Doctoral Thesis

Supersensitive Bio-marker Sensing using Photonic Crystal Nanolaser

(フォトニック結晶ナノレーザによる
超高感度バイオマーカーセンシング)

Yokohama National University
Department of Physics, Electrical and Computer Engineering

Shoji Hachuda
(羽中田　祥司)

March , 2016

要約

近年高齢化社会を迎え、医療費増大が深刻な問題となっている．平成 25 年の国民医療費が 40 兆円に迫るほど増大しており、さらに年平均 3%の増加を示し、医療費の増大が日本の深刻な問題となっている．この問題を解決するために、医療の高度化による疾病の早期発見や予防医療の重要性であり、これに対して疾病の早期発見や予防医療を実現するためにバイオマーカー診断の高度化が期待されている．バイオマーカーとは生物学的過程、病理学的過程、もしくは治療的介入に対する薬理学的応答の指標として、客観的に測定され評価される特性と定義され、広義では日常診断における血液検査、腫瘍マーカーなどが含まれる．病気の診断の指標となるバイオマーカーを日常的に検査することを求められている．しかし人の体には多種多様なバイオマーカーが存在し、その多くは簡便な測定法が確立されていないため、ELISA (酵素結合免疫吸着検定法 : Enzyme-Linked ImmunoSorbernt Assay)などにより診断が不可能なバイオマーカーも多数存在する．さらにバイオマーカーによっては検出された濃度では、すでに疾病の進行しているため早期発見に適さないものもあるためより高感度なバイマーカーが必要とされている．このような様々なバイオマーカーを日常的に診断するためには、低コストかつ簡便で高スループットなセンサーであることも要求されている．従って、ELISA 以上の高感度を実現し、かつ低コスト、簡便さ、高スループット等の性能を同時に満足するバイオセンサーが医療の現場から求められている．

バイオセンサーは酵素や抗体といった生体に関連する物質を利用し選択的に吸着する機能を持つバイオインターフェイス、目的の生体分子をとらえた反応をトランスデューサー、さらにトランデュサーからの信号を検出するセンサーにより構成される．現在いくつかのバイオマーカーが医療現場で使用されているが、低コスト、高スループット、簡易かつ高感度な診断は未だに実現していない．本研究室ではこれまでにフォトニック結晶 (PC) ナノレーザによるバイオセンシングを研究してきた．このナノレーザセンサは周囲の屈折率等をセンシングすることで波長がレッドシフトすることをセンシング原理とする．PC ナノレーザは媒質に利得を持つアクティブセンサであり、パッシブセンサにおいて現れる光学損失を打ち消し、自ら Q 値を高めるため狭線幅が可能である．さらにナノスロット (NS) を共振器部分に導入することでウシ血清アルブミン (BSA) で 255 fM という超高感度センシングを実現されてきた．これは一般的な

表面ラマン共鳴 (SPR) センサーの 1000 倍という超高感度である．このような超高感度なセンシングを実現している一方で、ナノレーザセンサには以下に示すいくつかの問題がある．

1. これまで主に測定してきた BSA が化学的に吸着を検出するもので、バイオマーカー検出に要求される選択性を実現しておらず、実際のバイオマーカーを診断できるか不明であること．
2. 不純物に対する選択性を未検証であること．
3. センシング時のブルーシフトや異なる測定での波長揺らぎ等の安定性．
4. センシング原理が未だ解明されておらず、実際に超高度できている不明であること．

そこで、本研究では以下の 4 つを目的とした．

1. 実際のバイオマーカーでの ELISA 以上の高感度検出の実証．
2. 不純物試料中からの選択的検出の実証．
3. センシング安定性の向上．
4. 超高感度で測定された濃度に対する検証．

第 2 章ではフォトニック結晶にナノスロット構造を導入したナノスロットナノレーザのモード局在による高感度化や狭線幅化のコンセプトを紹介し、液体センシング例を挙げた．

第 3 章では基本的なバイオマーカーのセンシング方法とバイオインターフェイスの構築方法を説明した．さらにバイオマーカーの検出の評価法としてシグナルとコントロール用のチップを準備し．チップ内に多数集積されたナノレーザアレイを比較し、統計処理することで検出することを説明した．

第 4 章ではモデルタンパク質に BSA を使用し、非特異吸着と特異吸着を評価した．非特異吸着では ALD による保護膜の形成でブルーシフトが抑制され、結果的により低濃度からのセンシングを実証した．特異吸着では BSA 抗体と BSA の吸着順による差から特異吸着を評価した．

第 5 章では SA を不純物あり／なしの試料中から SA 検出したところ、不純物なしでは検出限界 16 zM を評価した．不純物ありでは 10 兆倍の不純物環境で 100 zM の検出に成功した．このような実験には揺らぎがあるため、バイオインターフェイスの修飾条件の最適化した．

第 6 章では PSA を不純物あり／なしの試料中から PSA 検出した．さらに不安定性の改善のために PTES 条件の最適化や界面活性剤の一種であるエタノールによるセンサー表面の親水化した．PC ナノレーザセンサをもちいて不純物あり／なしの試料中から PSA 検出したところ、不純物あり／なしともに汎用的な ELISA の検出限界であるサブ pM より高感度な 1 fM PSA の検出に成功し、不純物選択比 (BSA / PSA) = 10 億倍の選択比が得られた．このように本デバイスは要

求される高感度、高選択性を有し、簡便かつ即時的なセンシングを実現した．さらにエタノールアミンを使用することで、センシング感度や波長シフトが増大することを発見した．これはセンサー表面が疎水化しているため、フォトニック結晶スラブ下部への抗体や抗原の浸透が抑制され、結果的に感度やシフトが抑制されたと考えられる．この抑制をエタノールアミンにより親水化することでスラブ下部への浸透が効率化されたため高価感度化が実現された．

第7章ではELISAによるPSA検出での親和定数と検出限界で規格化したfigure of merit (FOM) を再定義し、他のラベルフリーバイオマーカーおよびELISAとの性能を比較したところ、NSナノレーザのFOMが1.9-300と非常に高い値を示し、NSナノレーザの優れたセンシング性能を実証した．

第 8 章では以上のことをまとめ、フォトニック結晶ナノレーザがバイオマーカーセンサとして極めて有望であると評価した．さらにエタノールアミンやTween 20 の表面の親水化で高感度化、波長シフトの増大効果のバイオインターフェイスの改善によりバイオマーカーセンシングを安定化できた評価した．

Contents

Chapter 1
Introduction

1. 1 Biosensing

Figure 1.1 shows the population ratio as a function of year for the each age [1-1]. As seen in Fig. 1.1, the ratio of (labor/aging) was rapidly decreased with years and the supper aging society has come. Fig. 1.2 shows the annually national cost of medical care in Japan [1-2]. In 2015, the national cost approached 40 trillion yen and the average increasing rate has been 3%. If it remains increasing of the cost, it would break down the finance of Japan. Thus, Identification of severe diseases and advanced medical diagnoses are of increasing importance in aging societies [1-3]. Therefore, daily examinations of diagnostic biomarkers in blood and humor will have long demands. Although some easily-detectable biomarkers are already being serviced in health clinics, low-cost and high-throughput detection of very small amounts of specific biomarkers suitable for earlier and more reliable diagnoses is still a challenge [1-4]. For the purpose of easy and non-invasive diagnosis, the various biosensors were studied until now.

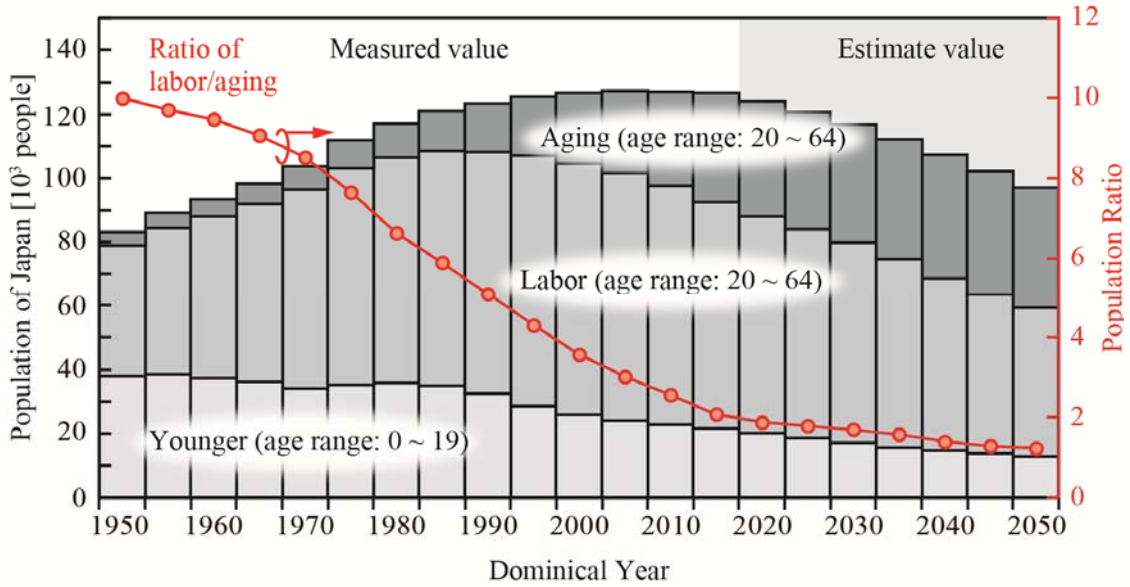

Fig. 1.1 The population ratio as a function of year for the each age in Japan.

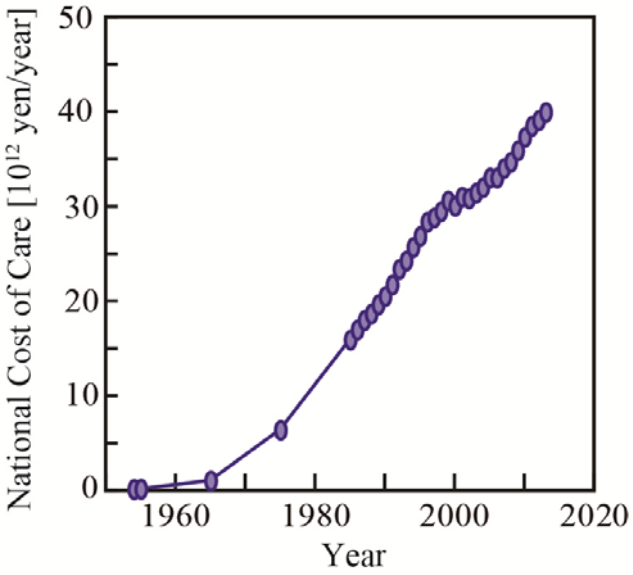

Fig. 1.2 National cost of care for each year.

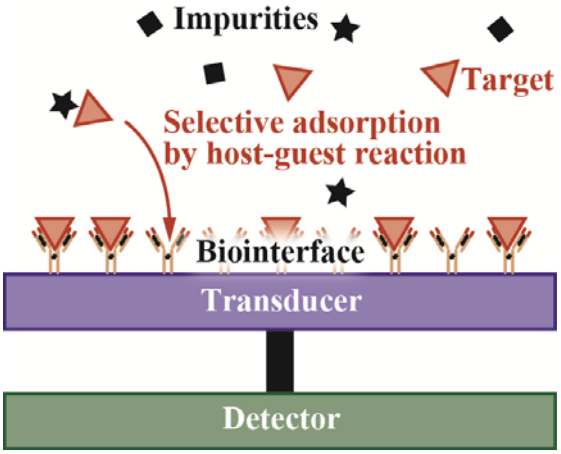

Fig. 1.3 Structure of biosensors. The biosensors consist of three parts such as the biointerface, the transducer, and the detector. The biointerface recognizes the target molecules, the transducer converts the specific adsorption of host-guest reaction to the signal, and the detector gets the signal.

The biosensor requires the specific recognition to the target molecules such as biomarkers. The recognition was obtained by the biological reaction such as host-guest reaction [1-5, 6] of enzyme reaction, antibody-antigen reaction, DNA hybridization, etc.

Fig. 1.3 shows the architectonics of the biosensors. The biosensors consist of the biointerface, the transistor and the detector. As mentioned above, the biointerface achieves the specific recognition to the target molecule, in the other words, selective

adsorption. The adsorption converses to light or electrical signal and then the signal is detected by the detector. Common immunological methods such as enzyme-linked immunosorbent assay (ELISA) allow a detection limit (DL) of pM order [1-7], which barely meets the requirement for these biomarkers, and yet has problems that they need time-consuming functionalization procedures of fluorescent labels where the labels themselves are suspected to change the original properties of the biomarkers. As label-free methods, photonic sensors [1-7–23] and those based on other physical parameters [1-3, 24–27] have been developed. Table 1.1 summarizes target biomarkers, the affinity constant K_A and the performance of detection limit (DL) using each label-free biomarker sensor such as PC waveguide/cavity, SiO_2 μ-toroidal, SiO_2 ring biosensor, surface plasmon resonance (SPR), localized SPR (LSPR), surface enhanced Raman scattering (SERS), field effect transistor (FET) and Impedance. Some biosensor achieved lower DL of f< pM order which is DL of ELISA. However, these biosensors have some issues. Here, LSPR, SERS and FET biosensors, which have a lower DL of ELISA, was introducted. SPR sensor measures light intensity as a function of resonance angle of incident light through prism due to the light coupling to plasmon mode on the metal surface and LSPR enhances the localization of electric field by the local pattern and improve the spatial resolution. However, the device footprint is large (10^4–10^6 μm^2) resulting in high cost for the using sample. μ-toroidal biosensor measures resonance wavelength shift by whispering gallery mode and achieves high sensitivity by the very high *Q*-factor. On the other hand, the sensing system is very complex. SERS identify sample from the spectrum of Raman scattering and is enhanced by local plasmon resonance which is one of most effective method for Raman scattering. However, the signal is noisy and unstable due to the lack of the uniformity of metal pattern which often has fabricated by Au nanoparticles. FET biosensor measures the changes in its electrical properties. FET biosensor has often improved by the modification of carbon nanotubes or grapheme, but the fabrication is the lack of reproducibility. In this way, none of them simultaneously satisfy all the requirements of practical medical sensors: low cost, disposable use, simple procedure, high sensitivity, and high selectivity against contaminants.

1.2 Photonic crystal nanolaser

For the satisfaction of the above requirements, photonic crystal nanolaser sensor was studied. PC nanolasers consists of a triangular lattice of holes in a GaInAsP single-quantum-well slab and 2–4 adjacent holes shifted to form a H0-type cavity shown in Fig. 1.4 [1-62]. A multi-dimensional Bragg diffraction formed photonic band gap (PBG) which is the forbidden band when the difference in index of refraction between the

Table 1.1 The performance of biosensors.

Biosensor	Biomarker *	K_A [M^{-1}]	DL [pM]	Ref.
PC waveguide/cavity	BSA	10^5	1.5×10^5	[1-28]
	Anti-biotin	10^7	233	[1-29]
	SA	10^{15}	1.9×10^{-7}	[1-30]
	CEA	10^{10}	5.6×10^{-4}	[1-31]
	avidin	10^{15}	10^{-3}	[1-32]
SiO_2 μ-toroidal	IL-2	10^9	5×10^{-6}	[1-33]
	IL-2	10^9	100	[7-34]
SiO_2 ring	BSA	10^7	100	[1-21]
	PSA	10^8–10^9	300	[7-35]
Interferometer	hCG	10^{10}	100	[1-36, 37]
SPR	IgG	10^8–10^9	0.27	[1-10]
	PSA	10^8–10^9	4.6	[1-38–40]
LSPR	PSA	10^8–10^9	280	[1-41]
	Tau	10^7	0.2	[1-42, 43]
	CEA	– **	8×10^{-6}	[7-44]
	PSA	10^8–10^9	30	[7-45]
	f-PSA	10^8–10^9	3×10^{-3}	[7-46]
SERS	PSA	10^8-10^9	0.12	[1-39, 40, 47]
	CEA	10^{10}	0.2	[7–48]
FET	SA	10^{15}	0.01	[1-49–51]
	PSA-ACT	10^{10}	11	[1-52]
	TnI	10^5–10^6	7000	[1-53–55]
	CEA	10^{10}	5.5×10^{-4}	[1-55, 56]
	IgG	10^9	7×10^{-3}	[1-57]
	PSA	10^8–10^9	2×10^{-3}	[1-58]
	PSA	10^8–10^9	3×10^{-5}	[7-59]
	TnI	10^5–10^6	0.2	[7-60]
	PSA-ACT	10^8–10^9	10^{-3}	[7-61]

* Note: Short of name biomarkers stand for bovine serum albmin (BSA), interleukin-2 (IL-2), human chorionic gonadotropin (hCG), immunoglobulin G (IgG), prostate specific antigen (PSA), streptavidin (SA), PSA-α1-antichymotripsin complex (PSA-ACT), free-PSA (f-PSA), troponin I (TnI), and carcinoembryonic antigen (CEA), respectivity.

** The affinity constant is no data because two aptamers were adopted as host molecules for CEA.

materials of the periodic structure is enough large [1-63]. PC forbids the light whose wavelength corresponds to the PBG. Using the characteristics, the cavity was formed in PC slab by the some shifted holes.

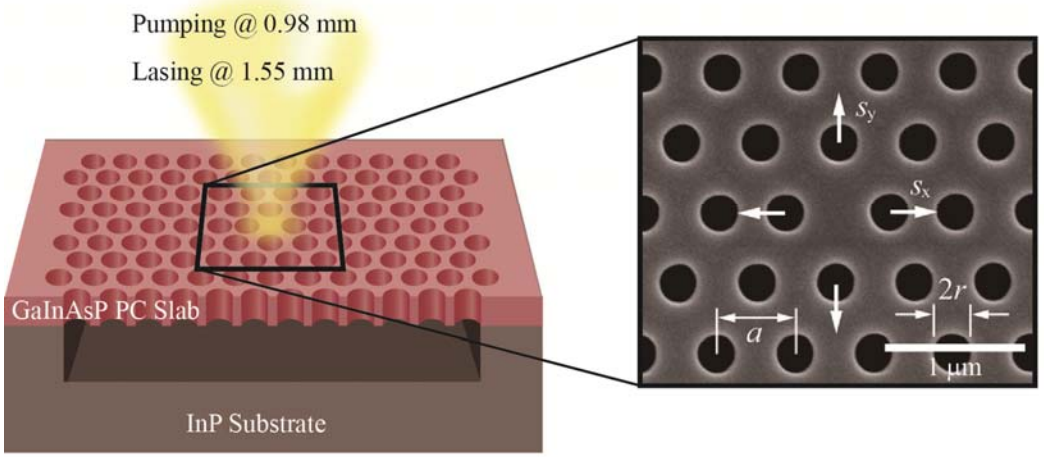

Fig. 1.4 Structure of a PC nanolaser.

In our laboratory, a photonic crystal nanolaser as a label-free sensor was developed [1-62]. When some medium is attached to the nanolaser cavity, which is exposed to an analyte, the laser wavelength redshifts due to the changes e.g., in the environmental index. The sensing area is within ~1 μm from the center of the cavitry. Let us compare the nanolaser sensor with common ELISA which is used in actual medical front. Since the total area of one nanolaser is no larger than 20 × 20 μm^2, its mass production is possible and cost effective, and supports its single-use, even using *e*-beam lithography, which is usually considered as a low-throughput process [1-64]. One chip including nanolasers is very small and so it is expected the chip cost will be of the order of $ 0.1. Additional cost will be necessary for the surface modification and packing, but still we expect it to be less than the expendable cost of ELISA because of the sensing method which does not require a secondary antibody and enzyme. As for the reader, the nanolaser needs the pump source, automatic stage, and optical spectrum analyzer (OSA). The OSA is the major cost, but will be comparable to the reader of ELISA. Thus, the cost of the nanolaser sensor is lower than that of ELISA. These chips after usage may have to be collected as the industrial waste because the GaInAsP semiconductor includes rare metals such as Ga and In and toxins such as As and P. However, it is not a particular issue, compared with other large amount of industrial waste of medical sites and the chips will be reused as a resource of the semiconductor. Previously, the performance of the nanolaser was the highly effective detection of some common proteins [1-65] and environmental toxin [1-66] was reported by our laboratory. Thus, the nanolaser was capable of a higher sensitivity than other label-free bio-sensors.

1.3 Biomarker and biointerface

Biomarker is defined as the accurate marker which indicates the reaction to the biological, pathological, or pharmacological process [1-67]. Therefore, the biomarkers are expected to be the marker to diagnose the health status and some biomarkers is actually used for the diagnosis such as PSA, CEA, TnI, etc. However, improving the sensitivity of biosensor has been required so that a very low concentrated biomarker included in blood can be diagnosed.

For the diagnosis from human sample such as blood, the diagnosis of target biomarker from high concentration contaminants. It is known that human serum includes total protein of 67 g/l (if molecular weight of the proteins is 66 kDa which is the molecular weight of albumin, the value can be converted to 1.3 mM). In this way, it is difficult to analyze the low concentration biomarkers from high concentration contaminant. Thus, the biointerface is needed for the selective detection from the contaminated samples. As mentioned above, the recognition of the biointerface is obtained by the biological reaction such as host-guest reaction of enzyme reaction, antibody-antigen reaction, DNA hybridization, etc. For the accurate detection, it is important to construct the biointerface which selectively adsorbs to the target biomarker and suppresses the non-specific adsorption.

1.4 Issues

This sensing using photonic crystal nanolaser has some issues. First, the issues are listed as follow:

1. The unexamined actual used biomarkers.
2. The unexamined selectivity against impurity
3. Blueshift noises occurred at the sensing.
4. The fluctuation of sensing in different trials.
5. The principle of the ultra-high sensitivity is not resolved.

First, the actual biomarkers and the selectivity against contaminants were not investigated using the nanolaser sensor. For the medical applications, it is required to investigate them. Next, the blueshift noise often has occurred in the sensing. So far, the noise was suppressed by thermal oxidization using strong pumping or the heating by an oven (180°C, >1 hour) [1-64]. Thereby, the sensor surface was covered with oxide layer of GaInAsP. This oxide layer prevented the sensor from further oxidization by photo-pumping at the sensing. However, the device with the thermal oxidization still blueshifted in charged polymers solution such as polyacrylic acid (PAA) or

polyethyleneimine (PEI). Because the oxide GaInAsP has weak resistance against acid or alkali solution, the oxide GaInAsP was etched or further oxidized by the charged polymers. Furthermore, the fluctuations in different trials were observed due to the un-uniformity of functionalization such as APTES and biotin. So, the stable and uniformity biointerface was not still structured between different treatment due to the manual errors or environmental errors. Finally, the principle of the ultra-high sensitivity is still unsolved. The ultra-high sensitivity has been discussed in ref. [1-65] and was described due to the light gradient force to the inside of NS and any forces in the wide area, which draw to the surrounding of the nanolaser cavity. However, this description cannot be explained for all questions.

1. 5 This work

As mentioned above, PC nanolaser sensors are potentially very useful for the medical application because the performance has ultra-high sensitivity, the low-cost fabrication and sensing method that do not need the enzyme and secondary antibody, and easy measurement. However, the nanolaser sensor has some issues such as blueshift noise, the stability of the sensing, an open question of the sensing principle and unexamined selectivity. Thehrefore, this work has following aims.

1. 5. 1 Demonstration of sensing actual biomarkers

So far, the biosensing using a NS nanolaser investigated mainly the chimisorption of BSA and the nanolaser achieved a supper-high sensitivity of DL = 255 fM for BSA [1-64]. However, the biomarker sensing which is required from medical fromt requires selective detection of the target biomarker. The BSA sensing does not have the selectivity because the chimisorption by GA couples to any proteins which include NH_2 goups and the selective detection of actual biomarkers have not established using the nanolaser sensor. Furthermore, a high sensitive biomarker is desired for early diagnosis and treatment for the lack of the sensitivity of ELISA (~pM order). Thus the main aims of this work are demonstration of sensing actual biomarker with higher sensitivity than that of ELISA and other labe-free biosensors shown in Table 1.1 and evaluation of the sensitivity by both values of DL and K_A because the sensitivity is limited by K_A which depends on the biomarker affinity.

1. 5. 2 **Demonstration of selectivity against a contaminant**

Biomarker sensing also needs the selectivity against a contaminant so as to detect very lower concentrated biomarkers than contaminants such as albumin included in blood. If 1 pM biomarker is detected from blood which includes with ~1 mM contaminants, the selectivity of 10^9 is necessary for the medical diagosis. Thus, this work aims to demonstrate the selective detection with the selectivity of > 10^9.

1. 5. 3 **Improvement of the stability for the biosensig**

As above mentioned, the sensing by a nanolaser sensor has some issues such as blueshift noise at laser pumping and the fluctuation of the sensing signal between different trials. So far, the blueshift noise was suppressed by thermal oxidization of the sensor surface by the advanced strong pumping or the heating by an oven [1-64]. However, the device with the thermal oxidization still blueshifted at bioseinsing of BSA or SA because the oxide GaInAsP has weak resistance against acid or alkali solution. The blueshift noise decreases the sensitivity of NS nanolaser. Thus, suppressing the noise is needed for the higher sensitivity and stability. Furthermore, the fluctuation of the

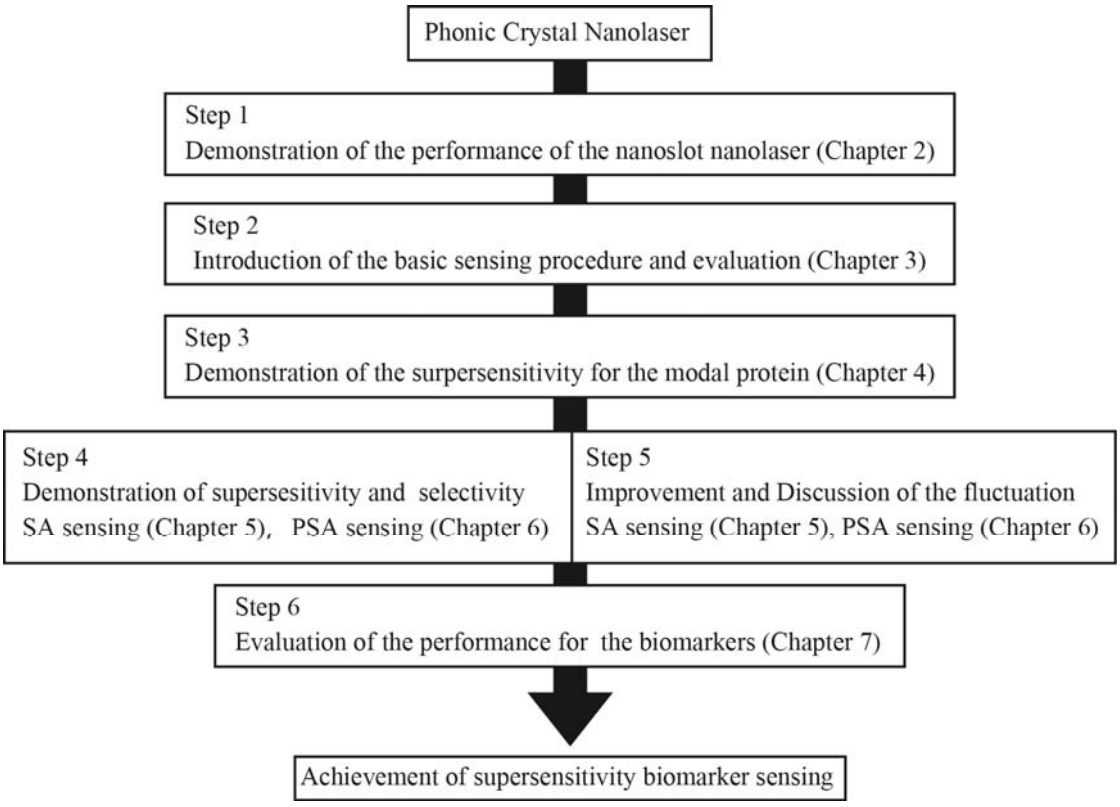

Fig. 1.5 Overview of this thesis.

sensing signal between different trials was obserbed and it was thought to be derived from unstable and/or ununiformity of the functionalization. For quantitative analysis, there is a need to suppress the fluctuation. Thus, Improvement of the stability for the bioseinsg by suppressing the blueshift noise and the fluctuation was one of aims for this work.

1. 5. 4 **Validation of the supper-sensitivity of NS nanolaser**

NS nanolaser achieved ultra-high sensitivity of DL = 16 zM SA in Chapter 5. Because this sensitivity is incredibly high value, it was suspected that the dilution of sample was inaccurate. There was a possibility that the unaccurate dilution of samples made it higher concentration than that of estimated by the dilution ratio. Therefore, the validation of supper-sensitivity of NS nanolaser was one of aims for this work.

1. 6 **This thesis**

Fig. 1.5 shows an overview of this thesis. Chapter 2 describes the principles of a photonic crystal nanolaser with NS and the demonstration of the ultra-high sensitivity for liquid sensing. For the demonstration of sensing actual biomarker, the selective detection of BSA and SA as model proteins was investigated. BSA was detected though the specific adsorption of antibody-antigen reaction by anti-BSA antibody in Chapter 4 for the confirmation of the possibility of the selective detection though antibody. SA was detected by specific adsorption of SA-biotin binding for the demonstration of the ideal performance with ultra-high K_A in Chapter 5. The sensing of PSA which is one of a famous biomarker was demonstrated in Chapter 6.Fothermore, the SA and PSA sensing from impure sampe was done for the demonstration of selectivity against contaminants in Chapter 5 and 6. For suppressing the blueshift noise was tried by the ALD protection which has strong resistance. The sensing for the device with ALD layer was investigated for each protein in Chapter 4, 5 and 6. For the improvement of functionalization of host molecule such as biotin and PSA antibody was tried in Chapter 5 and 6. Furthermore, APTES, which is the basic of the fuctionalization, also was otimalized in Chapter 6. Finally, Charpter 7 descries the evaluation of the sensor performance by the comparison with other label-free biosensors.

Reference

[1-1] Ministry of Internal Affairs and Communications, "About demographics at 2015," <http://www.ipss.go.jp/syoushika/tohkei/Popular/P_Detail2015.asp?fname=T02-09.htm>.

[1-2] Ministry of Health, Labour and Welfare," Brief overview about the annually national cost of medical care in Japan," < http://www.mhlw.go.jp/toukei/saikin/hw/k-iryohi/13/index.html>.

[1-3] G.-J. Zhang, Z. H. H. Luo, M. J. Huang, J. J. Ang, T. G. Kang, and H. Ji, "An integrated chip for rapid, sensitive, and multiplexed detection of cardiac biomarkers from fingerprick blood," *Biosens. Bioelectron.*, vol. 28, no. 1, 459–463, 2011.

[1-4] Y. D. Ivanov, V. M. Govorun, V. A. Bykov, and A. I. Archakov, "Nanotechnologies in proteomics," *Proteomics*, vol. 6, no. 5, 1399–1414, 2006.

[1-5] K. N. Houk, A. G. Leach, S. P. Kim, and X. Zhang, "Binding affinities of host–guest, protein–ligand, and protein–transition-state complexes," *Angew. Chemie Int. Ed.*, vol. 42, no. 40, pp. 4872–4897, 2003.

[1-6] Q. Chen, H. Chen, Y. Zhao, F. Zhang, F. Yang, J. Tang, and P. He, "A label-free electrochemiluminescence aptasensor for thrombin detection based on host–guest recognition between tris(bipyridine)ruthenium(II)-β-cyclodextrin and aptamer," *Biosens. Bioelectron.*, vol. 54, pp. 547–552, 2014.

[1-7] R. Wiese, Y. Belosludtsev, T. Powdrill, P. Thompson, and M. Hogan, "Simultaneous multianalyte ELISA performed on a microarray platform," *Clin. Chem.*, vol. 47, no. 8, 1451–1457, 2001.

[1-8] B. J. Luff, J. S. Wilkinson, J. Piehler, U. Hollenbach, J. Ingenhoff, and N. Fabricius, "Integrated optical Mach-Zehnder biosensor," *J. Lightwave Technol.*, vol. 16, no. 4, pp. 583–592, 1998.

[1-9] J. Homola, S. S. Yee, and G. Gauglitz, "Surface plasmon resonance sensors: review," *Sens. Actuators B Chem.*, vol. 54, no. 1−2, pp. 3–15, 1999.

[1-10] W. C. Law, K. T. Yong, A. Baev, R. Hu, and P. N. Prasad, "Nanoparticle enhanced surface plasmon resonance biosensing: application of gold nanorods," *Opt. Express*, vol. 17, no. 21, pp. 19041–19046, 2009.

[1-11] M. Piliarik, M. Bocková, and J. Homola, "Surface plasmon resonance biosensor for parallelized detection of protein biomarkers in diluted blood plasma," *Biosens. Bioelectron.*, vol. 26, no. 4, pp. 1656–1661, 2010.

[1-12] A. Yalcin, K. C. Popat, J. C. Aldridge, T. A. Desai, J. Hryniewicz, N. Chbouki, B. E. Little, O. King, V. Van, S. Chu, D. Gill, M. Anthes-Washburn, M. S. Unlu, and B. B. Goldberg, "Optical sensing of biomolecules using microring resonators," *IEEE J. Sel. Top. Quantum Electron.*, vol. 12, no. 1, pp. 148–155, 2006.

[1-13] A. M. Armani, R. P. Kulkarni, S. E. Fraser, R. C. Flagan, and K. J. Vahala, "Label-free, single-molecule detection with optical microcavities," *Science*, vol. 317, no. 5839, pp. 783–787, 2007.

[1-14] F. Vollmer and L. Yang, "Label-free detection with high-*Q* microcavities: a review of biosensing mechanisms for integrated devices," *Nanophotonics*, vol. 1, no. 3–4,

pp. 267–291, 2012.

[1-15] D.-K. Kim, S.M. Yoo, T. J. Park, H. Yoshikawa, E. Tamiya, J. Y. Park, and S. Y. Lee, "Plasmonic properties of the multispot copper-capped nanoparticle array chip and its application to optical biosensors for pathogen detection of multiplex DNAs," *Anal.Chem.*, vol. 83, no. 16, 6215–6222, 2011.

[1-16] M. P. Kreuzer, R. Quidant, J. P. Salvador, M. P. Marco, and G. Badenes, "Colloidal-based localized surface plasmon resonance (LSPR) biosensor for the quantitative determination of stanozolol," *Anal. Bioanal. Chem.*, vol. 391, no. 5, pp. 1813–1820, 2008.

[1-17] S.-H. Yeom, M.-E. Han, B.-H. Kang, K.-J. Kim, H. Yuan, N.-S. Eum, and S.-W. Kang, "Enhancement of the sensitivity of LSPR-based CRP immunosensors by Au nanoparticle antibody conjugation," *Sens. Actuators B,* vol. 177, pp. 376–383, 2013.

[1-18] A. Das, J. Zhao, G. C. Schatz, S. G. Sligar, and R. P. Van Duyne, "Screening of type I and II drug binding to human cytochrome P450-3A4 in nanodiscs by localized surface plasmon resonance spectroscopy," *Anal. Chem.*, vol. 81, no. 10, pp. 3754–3759, 2009.

[1-19] W. Zhou, Y. Ma, H. A. Yang, Y. Ding, and X. G. Luo, "A label-free biosensor based on silver nanoparticles array for clinical detection of serum p53 in head and neck squamous cell carcinoma," *Int. J. Nanomed.*, vol. 6, pp. 381–386, 2011.

[1-20] L. Guo, D. Wang, Y. Xu, B. Qiu, Z. Lin, H. Dai, H.-H. Yang, and G. Chen, "Discrimination of enantiomers based on LSPR biosensors fabricated with weak enantioselective and nonselective receptors," *Biosens. Bioelectron.*, vol. 47, no. 15, 199–205, 2013.

[1-21] K. De Vos, J. Girones, T. Claes, Y. De Koninck, S. Popelka, E. Schacht, R. Baets, P. Bienstman, "Multiplexed antibody detection with an array of silicon-on-insulator microring resonators," *IEEE Photon. J.*, vol. 1, no. 4, pp. 225–235, 2009.

[1-22] M. Lončar, A. Scherer, and Y. Qiu, "Photonic crystal laser sources for chemical detection," *Appl. Phys. Lett.*, vol. 82, pp. 4648, 2003.

[1-23] E. Chow, A. Grot, L.W. Mirkarimi, M. Sigalas, and G. Girolami, "Ultracompact biochemical sensor built with two-dimensional photonic crystal microcavity," *Opt. Lett.*, vol. 29, no. 10, pp.1093–1095, 2004.

[1-24] Y. Cui, Q. Q. Wei, H. K. Park, and C. M. Lieber, "Nanowire nanosensors for highly sensitive and selective detection of biological and chemical species," *Science*, vol. 293, no. 5533, pp.1289–1292, 2001.

[1-25] A. Kim, C. S. Ah, H. Y. Yu, J. H. Yang, I. B. Baek, C. G. Ahn, C. W. Park, M. S. Jun, and S. Lee, "Ultrasensitive, label-free, and real-time immunodetection using silicon field-effect transistors," *Appl. Phys. Lett.*, vol. 91, no. 10, pp. 103901, 2007.

[1-26] J. Chua, R. E. Chee, A. Agarwal, S. M. Wong, and G.-J. Zhang, "Label-free electrical detection of cardiac biomarker with complementary metal-oxide semiconductor-compatible silicon nanowire sensor arrays," *Anal. Chem.*, vol. 81, no. 15, pp. 6266–6271, 2009.

[1-27] M. G. von Muhlen, N. D. Brault, S. M. Knudsen, S. Y. Jiang, and S. R. Manalis, "Label-free biomarker sensing in undiluted serum with suspended microchannel resonators," *Anal. Chem.*, vol. 82, no. 5, pp. 1905–1910, 2010.

[1-28] R. G. Heideman and P. V. Lambeck, "Remote opto-chemical sensing with extreme sensitivity: Design, fabrication and performance of a pigtailed integrated optical phase-modulated Mach-Zehnder interferometer system," *Sensors Actuators, B Chem.*, vol. 61, pp. 100–127, 1999.

[1-29] S. Zlatanovic, L. W. Mirkarimi, M. M. Sigalas, M. A. Bynum, E. Chow, K. M. Robotti, G. W. Burr, S. Esener, and A. Grot, "Photonic crystal microcavity sensor for ultracompact monitoring of reaction kinetics and protein concentration," *Sensors Actuators, B Chem.*, vol. 141, no. 1, pp. 13–19, 2009.

[1-30] D. Yang, S. Kita, F. Liang, C. Wang, H. Tian, Y. Ji, M. Lončar, and Q. Quan, "High sensitivity and high *Q*-factor nanoslotted parallel quadrabeam photonic crystal cavity for real-time and label-free sensing," *Appl. Phys. Lett.*, vol. 105, no. 6, p. 063118, 2014.

[1-31] F. Liang, N. Clarke, P. Patel, M. Loncar, and Q. Quan, "Scalable photonic crystal chips for high sensitivity protein detection," *Opt. Express*, vol. 21, no. 26, pp. 6071–6077, 2013.

[1-32] S. Chakravarty, A. Hosseini, X. Xu, L. Zhu, Y. Zou, and R. T. Chen, "Analysis of ultra-high sensitivity configuration in chip-integrated photonic crystal microcavity bio-sensors," *Appl. Phys. Lett.*, vol. 104, p. 191109, 2014.

[1-33] A. M. Armani, R. P. Kulkarni, S. E. Fraser, R. C. Flagan, and K. J. Vahala, "Label-free, single-molecule detection with optical microcavities," *science*, vol. 317, no. 5839, pp. 783–787, 2007.

[1-34] E. Ozgur, P. Toren, O. Aktas, E. Huseyinoglu, and M. Bayindir, "Label-free biosensing with high selectivity in complex media using microtoroidal optical resonators.," *Sci. Rep.*, vol. 5, p. 13173, 2015.

[1-35] T. Taniguchi, A. Hirowatari, T. Ikeda, M. Fukuyama, Y. Amemiya, A. Kuroda, and S. Yokoyama, "Detection of antibody-antigen reaction by silicon nitride slot-ring biosensors using protein G," *Opt. Commun.*, vol. 365, pp. 16–23, 2016.

[1-36] I. T. Huhtaniemi, C. C. Korenbrot, and R. B. Jaffe, "hCG binding and stimulation of testosterone biosynthesis in the human fetal testis," *J. Clin. Endocrinol. Metab.*, vol. 44, no. 4, 963–967, 1977.

[1-37] B. H. Schneider, J. G. Edwards, and N. F. Hartman, "Hartman interferometer:

versatile integrated optic sensor for label-free, real-time quantification of nucleic acids, proteins, and pathogens," *Clin. Chem.*, vol. 43, no. 9, pp. 1757–1763, 1997.

[1-38] G. A. J. Besselink, R. P. H. Kooyman, P. J. H. J. van Os, G. H. M. Engbers, and R. B. M. Schasfoort, "Signal amplification on planar and gel-type sensor surfaces in surface plasmon resonance-based detection of prostate-specific antigen," *Anal. Biochem.*, vol. 333, pp. 165–173, 2004.

[1-39] D. A. Zubtsov, E. N. Savvateeva, A. Yu. Rubina, S. V. Pan'kov, E. V. Konovalova, O. V. Moiseeva, V. R. Chechetkin, and A. S. Zasedatelev, "Comparison of surface and hydrogel-based protein microchipsm," *Anal. Biochem.*, vol. 368, no. 2, pp. 205–213, 2007.

[1-40] P. S. Katsamba, I. Navratilova, M. Calderon-Cacia, L. Fan, K. Thornton, M. Zhu, T. V. Bos, C. Forte, D. Friend, I. Laird-Offringa, et al., "Kinetic analysis of a high-affinity antibody/antigen interaction performed by multiple Biacore users," *Anal. Biochem.*, vol.352, pp. 208–221, 2006.

[1-41] S. W. Lee, K. S. Lee, J. Ahn, J. J. Lee, M. G. Kim, and Y. B. Shin, "highly sensitive biosensing using arrays of plasmonic Au nanodisks realized by nanoimprint lithography," *ACS Nano*, vol. 5, pp. 897–904, 2011.

[1-42] M. Vestergaard, K. Kerman, D. K. Kim, H. M. Hiep, and E. Tamiya, "Detection of Alzheimer's tau protein using localised surface plasmon resonance-based immunochip," *Talanta*, vol. 74, pp. 1038–1042, 2008.

[1-43] G.o A. Farias, J. P. Muñoz, J. Garrido, and R. B. Maccioni, "Tubulin, actin, and tau protein interactions and the study of their macromolecular assemblies," *J. Cell. Biochem.*, vol. 85, no. 2, pp. 315–324, 2002.

[1-44] D. Wang, Y. Li, Z. Lin, B. Qiu, and L. Guo, "Surface-enhanced electrochemiluminescence of $Ru@SiO_2$ for ultrasensitive detection of carcinoembryonic antigen," *Anal. Chem.*, vol. 87, no. 12, pp. 5966–5972, 2015.

[1-45] S. S. Aćimović, M. A. Ortega, V. Sanz, J. Berthelot, J. L. Garcia-Cordero, J. Renger, S. J. Maerkl, M. P. Kreuzer, and R. Quidant, "LSPR chip for parallel, rapid, and sensitive detection of cancer markers in serum," *Nano Lett.*, vol. 14, no. 5, pp. 2636–2641, 2014.

[1-46] M. Sanders, Y. Lin, J. Wei, T. Bono, and R. G. Lindquist, "An enhanced LSPR fiber-optic nanoprobe for ultrasensitive detection of protein biomarkers," *Biosens. Bioelectron.*, vol. 61, pp. 95–101, 2014.

[1-47] D. S. Grubisha , R. J. Lipert , H.-Y. Park , J. Driskell, and M. D. Porter, "Femtomolar detection of prostate-specific antigen: an immunoassay based on surface-enhanced Raman scattering and immunogold Labels," *Anal. Chem.*, vol. 75, no. 21, pp. 5936–5943, 2003.

[1-48] X. Miao, S. Zou, H. Zhang, and L. Ling, "Highly sensitive carcinoembryonic

antigen detection using Ag@Au core-shell nanoparticles and dynamic light scattering," *Sensors Actuators, B Chem.*, vol. 191, pp. 396–400, 2014.

[1-49] Y. Cui, Q. Q. Wei, H. K. Park, and C. M. Lieber, "Nanowire nanosensors for highly sensitive and selective detection of biological and chemical species," *Science*, vol 293, pp.1289–1292, 2001.

[1-50] E. Stern, J.F. Klemic, D. A. Routenberg, P. N. Wyremebak, D. B. Turner-Evans, A. D. Hamilton, D. A. Lavan, T. M. Fahmy, and M. A. Reed, "Laabel-free immunodetection with CMOS-compatible semiconducting nanowires," *Nature*, vol. 445 pp. 519–522, 2007.

[1-51] E. Stern, R. Wagner, F. J. Sigworth, R. Breaker, T. M. Fahmy, and M. A. Reed, "Importance of the Debye screening length on nanowire field effect transisitor sensors," *Nano Lett.*, vol. 7, pp. 3405–3409, 2007.

[1-52] Jun Pyo Kim, Byung Yang Lee, Joohyung Lee, Seunghun Hong, and Sang Jun Sim, "Enhancement of sensitivity and specificity by surface modification of carbon nanotubes in diagnosis of prostate cancer based on carbon nanotube field effect transistors," *Biosens. Bioelectron.*, vol. 24, no. 11, pp. 3372–3378, 2009.

[1-53] T. W. Lin, P. J. Hsieh, C. L. Lin, Y. Y. Fang, J. X. Yang, C. C. Tsai, P. L. Chiang, C. Y. Pan, and Y. T. Chen, "Label-free detection of protein-protein interactions using a calmodulin-modified nanowire transistor," *Proc. Natl. Acad. Sci. U. S. A.*, vol. 107, pp. 1047–1052, 2010.

[1-54] X. Liu, J. Wei, D. Song, Z. Zhang, H. Zhang, and G. Luo, "Determination of affinities and antigenic epitopes of bovine cardiac troponin I (cTnI) with monoclonal antibodies by surface plasmon resonance biosensor," *Anal. Biochem.*, vol. 314, no. 2, pp. 301–309, 2003.

[1-55] L. V. Levin, T. W. Griffin, L. R. Childs, S. Davis, and D. E. HaagensenJr., "Compa Debye screening rison of multiple anti-CEA immunotoxins active against human adenocarcinoma cells," *Cancer Immunol. Immunother.*, vol. 24, no. 3, pp. 202–206, 1987.

[1-56] G. Zheng, F. Patolsky, Y. Cui, W.U. Wang, and C.M. Lieber, "Multiplexed electrical detection of cancer marlers with nanowire sensor arrays," *Nat. Biotechnol.*, vol. 23, pp. 1294–1301, 2005.

[1-57] J. P. Kim, B. Y. Lee, S. Hong, and S. Jun Sim, "Ultrasensitive carbon nanotube-based biosensors using antibody-binding fragment," *Anal. Biochem.*, vol. 381, no. 2, pp. 193–198, 2008.

[1-58] E. Stern, A. Vacic, N. K. Rajan, J. M. Criscione, J. Park, B. R. Ilic, D. J. Mooney, M. A. Reed, and T. M. Fahmy, "Label-free biomarker detection from whole blood," *Nat. Nanotechnol.*, vol. 5 pp. 138–142, 2010.

[7-59] A. Kim, C. S. Ah, H. Y. Yu, J. H. Yang, I. B. Baek, C. G. Ahn, C. W. Park, M. S.

Jun, and S. Lee, "Ultrasensitive, label-free, and real-time immunodetection using silicon field-effect transistors," *Appl. Phys. Lett.*, vol. 91, p. 103901, 2007.

[7-60] K. Kim, C. Park, D. Kwon, D. Kim, M. Meyyappan, S. Jeon, and J. S. Lee, "Silicon nanowire biosensors for detection of cardiac troponin I (cTnI) with high sensitivity," *Biosens. Bioelectron.*, vol. 77, pp. 695–701, 2016.

[7-61] D. J. Kim, I. Y. Sohn, J. H. Jung, O. J. Yoon, N. E. Lee, and J. S. Park, "Reduced graphene oxide field-effect transistor for label-free femtomolar protein detection," *Biosens. Bioelectron.*, vol. 41, no. 1, pp. 621–626, 2013.

[1-62] S. Kita, K. Nozaki, S. Hachuda, H. Watanabe, Y. Saito, S. Otsuka, T. Nakada, Y. Arita, and T. Baba, "Photonic crystal point-shift nanolaser with and without nanoslots −−− design, fabrication, lasing and sensing characteristics," *IEEE J. Sel. Top. Quantum Electron.*, vol. 17, no. 6, pp. 1632–1647, 2011.

[1-63] E. Yablonovitch, and T. J. Gmitter, "Photonic band structure: the face-centered-cubic case," *Phys.Rev. Lett.*, vol. 63, pp. 1950–1953, 1989.

[1-64] S. Kita, "Photonic crystal nanolaser sensor," Doctoral thesis (*Yokohama Nat'l Univ.*), 2012.

[1-65] S. Kita, S. Hachuda, S. Otsuka, T. Endo, Y. Imai, Y. Nishijima, H. Misawa, and T. Baba, "Super-sensitivity in label-free protein sensing using a nanoslot nanolaser," *Opt. Express.*, vol. 19, no. 18, pp. 17683-17690, 2011.

[1-66] D. Takahashi, S. Hachuda, T. Watanabe, Y. Nishijima and T. Baba, "Detection of endotoxin using a photonic crystal nanolaser", *Appl. Phys. Lett.*, vol. 106, no. 13, pp. 131112, 2015.

[1-67] B. Definitions and W. Group, "Biomarkers and surrogate endpoints: Preferred definitions and conceptual framework," *Clin. Pharmacol. Ther.*, vol. 69, no. 3, pp. 89–95, 2001.

Chapter 2
Nanoslot Nanolaser

2. 1 Overview

This chapter demonstrates the fundamental principles involved in improving the sensitivity and resolution of a nanoslot (NS) nanolaser. Variations in the conventional fabrication process and the fundamental measurement setup are also described. Furthermore, the characteristics of an NS nanolaser in water are explained.

2. 2 Principle

Index resolution n_{res} is a crucial quantity for improving the sensitivity of biosensors that detect biomolecules through changes in the refractive environmental index Δn_{env} due to adsorption of the biomolecules. Δn_{res} for liquid and gas sensing is given as:

$$\Delta n_{res} = \frac{\Delta \lambda_s}{(\Delta \lambda / \Delta \lambda_{env})} \tag{2-1}$$

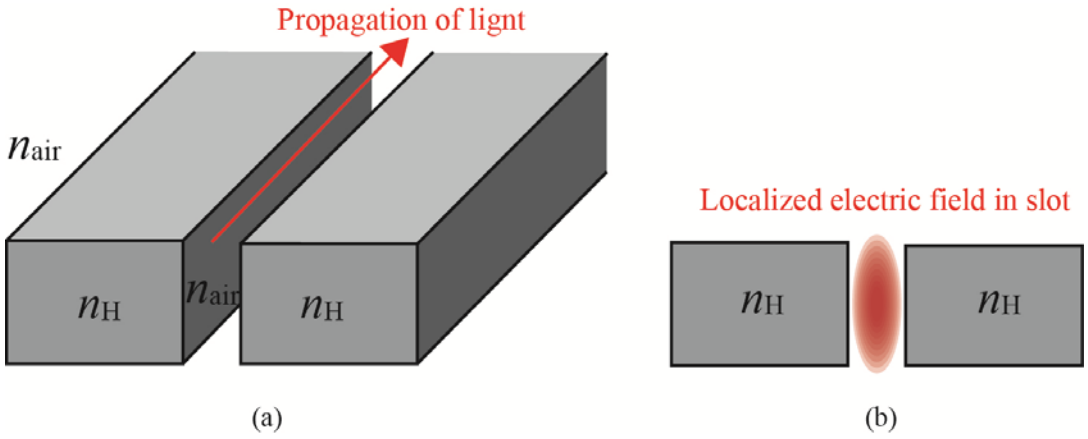

Fig. 2.1 A typical NS structure, i.e., a slot waveguide. (a) Structure of the slot waveguide and (b) the cross section. The electric field Localizes in the low-index NS.

Here, $\Delta\lambda_s$ and $\Delta\lambda$ are the spectral line width and the laser wavelength shift, respectively. $\Delta\lambda/\Delta n_{env}$ denotes the refractive index sensitivity s_{env}. To improve Δn_{res} for biosensing, Eq. (2.1) requires a narrow $\Delta\lambda_s$ or high s_{env}. A NS structure satisfies both requirements. A fundamental NS structure, i.e., a slot waveguide, shown in Fig. 2.1, consists of two strips of a high-index material separated by a nanoscale low-index region. In such a waveguide, the optical field can be enhanced and confined in a low-index medium, even when the light is guided by total internal reflection [2-2, 3, 4]. The enhancement of the electron field is proportional to the ratio of the dielectric constants between the high and low index materials due to the discontinuity of the electron field at the boundary. The strong localization of the laser mode in the NS enhances the light-matter interaction in the NS [2-5]. For biosensing, the NS is filled with water because biosensing using a PC nanolaser is performed in water [2-6]. This is expected to suppress the thermo-optic (TO) effects because the positive TO effect in the GaInAsP slab is canceled by the negative effect in water. Thus, it is expected to reduce λ_s. Furthermore, a narrow NS enhances strong localization of the laser mode in the NS and enables the above requirements.

In previous research, H0 type cavities with an NS calculated for a small modal volume [2-7], *Q*-optimization [2-8], and the *Q*-factor were balanced with the detection efficiency.

2. 3 Fabrication

For this thesis, PC nanolasers were fabricated on a 180-nm-thick GaInAsP quantum-well epitaxial wafer grown on a (100) InP substrate by Furukawa Elec. This

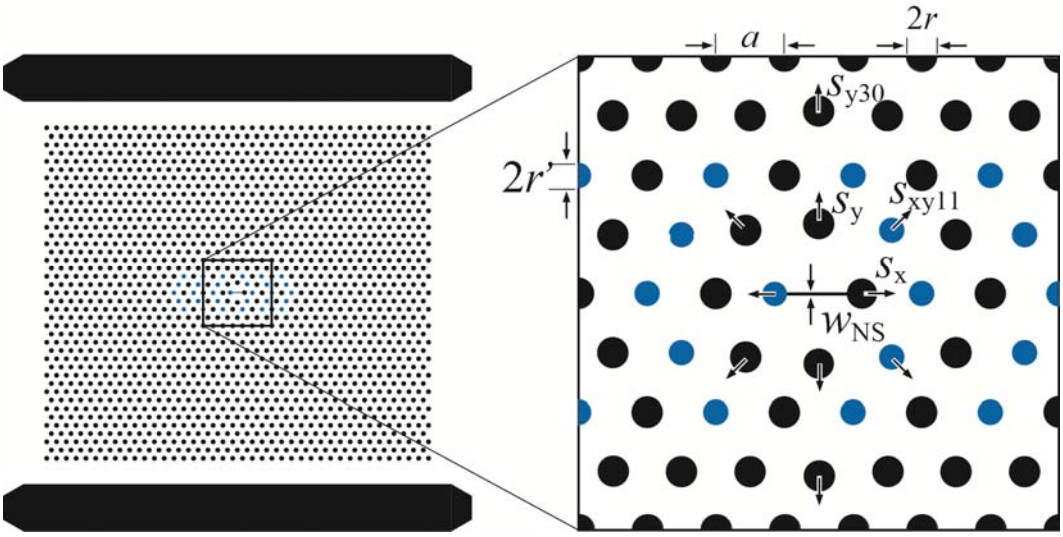

Fig. 2.2 A typical CAD image of a single NS nanolaser for the EB lithography and an enlarged figure of the cavity. Patterns were formed at back or blue area. Furthermore, asymmetric modification was added at blue area.

work used single-quantum-well (SQW) wafer 1 (F1206354 and F1207380) and SQW wafer 2 (M8-11115 and M8-130304) shown in Ref [2-8]. The fabrication process of a nanolaser is well summarized in Ref [2-8]. In brief, a device was fabricated by forming an electron-beam (EB) lithography resist pattern, transcribing the pattern on the active layer using hydrogen iodide (HI) inductively coupled plasma (ICP) dry etching, and forming an air-bridge structure by wet etching using hydrochloric acid (HCl). However, SQW wafer 1 requres additional process which is echting unnessary layers by HCl and H_2SO_4 etchent. The following changes to the usual fabrication process were applied:

1. Final design changes.
2. A surface treatment for stable electron-beam lithography.

Change 1 was applied to the final design of the NS nanolasers. A structure whose Q-factor was balanced with its detection efficiency was adopted. Conventional NS nanolasers often fail to operate or operate poorly. For biosensing using a nanolaser array for batch measurement, there are drawbacks such as low throughput and reduction in the number of measured devices due to weak lasing. Thus, a structure was adopted with radiation pattern control for the vertical emission related to the detection efficiency from above [2-9] and with Q-factor optimization with the above modulation. Fig. 2.2 shows a typical computer aided design (CAD) of a single NS nanolaser and Table 2.1 summarizes the parameters of the basic structure and the Q-optimized and asymmetric modified structure. During the biosensing process, the measurements of all the nanolasers, which were integrated over for the array configuration in a chip, were performed simultaneously and used for statistical analysis. It is necessary that the NS widths w_{NS} of the nanolasers are constant in

Table 2.1 Parameters of the CAD design.

Structure	Basic	Optimized for high Q and light extraction
Lattice constant a	500 nm	500 nm
Airhole diameter $2r$	220–240 nm	220–240 nm
NS width w_{NS}	0–60 nm	30 nm
Airhole shift (s_x, s_y)	(90–130 nm, 0–80 nm)	(120 nm, 60–80 nm)
Airhole shift (s_{xy11}, s_{y30}) (for Q optimization)	–	(0–20 nm, 0–20 nm)
Asymmetric modification Δr (along the E_y field)	–	−30–0 nm

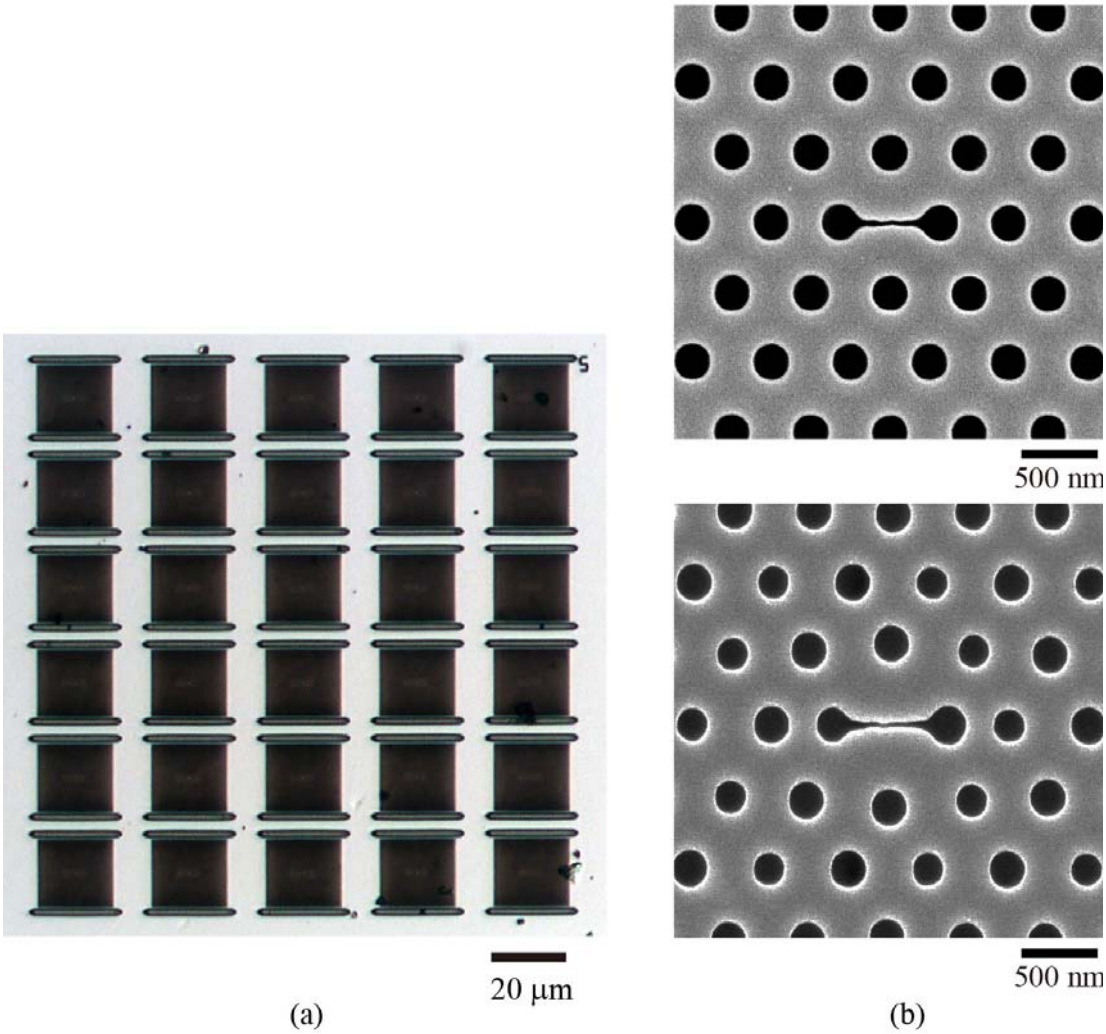

Fig. 2.3 A typical fabricated NS nanolaser array. (a) Optical microscope image of the nanolasers integrated in a 6 × 5 arrayed configuration within a footprint of less than 150 × 150 μm^2. (b) Upper and lower figures show the SEM images of a fabricated basic structure and a *Q*-optimized and asymmetric modified structure, respectively.

the array configuration to reduce biosensing measurement errors. Fig. 2.3 shows a typical fabricated NS nanolaser array. Fig. 2.3(a) shows an optical microscope image of an overall nanolaser array and Fig. 2.3(b) shows the scanning electron microscope (SEM) images of a cavity area in a nanolaser for both structures. We set the minimum w_{NS} to ~30 nm by adjusting the dose time and the design w_{NS}. Fig. 2.4 shows plots of the measured w_{NS} as a function of the design w_{NS} for the different dose times, and Fig. 2.5 shows the fabricated NS nanolasers at the same dose time for a series of design w_{NS} (22.5–60 nm). The NS was formed like a threshold and the measured w_{NS} increased with both dose time

and design w_{NS}. This suggests that the narrowest w_{NS} can be obtained by adjusting the dose time and/or design w_{NS}. Furthermore, a dose time of 1.4 μs/dot and a design w_{NS} of over 30 nm are required to remove a 400-nm-thick resist. For a nanolaser array with a constant w_{NS}, a design w_{NS} of 30 nm with a stable minimum w_{NS} was adopted, and alignment of the fabricated w_{NS} values was ensured by fabricating the nanolaser arrays with different dose times.

Change 2 was the use of a surface treatment to increase the success rate of EB lithography when the EB resist is directly coated onto the InP surface without any buffer layer or coating. A resist such as ZEP 520A generally has poor compatibility with water and the hydrophilicity of an InP substrate degrades the adhesion of the resist and substrate [2-8]. This poor adhesion reduces the chance of constructing a nanolaser. The following three surface treatments were used in the hope of improving the adhesion.

1. Tydrophobization using HCl etchant (4°C, HCl : water = 4 :1)
2. Oxidization of the InP surface by thermal annealing (180°C, 1 h) with organic washing
3. Oxidization of the InP surface by thermal annealing (180°C, 1 h) without organic washing

Treatment 1 is the same as that used in Refs [2-8], and consists most importantly of a brief soaking in a HCl etchant, resulting in hydrophobization of the substrate. This was performed by repeated short soaking in the HCl etchant until the contact angle with water was more than 90°. A low contact angle represents the hydrophilicity of a substrate and a

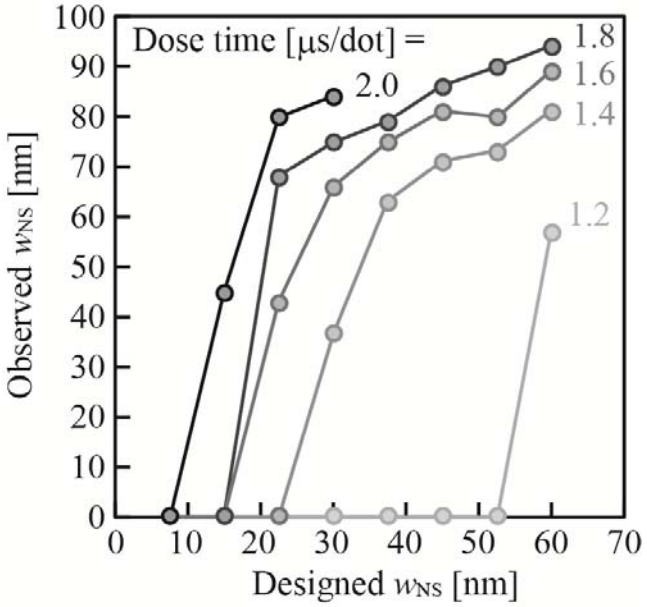

Fig. 2.4 Observed w_{NS} as a function of the designed w_{NS} for the various dose times.

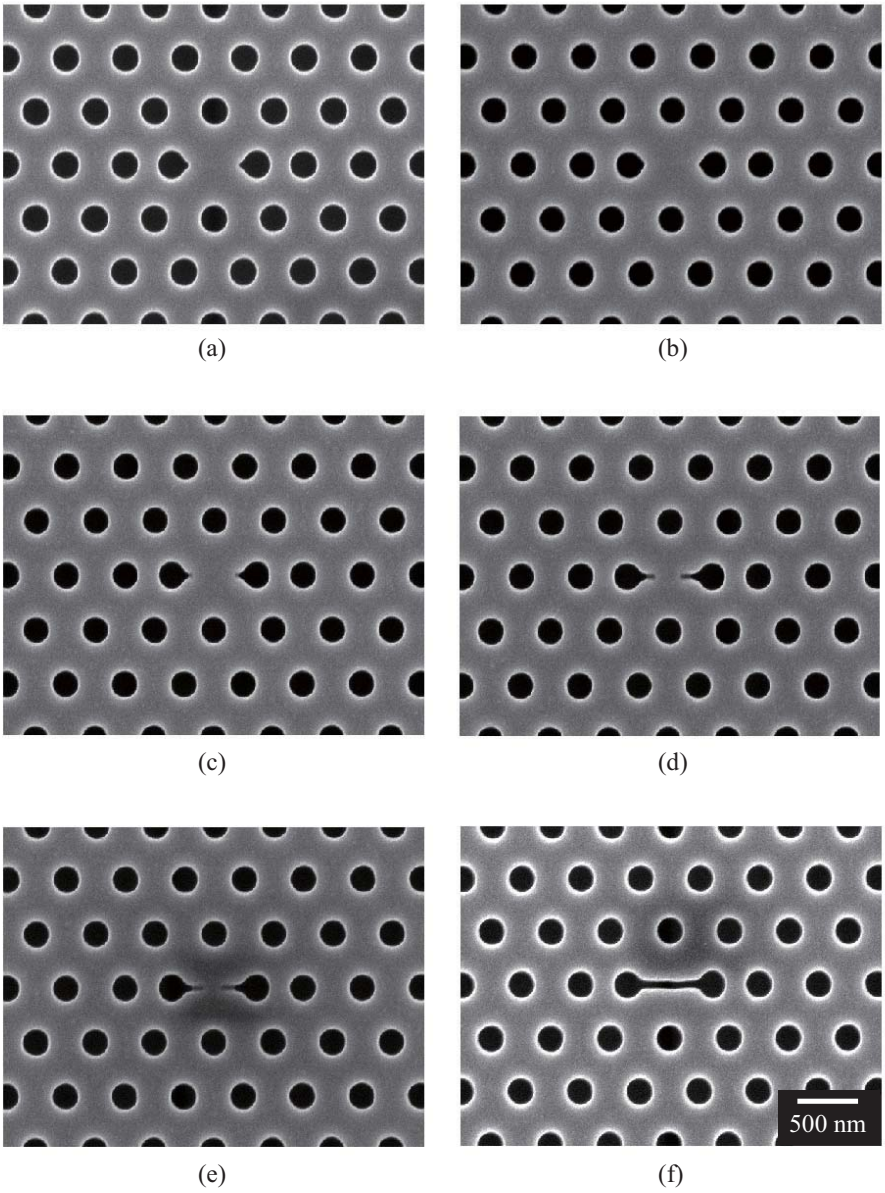

Fig. 2.5 SEM images of the NS nanolaser for different w_{NS} (basic structure) with the same dose time. (a) 22.5, (b) 30, (c) 37.5, (d) 45, (e) 52.5, and (f) 60 nm.

large contact angle shows the hydrophobicity (see Fig. 2.6). However, repeated HCl treatment etches the upper InP cladding layer and makes the thickness of the layer thinner than the expected thickness, or eliminates it entirely. This causes damage to the GaInAsP active layer and errors in the creation of the air holes following HI-ICP etching. Treatments 2 and 3 were used for SQW wafer 2. This wafer has p-type doping in the surface of an InP capping layer and decent adhesion against a resist even without

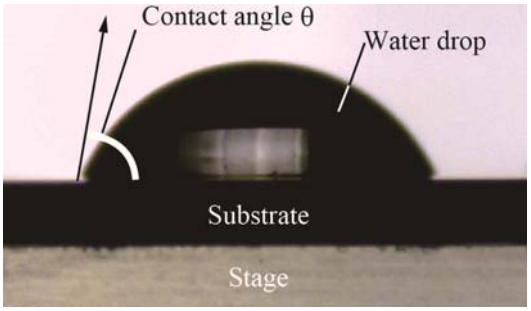

Fig. 2.6 A optical microscope image of the contact angle between a substrate and a water drop. The angle is related to the hydrophilic properties of the substrate.

Treatment 1. Furthermore, hydrophobization was achieved by the oxidization of thermal annealing. The difference between treatments 2 and 3 is an organic washing process after the annealing. This organic washing was performed to remove the oil spot, with the process taking place as follows:

1. The substrate was boiled in dichloromethane (CH_2Cl_2) (~120°C, 20 min).
2. The substrate was rinsed three times with acetone and methanol, respectively.
3. The substrate was boiled in methanol.
4. The substrate was dried using a blower and filament lamp.

Treatments 2 and 3 improved the resist adhesion thanks to the p-type doping and the annealing process. However, Treatment 2 often had poor adhesion due to the organic washing. Quick drying was required after washing to prevent the adherence of the dirt. Therefore, methanol boiling of the substrate, a blower, and a filament lamp were used. However, the drying process can go wrong, resulting in droplets of methanol forming on the substrate. The dirt agglutinated on the position of the droplets and degraded the adhesion of the resist. On the other hand, Treatment 3 resulted in good adhesion and was almost as successful as the following EB lithography. Due to the above results, Treatment 3 was adopted to produce a stable resist mask.

2. 4 **Measurement**

A nanolaser was photopumped at λ = 0.98 μm through a micro-photoluminescence (μ-PL) setup [2-10, 11] with a computer-controlled stage. The laser emission was coupled to an optical fiber and its wavelength was measured using an OSA. Fig. 2.7(a) shows a schematic of the μ-setup with a customized microscope system (Mitsutoyo, F870). A 0.98 μm high-power laser diode (LD) with multimode fiber output (IC-718, Opotopower Co.)

was used as the pumping source. It used a pulse-driven power supply, which was driven under the conditions: pulse width: 100, 200, 500, and 1000 ns; cycle time (repetition frequency): 100 (10), 200 (5), 500 (2), and 1000 (1) μs (kHz). The pumping was irradiated by a nanolaser (set on the sample stage with a diameter of ~25 μm) through a dichroic mirror, a half mirror, and a 50 × objective lens (Mitsutoyo Mplan NIR50). The emission radiation, including laser emission, spontaneous emission, and reflection emission from a nanolaser was collected by the same lens and split at the half mirror into an InGaAs near-infrared image sensor (Indigo, Alpha NIR) and an OSA (OSAs: Advantest, Q8383 (resolution limit: 100 pm) or Q8384 (10 pm)). The reflection of the pumping from a nanolaser was cut at the polished Si filters before coupling with an InGaAs image sensor or an OSA. A sample stage was connected to a Peltier temperature controller (Trio-Tech International, TC1000).

Real-time monitoring of the near-infrared image on the sample stage was performed using the InGaAs image sensor to ensure alignment of the pumping area and the focus. In this real-time monitoring, a pumping spot was simultaneously monitored with an idol spot created by reflection in the μ-setup and was identified by displacing the objective lens. Displacing the objective lens quenched the pumping spot and did not affect the idol spot. The pumping spot position was aligned by moving a sample stage or an objective lens. Sample stages were manually moved with the alignment of a micrometer. Objective lens positions were adjusted by computer. Optimization of the light axes was performed using the micrometer at the input and output sides for maximizing the power intensity measured by OSA.

The laser wavelength was detected by OSA and was analyzed by a computer though a GPIB cable. The spectra in the wide and narrow bands (wide band: bandwidth = 200 nm, center wavelength = 1.55 μm; narrow band: bandwidth = 5 nm, center wavelength = the laser wavelength at the wide band measurement) were continuously measured to improve the accuracy of the laser wavelength. In the batch measurement of nanolaser arrays, the wavelength of each device was automatically measured individually using apparatus control software (Lab VIEW, National Instruments Corporation) [2-12]. Each device was arranged in an array configuration (configurations: 5 × 5 or 5 × 6) at equal intervals. The coordinates of the objective lenses at three corners were obtained and used to decide the coordinates of each device. The alignment of the sample stage was not used to prevent displacement of the coordinates after the coordinates were obtained.

Figs. 2. 7(b) and (c) show the process of setting up a sample for sensing. The device was put on a slide glace, was covered with a cover glace, and was soaked in deionized water or index-matched liquid, which was injected through the gap between the slide

glace and cover glace. All the characteristics were measured at room temperature (~25°C) except for the temperature dependency, which was measured using the above temperature controller.

2. 5 Lasing characteristics

Fig. 2.8 shows the L−L characteristics for the above basic structure and the *Q*-optimized and asymmetric modified structure in water.The effective pump power P_{eff} is not clearly defined for an NS nanolaser and the effective P_{th} for an NS nanolaser has not been adequately investigated. Thus, we show the L–L characteristics for the P_{irr} on the horizontal axis. Fig. 2.8(a) shows that lasing occurs in both structures with thresholds of

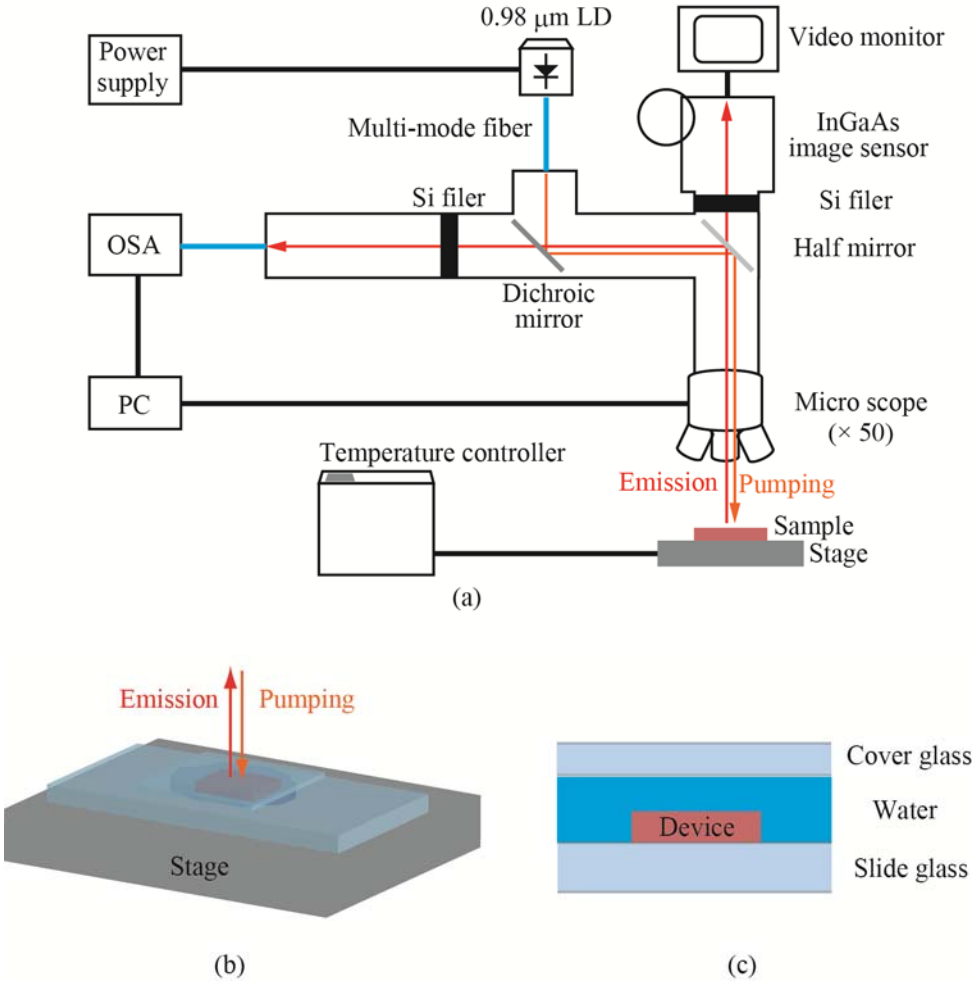

Fig. 2.7 (a) Schematic of a measurement setup for the μ-PL measurement, (b) typical configuration of a slide glass, a cover glass, and a device for biosensing in a water environment, and (c) an enlarged image of the configuration.

P_{th} = 7–10 mW and ~5 mW, respectively. The differences in the thresholds are due to the Q-factors, which are ~1400 and 23000 [2-8], respectively. Since the former structures have low Q-factors and high thresholds, the device was often not operated or was weakly operated due to fabrication errors. These structures are not suitable for the batch biosensing of many nanolasers. Furthermore, atomic layer deposition (ALD), which is a latter process (see Chapter 3) and is coated on a nanolaser for the stability of the wavelength, decreased the laser intensity (~ −15 dB). Due to this result, the former structure is impractical for batch measurements. On the other hand, the latter structure improved the coupling efficiency for the objective lens [2-9] and enabled measurement of the laser wavelength with low power pumping. Fig. 2.8(b) shows a typical single-mode spectrum with a peak intensity of 38 dB for the latter structure. It is easily operated by room-temperature photopumping with low power and is suitable for batch measurements.

2. 6 Liquid sensing

2. 6. 1 Evaluation of the refractive index sensitivity

To evaluate s_{env} of an NS nanolaser, the laser wavelengths were measured in various index-matching liquids (Cargille Labs, series AAA: range n_D = 1.3–1.395, adjustment ±

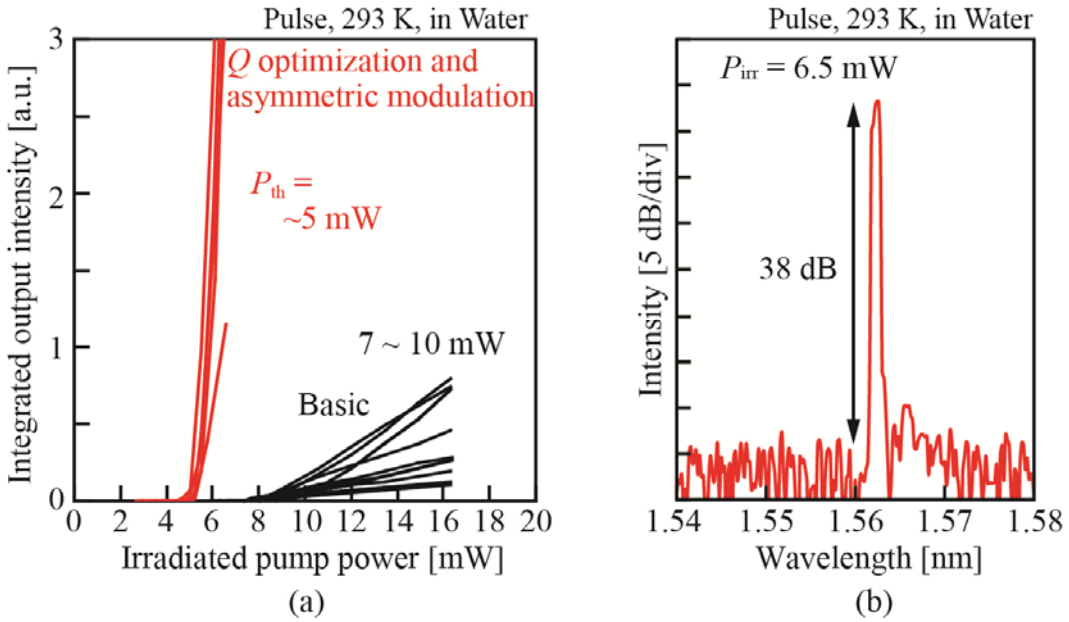

Fig. 2.8(a) Laser output versus pump light input (L-L) characteristics in water for the basic structure (black) and the Q-optimization and asymmetric modulated structure (red). (b) The typical laser spectrum of the latter structure.

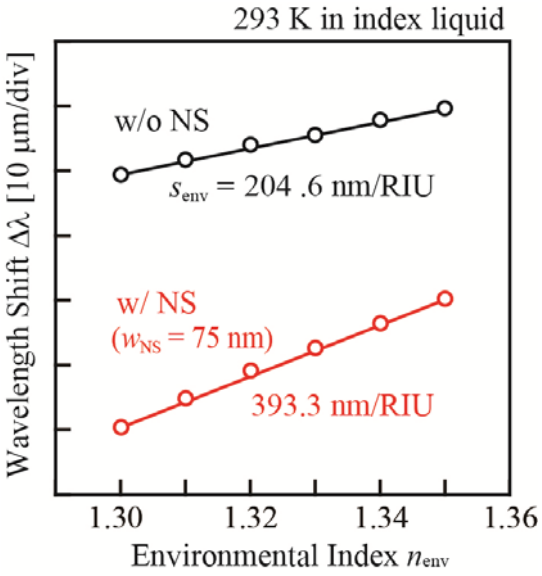

Fig. 2.9 n_{env} dependency of the laser wavelength Δλ. The back and red plots show Δλ with and without an NS, respectively.

0.0002) [2-13]. Fig. 2.9 shows a comparison between the typical s_{env} with and without a NS. We compared the same structure (the basic structure) with and without an NS and found that the s_{env} of the device with the NS is twice that of the one without. The higher s_{env} was caused by the increase in the evanescent field, which penetrates outwards from the PC slab, and the localization of the laser mode in an NS. A higher s_{env} of 350–410 nm/RIU was repeatedly obtained and is very high in the nano/micro-cavities while maintaining a high Q-factor [2-14], which has a trade-off with s_{env}. There is a tendency to increase s_{env} with increasing w_{NS} and this tendency indicates that it is not the localization of the laser mode in an NS but the evanescent field that dominates the bulk s_{env}. However, it is expected to increase the wavelength shift due to the adsorption of biomolecules by the localization, because the localization of the laser mode in an NS overlaps a several nm thick range of the adsorption of biomolecules.

2. 6. 2 **Evaluation of the dependency of temperature**

Fig. 2.10 shows a comparison of the laser spectra for a NS nanolaser. The spectra have λ_s of < 40 ps (and the device with an NS was measured using Q8384 due to the resolution limit of the OSA). This reduction of the thermal chirping is caused by the cancellation of the TO effects between the GaInAsP slab and water. When a nanolaser was operated in water by pulse pumping, the temperature of the GaInAsP slab fluctuated due to repeated heating by the pulse pumping. The fluctuation raised the variation of the equivalent

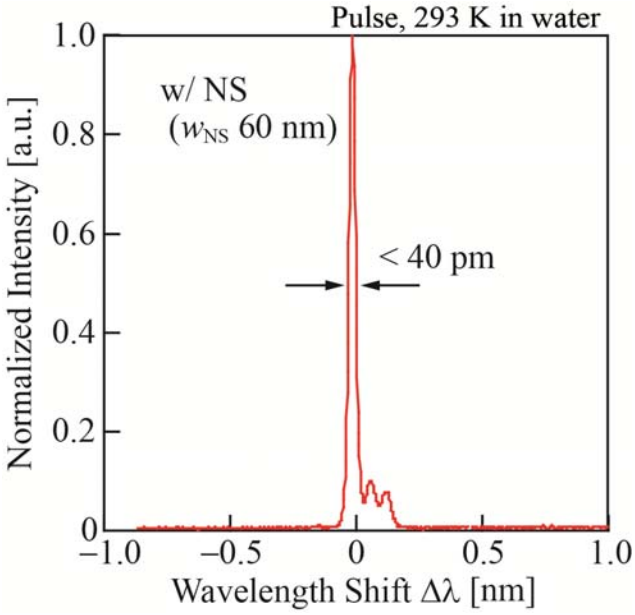

Fig. 2.10 Typical laser spectrum for a NS nanolaser.

refractive index n_{eq} due to the positive and negative TO effects of the slab and water, respectively. When a nanolaser was operated in air by pulse pumping, the repeated heating made the fluctuation of the temperature and n_{eq} bigger than those in water and broad λ_s values of > 10 nm was observed. With the laser operating in water, the fluctuation of the temperature was suppressed due to the heat capacity of water and the fluctuation of n_{eq} was suppressed due to the cancellation of the TO effects. The spectrum for the device without NS has often been λ_s of > 500 in water. Furthermore, the NS enhanced the cancellation due to the localization of the laser mode in a NS filled with water. In these results, we observed a minimum λ_s of < 40 ps for the device with an NS.

$\Delta\lambda$ dependency of the surrounding temperature with and without an NS was reported in Ref [2-8]. The $\Delta\lambda$ of both structures increased with temperature and the NS suppressed the variation. A saturation point of the increasing $\Delta\lambda$ was observed and this point is expected to be independent of fluctuations in temperature. Fig. 2.11 shows the laser spectra for the same device, whose SEM image is inserted, with various pumping pulses of 100 ns, 200 ns, 500 ns, and 1000 ns (and the other pumping source conditions were the same). We observed that full width at half maximum (FWHM) λ_s = 33–98 ps at the different pulse widths. The pumping pulse width increased with the time-averaged pumping power P_{ave} and it increased the heating fluctuations at the slab. This suggests that the narrowest λ_s can be obtained by controlling not only T but also the pumping conditions. Low power pumping suppresses the heating of the slab and the broadening of λ_s. However, low power pumping also decreases the lasing ratio (lasing/un-lasing) in the

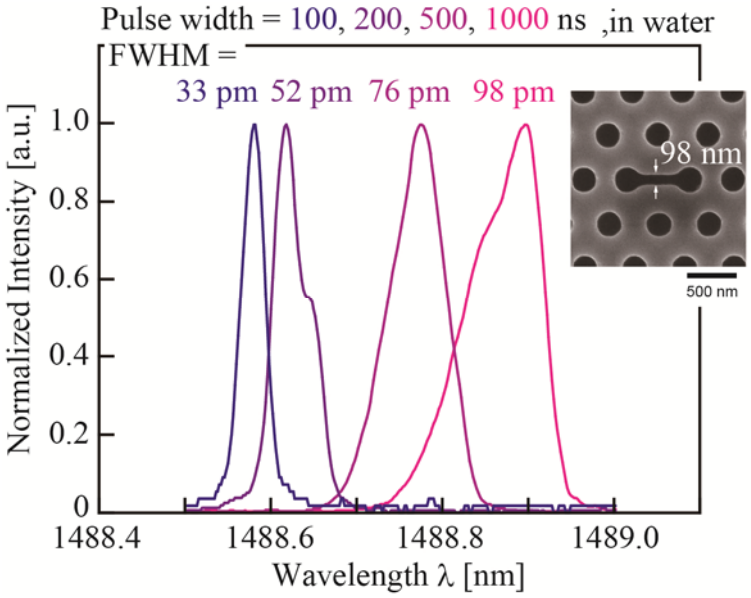

Fig. 2.11 Typical laser spectra for the various pumping pulses of 100 ns, 200 ns, 500 ns, and 1000 ns.

batch measurement of many devices due to fabrication errors. We therefore adopted pumping conditions for which P_{ave} is not extremely low (typical pumping conditions: Input current I_{in} = 600 to 800 mA; Pulse width = 500 ns; cycle time = 100 μs, P_{ave} = 40 to 60 μW).

Reference

[2-1] S. Kita, K. Nozaki, S. Hachuda, H. Watanabe, Y. Saito, S. Otsuka, T. Nakada, Y. Arita, and T. Baba, "Photonic crystal point-shift nanolaser with and without nanoslots --- design, fabrication, lasing and sensing characteristics," *IEEE J. Sel. Top. Quantum Electron.*, vol.17, 2011.

[2-2] V. R. Almeida, Q. Xu, C. A. Barrios and M. Lipson, "Guiding and confining light in void nanostructure," *Opt. Lett.*, vol. 29. pp. 1209−1211, 2004.

[2-3] T. B. Jones, M. Hochberg, C. Walker and A. Scherer, "High-Q optical resonators in silicon-on-insulator-based slot waveguides," *Appl. Phys. Lett.*, vol. 86, p. 081101, 2005.

[2-4] C. A. Barrios and M. Lipson, "Electrically driven silicon resonant light emitting device based on slot-waveguide," *Opt. Exp.*, vol. 13. pp. 10092−10101, 2005.

[2-5] S. Kita, S. Hachuda, K. Nozaki and T. Baba, "Nanoslot laser," *Appl. Phys. Lett.*, vol. 97, p. 161108 (2010).

[2-6] S. Kita, "Simple and high accuracy chemical/biosensing utilizing photonic crystal

nanolaser," Master's thesis *(Yokohama Nat'l Univ.)*, 2009.

[2-7] K. Nozaki, "Ultimately-Small Semiconductor Photonic Crystal Lasers and Spontaneous Emission Control," Doctoral thesis *(Yokohama Nat'l Univ.)*, 2007.

[2-8] S. Kita, "Photonic crystal nanolaser sensor," Doctoral thesis *(Yokohama Nat'l Univ.)*, 2012.

[2-9] M. Narimatsu, S. Kita, H. Abe, and T. baba, "Enhancement of vertical emission in photonic crystal nanolasers," *Appl. Phys. Lett.*, vol. 100, p. 121117, 2012.

[2-10] M. Lončar, A. Scherer, and Y. M. Qiu, "Photonic crystal laser sources for chemical detection," *Appl. Phys. Lett.*, vol. 82, no. 26, pp. 4648–4650, 2003.

[2-11]. T. W. Lu, P. T. Lin, K. U. Sio, and P. T. Lee, "Optical sensing of square lattice photonic crystal point-shifted nanocavity for protein adsorption detection," *Appl. Phys. Lett.*, vol. 96, no. 21, p. 213702, 2010.

[2-12] National Instruments homepage, "LabVIEW system design software," < http://www.ni.com/labview/# >

[2-13] "Cargille Labs – Refractive Index (matching) Liquids," <http://www.cargille.com/refractivestandards.shtml>.

[2-14] D. Yang, S. Kita, F. Liang, C. Wang, H. Tian, Y. Ji, M. Loncár, and Q. Quan, "High sensitivity and high *Q*-factor nanoslotted parallel quadrabeam photonic crystal cavity for real-time and label-free sensing," *Appl. Phys. Lett.*, vol. 105, p. 063118, 2014.

Chapter 3
Procedures and evaluations

3. 1 Overview

This chapter introduces the fundamental concepts of biosensing using a NS nanolaser and the procedures and evaluations involved in the biosensing process. In particular, the surface treatment process is discussed and the evaluation methods of the detection limit and the measurement errors using statistical analysis are presented.

3. 2 Concepts of biosensing

To detect biomarkers in a patient's blood, there are certain requirements. One is the selective detection of the biomarkers despite the high concentration of impurities. A PC nanolaser sensor detects the adsorption of the molecules on the sensor surface as the wavelength shifts. Causes of wavelength shifts include the specific binding of the target biomarkers and the non-specific binding of the impurities. The specific binding gives the sensing signals, but the non-specific binding gives the sensing noise. The noise of non-specific binding reduces the accuracy of the biosensing, which detects a low concentration of target biomarkers. Furthermore, there is noise due to the wavelength fluctuations of the individual nanolasers. The standard deviation of all the fluctuations for biosensing (σ) can be categorized as either temporal (σ_{time}) or spatial (σ_{space}) [3-1]. The sources of σ_{time} are derived from the target, the biointerface, the transducer, the environment, etc. Thermal and vibrational fluctuations of these sources give σ_{time}. Thermal fluctuations can be controlled through the athermal effect of the NS nanolaser and the controlled environment temperature. On the other hand, the vibrational fluctuations, which depend on the biointerface, are not controllable due to the difficulties involved in constructing a robust and uniform biointerface. Therefore, σ_{space}, which depends on parameters such as the adsorption state and the biointerface, is also not controllable. A biointerface is made through the linkage of a self-assembled monolayer (SAM) such as APTES. However, achieving high densities of APTES on a SiO_2 surface is challenging, and typically only 10–50% surface coverage can be expected [3-2]. The unstable and non-uniform biointerface enhances the fluctuations to create sensing noise

and reduces the biosensing accuracy.

The concepts behind biosensing aim to improve the detection accuracy using statistical analysis with many devices, and to compare the sensing signal with a negative control (see Fig. 3.1). It is easy to integrate over many nanolasers in an array configuration [3-3, 4] that is suitable for statistical analysis, and the measurement for all of the devices can be done automatically with the μ-PL setup in the computer-controlled sample stage [3-5]. Statistical analysis can overcome fluctuations of the adsorption state due to averaging the fluctuation over the adsorption and desorption of the impurities, and can suppress the estimated error range by using measurements from many devices. Furthermore, selective detection of the biomarker can be achieved from statistical differences between the sensing signal and the negative control. The negative control is a reference wavelength shift and is measured by the biointerface of the sensor, which is similar to that of the sensor for the sensing signal except for the immobilization of the host. Thus, the noise due to the non-specific binding can be estimated from the negative control.

In previous research, statistical analysis was used to reduce the blind window, which is the unresponsive area in the concentration of the biomolecule [3-1]. The size of the blind window was reduced through statistical analysis of the wavelength shifts with various NS widths, a parameter on which the blind window depends. In this thesis, statistical analysis was used to identify the wavelength shift from a negligible amount of biomarkers against the non-specific adsorption of the impurities and the fluctuations of the adsorption state.

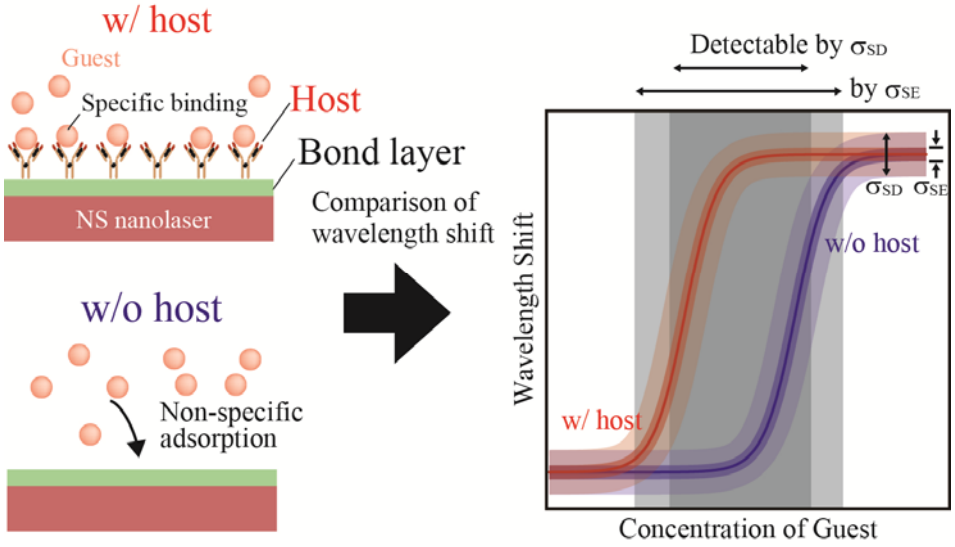

Fig. 3.1 Schematic concept of biosensing using a comparison of devices with and without a host.

3. 3 **Procedure**

As mentioned in Chapter 1, all biosensors use host–guest interactions to detect target molecules [3-6]. To achieve stable biosensing in water using nanolasers, two devices used for sensing and for negative control were prepared and the following five processes, as shown in Fig. 3.2, were performed:

1. A surface treatment was applied to stabilize the laser wavelength.
2. Hydrophilization was performed for uniform modification.
3. Silanization was used to introduce the functional group to the host.
4. Host functionalization was used to select the guest molecule (only for the sensing device).

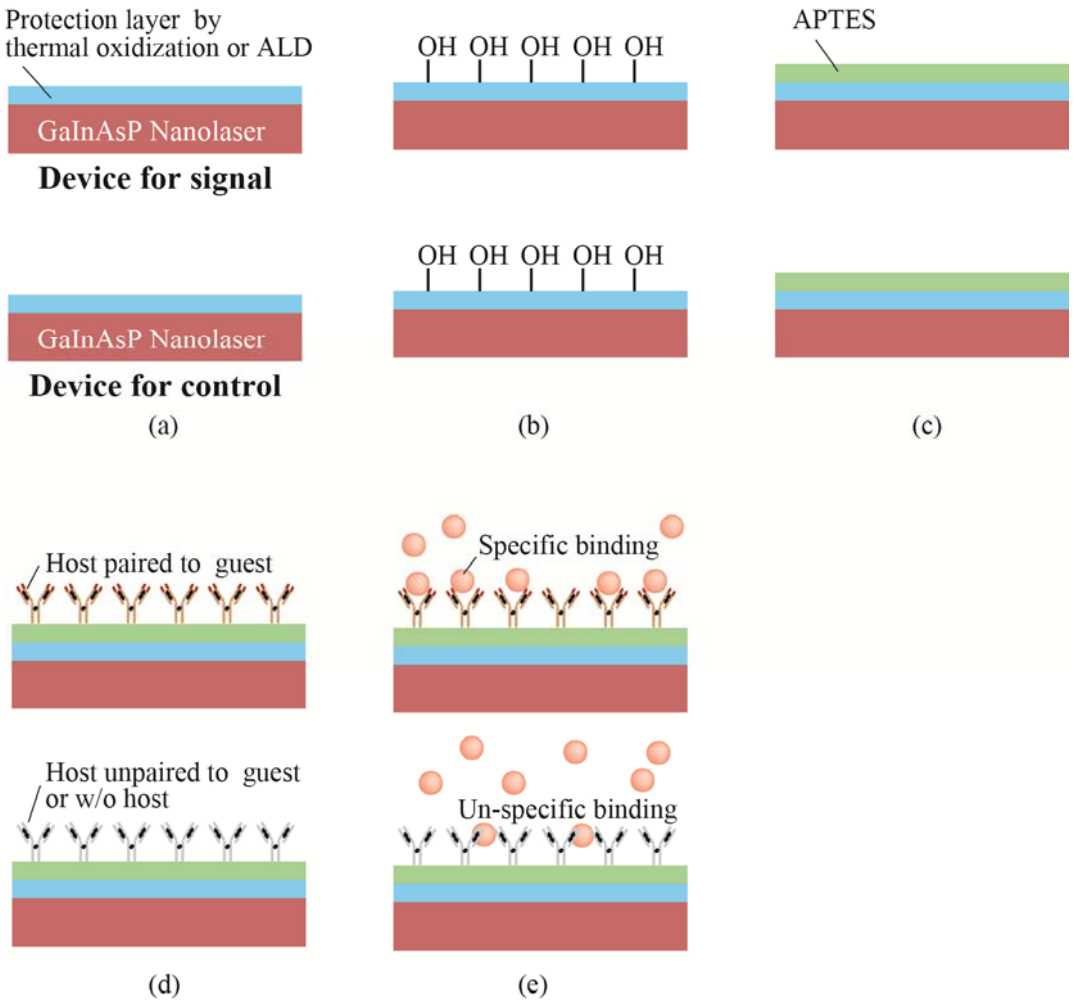

Fig. 3.2 Schematic of the biosensing procedure for signal and control using nanolasers. Each procedure is (a) surface treatment, (b) hydrophilization, (c) silanization, (d) host functionalization and (e) guest binding.

5. Guest binding was performed.

The first procedure was a surface treatment to stabilize the laser wavelength. The fluctuation of the spectrum during biosensing using a nanolaser appears due to various causes such as TO effects, thermal oxidization of GaInAsP due to the lasing, and etching of the surface due to biomolecules [3-7, 8] In particular, the thermal oxidization and etching are causes of consecutive blueshifts in biosensing. This blueshift negates the redshift (the sensing signal) for the adsorption of biomolecules and mar the sensitivity of a nanolaser. The surface treatment aims to suppress the consecutive blueshifts due to the oxidization or etching and to improve the stability against fluctuations. Thus, the surface treatment is a critical step for allowing stable biosensing using a nanolaser.

The second procedure is hydrophilization for uniform modification. As mentioned above, SAM is a necessary layer for further cross-linking. Silanization is a well-known method of SAM formation, and is suitable for a cross-link between organic materials and inorganic sensor surfaces such as semiconductors. Because the silanization process requires a hydroxyl group on the surface, it is necessary to hydrophilize the sensor surface for uniform and stable modification.

The third procedure is silanization, which is used to introduce the functional group for the host molecules. In biosensing, silanization is used to add the functional groups such as carboxy and amino to the sensor surface and to functionalize the host molecules. The cross-link of silanization is due to the dehydration condensation of hydroxyl groups; this functional group is used to immobilize host molecules through coupling, such as peptide binding.

The fourth procedure is host functionalization to select the guest molecule. This is a final treatment for the termination in the biointerface. As mentioned in Chapter 1, host molecules possess a highly complementary combining site structure to that of their guest molecules and give the selectivity of a nanolaser sensor to their guest molecules.

The final procedure is guest binding. The lasing wavelength shifts before and after the binding and it is detected by monitoring $\Delta\lambda$. The $\Delta\lambda$ values of the devices for sensing and the control are compared.

3. 3. 1 **Surface treatment to stabilize the laser wavelength**

The aim of surface treatment is to suppress the blueshift noise in biosensing. As mentioned above, a blueshift due to the thermal oxidization of the GaInAsP slab by the lasing of a nanolaser has been reported. A blueshift due to a chemical reaction, such as the etching and oxidization of the GaInAsP slab by the polymers with the carboxy group or amino group, was also reported. Etching and oxidization were also observed in

biosensing at the pH 7.4 PBS buffer, which is often used in biosensing. These decrease the wavelength due to the reduction of the equivalent refractive index n_{eq}. To suppress the blueshift in biosensing, the following three approaches were applied:

1. Advance thermal oxidization by lasing with strong pumping or baking.
2. Advance thermal oxidization by baking.
3. Application of a protective layer coating using ALD.

Fig. 3.3(a) shows typical real-time observation of Δλ and compares Δλ with and

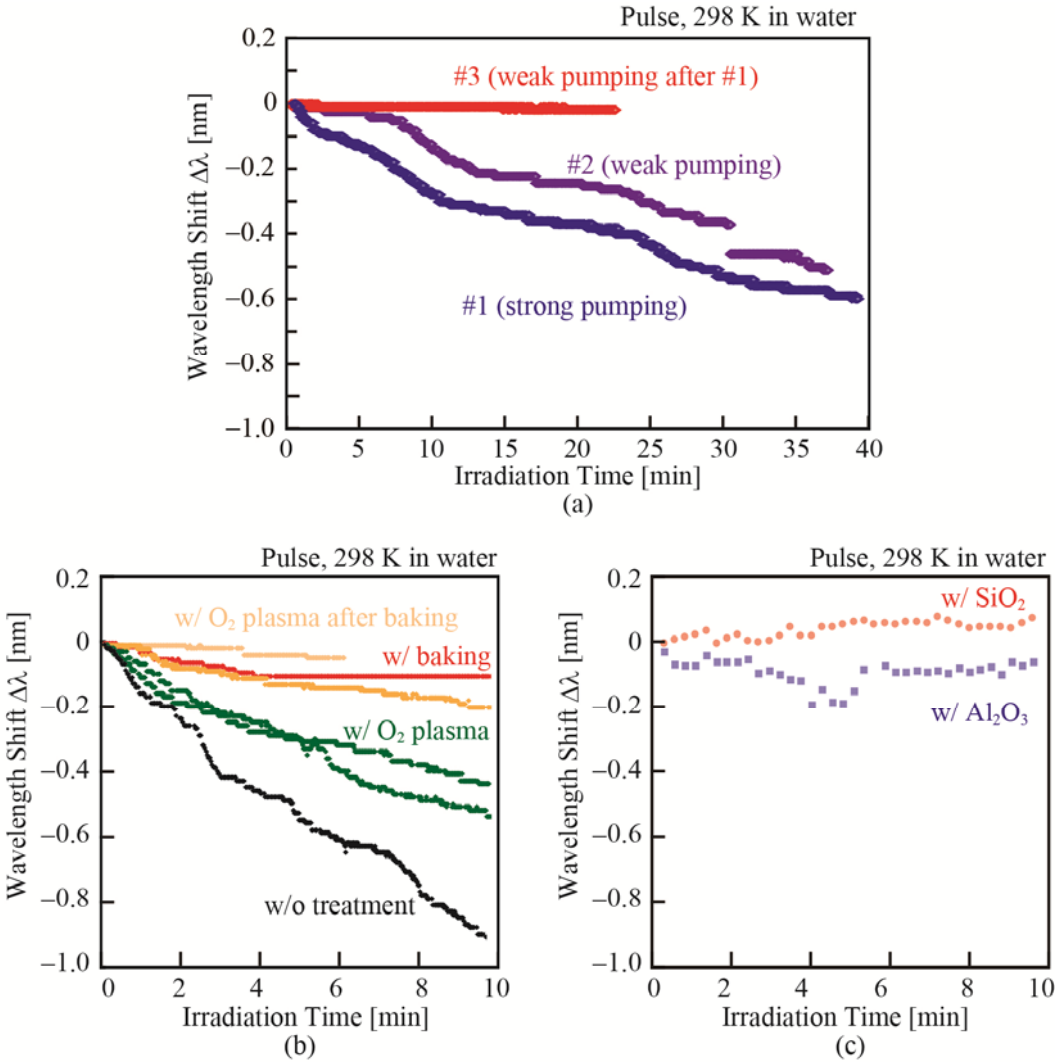

Fig. 3.3 Real-time observations of Δλ for various surface treatments. Comparison of (a) the irradiation power (strong pumping: Pave = 65 μW, weak pumping: Pave = 49 μW), (b) the advance treatment before the observation (Pave = 65 μW), and (c) the ALD protective layer (Pave = 65 μW).

without advance thermal oxidization by lasing with strong pumping. $\Delta\lambda$ was measured during strong Irradiation #1, during weak Irradiation #2, and during weak irradiation after strong Irradiation #3. The $\Delta\lambda$ of the device number #1, #2, and #3 shows the blueshift for 10 min of ~0.3, ~0.2, and <0.05 nm, respectively. The blueshift depends on the pumping power and tended to saturate. The weak irradiation after the oxidization of Irradiation #1 shows that it is possible to suppress the blueshift. Fig. 3.3(b) shows $\Delta\lambda$ measured for 10 min with and without advance oxidization by baking. This test also investigated the influence of O_2 plasma, which is a further process in biosensing. The blueshift of $\Delta\lambda$ after the baking was suppressed, in a similar way to that after oxidization by the irradiation with strong pump power. O_2 plasma also reduced the blueshift because the process caused oxidization. Thus, the suppression of thermal oxidization was maintained after the O_2 plasma process. Fig. 3.3(c) shows $\Delta\lambda$ for the devices with the ALD coating. The fluctuation of $\Delta\lambda$ in 10 min was less than 0.1 nm and the ALD coating also reduced the blueshift. These approaches enable suppression of the blueshift due to oxidization at the lasing stage with pumping. In biosensing, low irradiation has significant effects for reducing the local heating, which denatures the GaInAsP slab and/or the biomolecules.

Approach 1 has a low throughput for the measurement with many devices because this method requires individual advance oxidization due to the limit of the pump light's spot size, which covers only a single device (~25 μm^2). Approach 2 improves the throughput by batch oxidization. However, these thermal oxidization approaches cause problems as the blueshift is still observed in biomolecule sensing. As mentioned above, the carboxy group and/or the amino group of the polymer etch and oxidize the GaInAsP slab due to the weak stability of the chemical reactions. The biomolecules can etch and oxidize it the

(a) (b)

Fig. 3.4 Instruments for generating the O_2 plasma, (a) Samco ICP-10ip, (b) Sakigake YHS-R.

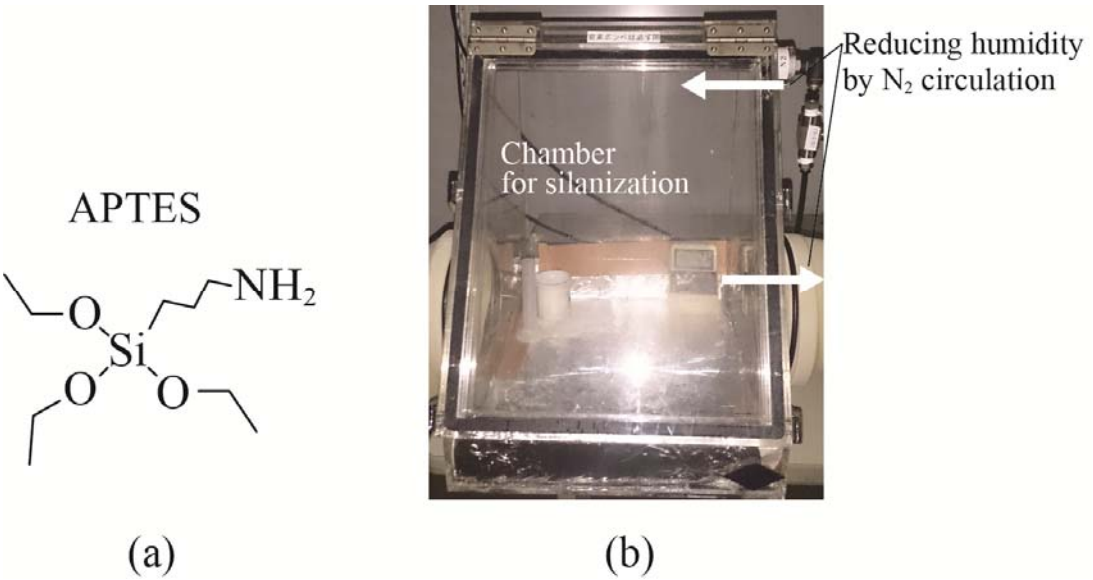

Fig. 3.5 (a) Structure of the APTES. (b) Reduction of humidity by N_2 circulation.

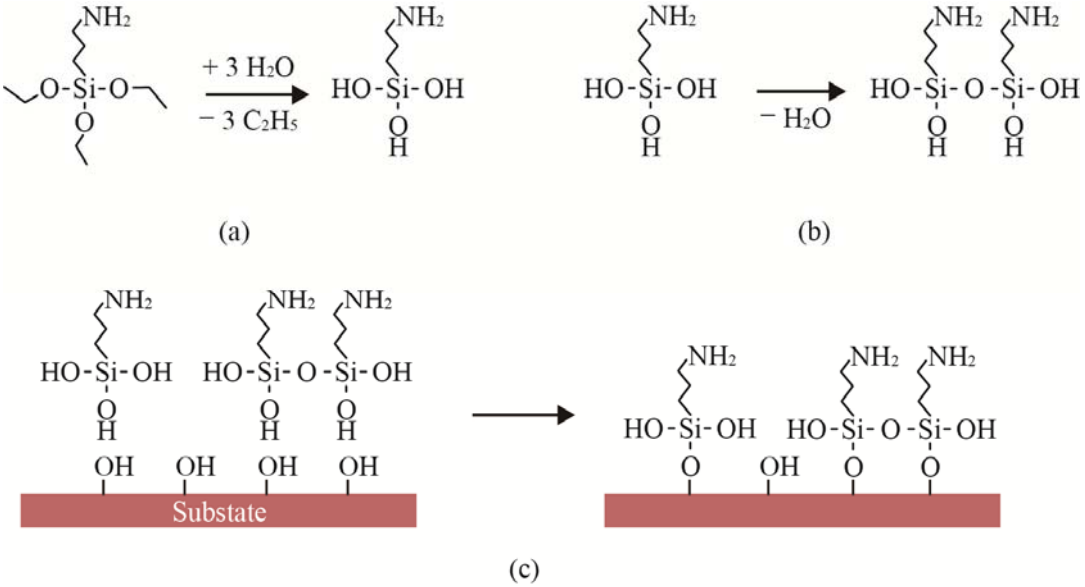

Fig. 3.6 Overview of the silanization process. (a) Hydrolysis of APTES, (b) polymerization of APTES due to dehydration, (c) immobilization of APTES to the sensor surface.

same manner. Approach 3 was found to overcome the stability for the chemical reactions because an ALD coated oxide film such as SiO_2 or ZrO_2 has sufficient resistance. The device with an ALD coating was used for biosensing and its usefulness was discussed

(see Chapter 6). For the reasons described above, Approach 3 is the most suitable for biosensing and for reducing the fluctuations of the oxidization and etching. A 3-nm ZrO_2 coating on the device was adopted as a final surface treatment.

3. 3. 2 Hydrophilization for uniform modification

Hydrophilization improves the homogeneity and stability of the procedure because silanization is enhanced on hydrophilic surfaces with the presence of a hydroxyl group and/or an O_2-functional group [3-9]. Various procedures have been reported for the oxidation of surfaces including O_2 plasma [3-9, 10, 11] and electrochemical techniques [3-12], ozone treatment [3-13, 14], etc. O_2 plasma was used for hydrophilization and was also used for surface cleaning [3-15, 16]. Organic washing of the substrate was performed before the O_2 plasma was applied. Table 3.xx lists the conditions of the O_2 plasma for Samco ICP-10ip or Sakigake YHS-R shown in Fig. 3.4. The contact angle of a GaInAsP substrate was typically ~50° and the O_2 plasma reduced the angle to less than 10° even if the process time was 10 s. So a process time of 10 s was found to be sufficient for hydrophilization. Excess irradiation should be avoided to prevent the surface of a sensor chip being physically etched, and the chip should not be set in the center of the chamber for the same reason.

3. 3. 3 Silanization to introduce the functional group to the host

A silanization reaction was performed using 3-aminopropyltriethoxysilane (APTES) in a dry environment shown as Fig. 3.5. Fig. 3.6 shows an overview of the silanization process of APTES to the sensor surface, and the procedure can be summarized as follows:

1. The sensor chip was immersed in toluene after hydrophilization.
2. The chip was boiled in toluene (130°C, 5 min).
3. 0.0005– 0.5% dehydrated APTES solution was mixed with dehydrated toluene in a dry environment using a glove box (humidity of < 20%) for 8 min. 0.05% APTES solution was generally used for the following sensing results.
4. The chip was immersed in the above APTES solution for 5 min.
5. The chip was rinsed three times with toluene, acetone, methanol, and deionized water.

This procedure is almost the same as that detailed in Ref. [3-1], except for the APTES concentration. Methyl groups including APTES convert hydroxyl groups due to the hydrolysis and then the APTES couple with each other or the sensor surface by the dehydration condensation of the hydroxyl groups. This overview has been simplified significantly and the silanization reaction is actually more complex due to physical

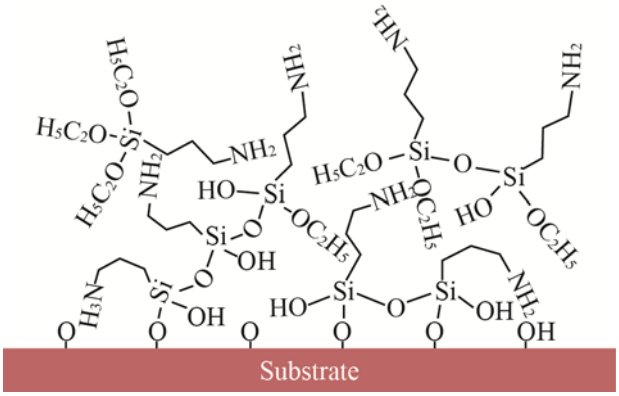

Fig. 3.7 Estimated actual surface functionalized APTES in toluene.

adsorption, hydrogen bonds, and the complex cross-link of APTES [3-17, 18] (see Fig. 3.7). After the silanization reaction, the contact angle, which reflects the hydrophilicity of the surface, was confirmed for the sake of uniform functionalization. Fig. 3.8 summarizes the measured contact angles as a function of the APTES concentration and shows the reported dependency of the APTES thickness on the contact angle [3-17]. The measured contact angle was increased to a contact angle of 30–50° with increasing APTES concentrations. When the APTES thickness was 10 Å (monolayer thickness = 7–9 Å), the contact angle was already saturated due to the lack of the hydroxyl group and the monolayer showed an angle of ~50° [3-17]. The fluctuation of the measured contact angles was large and one of the causes of this was determined to be the physical absorption of APTES, which has hydroxyl groups due to the lack of ultrasonic washing. Assuming that the saturated angle showed the adsorption of one or more layers, the silanization in the conventional concentration of 0.5% APTES could possess instability due to the multi-layer adsorption. The instability of APTES is investigated in Chapter 6.

3. 3. 4 **Host functionalization to select the guest molecule**

Biomolecules such as the DNA, aptamer, biotin, and antibodies are widely used as hosts. In this thesis, biotin and antibodies, which have selectivity for the SA and the corresponding antigen, respectively, were used as the host molecules. On the other hand, the control device was used without host molecules or with molecules un-paired to the guest.

Glutaraldehyde (GA) was used for non-specific detection. GA is a molecule with two aldehyde groups. Protein is immobilized on the sensor surface through the coupling of an amino group and an aldehyde group. Immobilization of the host or GA was used for the

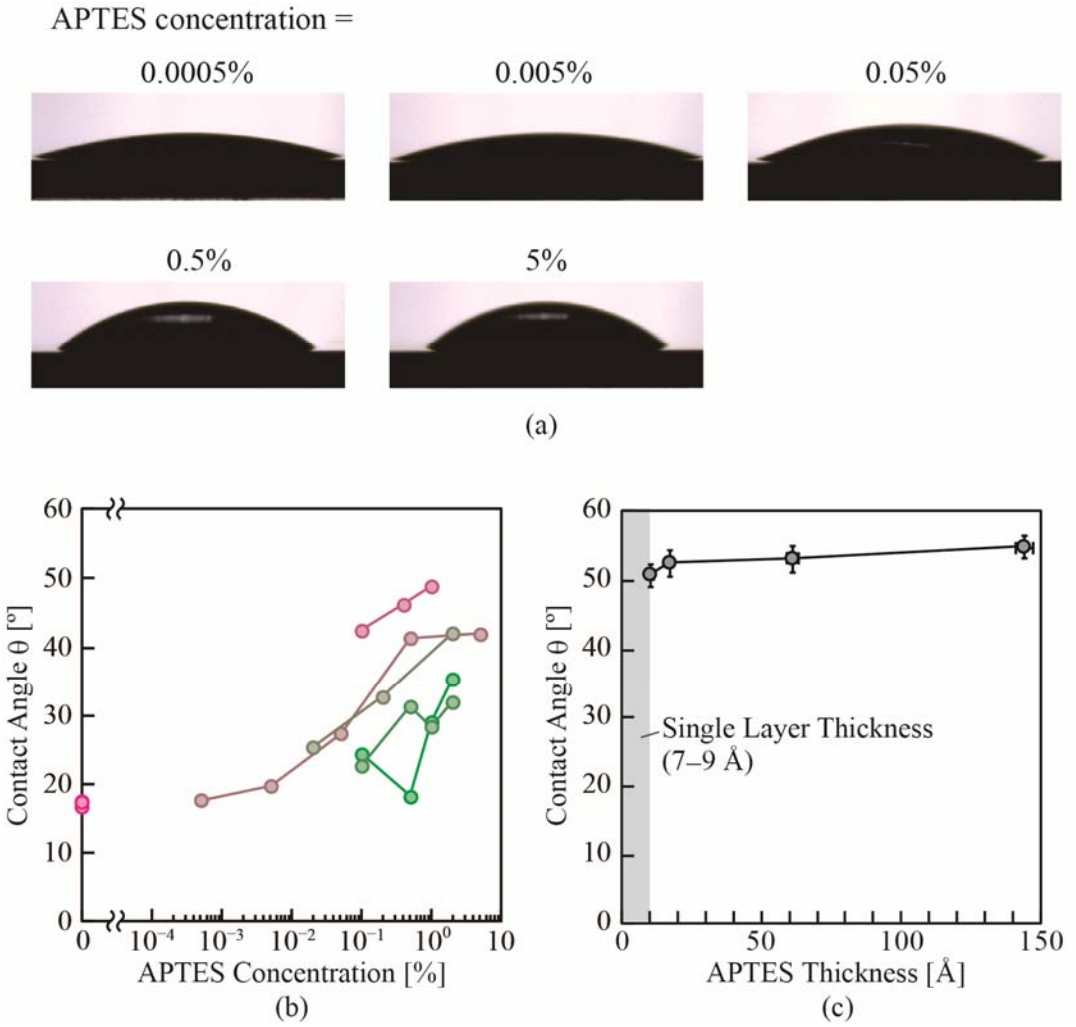

Fig. 3.8 (a) Optical microscope images of 5 μl water drop on GaInAsP with 3 nm ZrO_2 after each concentration of APTES was functionalized. (b) The concentration of the APTES dependency on θ. Each color in the plot shows a different trial. (c) θ as a function of APTES thickness.

immobilization of the host and the detection of BSA.

3. 4 **Evaluation**

The selective detection and DL were estimated with the following two approaches. First, the DL was estimated using Langmuir fitting. The laser wavelength shift Δλ and the DL of concentration for biosensing were respectively given by [3-19, 20]:

$$\Delta\lambda = \frac{\Delta\lambda_{\max} K_A C}{1 + K_A C} \tag{3-1}$$

$$\mathrm{DL} = \left(\frac{\Delta\lambda_{\min}}{\Delta\lambda_{\max} - \Delta\lambda_{\min}} \right) \tag{3-2}$$

where $\Delta\lambda_{max}$ is the wavelength shift after saturated adsorption of the biomolecule, $\Delta\lambda_{min}$ is the minimum resolvable shift, K_A is the affinity constant for host-guest interaction, and C is molar concentration of the solution with the guest. $\Delta\lambda_{min}$ is limited by the spectral noise caused by fluctuations in the device temperature and the OSA performance. Thus, $\Delta\lambda_{min}$ was evaluated as a spectral line of width λ_s. $\Delta\lambda_{max}$ is also limited by the sensitivity to the adsorption of the biomolecule. In this approach, the performance of the nanolaser was evaluated from DL.

Second, the selective detection was evaluated by statistical analysis. According to the error theory, the observed value consists of the true value and the measurement error. The true value of $\Delta\lambda$ was estimated from the average $\Delta\lambda$ of the multimeasurement and the measurement error was estimated from the standard deviation σ_{SD} and the standard error σ_{SE}. Taking the average value of the measurement from many devices can offset the fluctuations of the adsorption state due to the averaging of the fluctuation with both adsorption and desorption of the impurities. The measurement error depends on the uniformity of the biointerface, which is the host molecule layer on each nanolaser surface, because $\Delta\lambda$ gives the adsorption of the guest to the host. Considering the surface coverage θ_{host} of the host molecule, Eq. (3-1) can be expressed as:

$$\Delta\lambda = \frac{\Delta\lambda_{\max 1} K_{A1} C \theta_{host}}{1 + K_{A1} C} - \frac{\Delta\lambda_{\max 2} K_{A2} C (1 - \theta_{host})}{1 + K_{A2} C} \tag{3-3}$$

where the first term denotes the wavelength shift for specific adsorption on the surface with host molecules, and the second term denotes the same for non-specific adsorption on the surface without host molecules. Fig. 3.9 shows the concentration dependency of the wavelength shift for various values of θ_{host} and for $K_{A1} = 10^8$ $M^{-1}$and $K_{A2} = 10^5$ M^{-1} although the concentration range where $\Delta\lambda$ increases was different from that of the PSA ($K_A = 10^8$–10^9) sensing using NS nanolaser. It is considered that this different is due to the enhancement of the sensitivity by NS which was reported as > 10^4 [3-1, 5]. Futhermre, Reducing θ_{host} decreases $\Delta\lambda$ for the specific adsorption, and the fluctuation of θ_{host} for each nanolaser surface causes a measurement error in the multi-measurement. As per the above description for identifying the selective detection, a redshift within the region of the measurement error of the devices for the signal or control cannot be identified as a detection. The selective detection of the biomarker was identified by taking the statistical difference between the sensing signal and the negative control. To improve sensitivity and accuracy, the degree of the measurement error was estimated from σ_{SD}, and the accuracy of the average value was evaluated from σ_{SE}. When the distribution

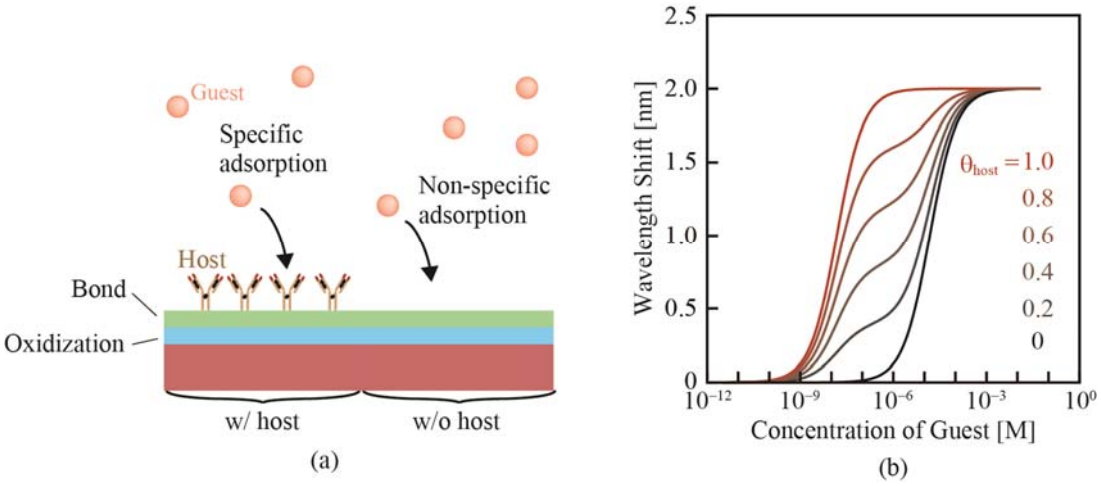

Fig. 3.9 Description of the effect of θ_{host}. (a) Biosensing model for plaque immobilization of the host molecule (θ_{host} = 0.5). (b) Wavelength shift $\Delta\lambda$ as a function of guest molecule concentration wchich was calculated from Eq. (3-3) for different values of θ_{host}, $K_{A1} = 10^8$ M^{-1}, $K_{A2} = 10^5$ M^{-1}, λ_{max1} = 2 nm and λ_{max2} = 2 nm.

follows a normal distribution, the average value $\pm 2\sigma_{SE}$ ($\pm 3\sigma_{SE}$) represents a probability of 95% (99%) that the true value will be within that range. More measurements with the devices reduces σ_{SE} and makes the average value more accurate because SE is inversely proportional to the square root of the number of measurements. Furthermore, statistical differences between the wavelength shifts for the signal and control were determined using *t*-test. *t* is a probability distribution that is closely related to the standard normal distribution. The *p*-value probability, where wavelength shifts for the signal and control become equal by chance, can be obtained from the *t*-test. As described above, the difference in the wavelength shift between the signal and control was evaluated using σ_{SD}, σ_{SE}, and the *t*-test, and the detection of the guest was determined from the difference.

Reference

[3-1] S. Kita, "Photonic crystal nanolaser sensor," Doctoral thesis (*Yokohama Nat'l Univ.*), 2012.

[3-2] P. G. Fernandes, H. J. Stiegler, M. Zhao, K. D. Cantley, B. Obradovic, R. A. Chapman, H. C. Wen, G. Mahmud, and E. M. Vogel, "SPICE macromodel of silicon-on-insulator-field-effect-transistor-based biological sensors," *Sensors Actuators, B Chem.*, vol. 161, no. 1, pp. 163–170, 2012.

[3-3] H. Abe, M. Narimatsu, T. Watanabe, T. Furumoto, Y. Yokouchi, Y. Nishijima, S. Kita, A. Tomitaka, S. Ota, Y. Takemura and T. Baba, "Living-cell imaging using

a photonic crystal nanolaser array," *Opt. Express*, vol. 23, no. 13, pp. 17056–17066, 2015.

[3-4] T. Watanabe, H. Abe, Y. Nishijima and T. Baba, "Array integration of thousands of photonic crystal nanolasers," *Appl. Phys. Lett.*, vol. 104, no. 12, pp. 121108, 2014.

[3-5] S. Hachuda, S. Otsuka, S. Kita, T. Isono, M. Narimatsu, K. Watanabe, Y. Goshima and T. Baba, "Selective detection of sub-atto-molar streptavidin in 10^{13}-fold impure sample using photonic crystal nanolaser sensors," *Opt. Express*, vol. 21, no. 10, pp. 12815–12821, 2013.

[3-6] P. N. Prasad, "Introduction to biophotonics," *Wiley-Interscience*, Apr 2003.

[3-7] K. Watanabe, S. Hachuda, T. Isono, and T. Baba, "Photonic crystal nanolaser sensors with ALD coating," *Conference on Lasers and Electro Optics-Pacific Rim and OptoElectronics and Communications Conference/Photonics in Switching (CLEO-PR & OECC/PS)*, Kyoto, no. TuJ2–2, 2013.

[3-8] K. Watanabe, Y. Kishi, S. Hachuda, T. Watanabe, M. Sakemoto, Y. Nishijima and T. Baba, "Simultaneous detection of refractive index and surface charges in nanolaser biosensors," *Appl. Phys. Lett.*, vol. 106, no. 2, pp. 021106, 2015.

[3-9] M. Yoshinari, T. Hayakawa, K. Matsuzaka, T. Inoue, Y. Oda, M. Shimono, T. Ide and T. Tanaka, "Oxygen plasma surface modification enhances immobilization of simvastatin acid," *Biomed. Res.*, vol. 27, no. 1, pp. 29–36, 2006.

[3-10] T. Suni, K. Henttinen, I. Suni and J. Mäkinen, "Effects of plasma activation on hydrophilic bonding of Si and SiO_2," *J. Elechem. Soc.*, vol. 149, no. 6, pp. G348–G351, 2002.

[3-11] S. Szunerits and R. Boukherroub, "Different strategies for functionalization of diamond surfaces," *J. Solid State Electrochem.*, vol. 12, no. 10, pp. 1205–1218, 2008.

[3-12] D. Delabouglise, B. Marcus, M. Mermoux, P. Bouvier, J. Chane-Tune, J.-P. Petit, P. Mailley, T. Livache, "Biotin grafting on boron-doped diamond," *Chem. Commum. (Camb).*, vol. 1, no. 21, pp. 2698–2699, 2003.

[3-13] H. Valdés, M. Sánchez-Polo, J. Rivera-Utrilla and C. A. Zaror, "Effect of ozone treatment on surface properties of activated carbon," *Langmuir*, vol. 18, pp. 2111–2116, 2002.

[3-14] E. Najafi, J.-Y. Kim, S.-H. Han, and K. Shin, "UV-ozone treatment of multi-walled carbon nanotubes for enhanced organic solvent dispersion," *Colloids Surfaces A Physicochem. Eng. Asp.*, vol. 284–285, pp. 373–378, 2006.

[3-15] R. Takei, K. Yoshida and T. Mizumoto, "Effects of wafer precleaning and

plasma irradiation to wafer surfaces on plasma-assisted surface-activated direct bonding," *Jpn. J. Appl. Phys.,* vol. 49, p. 086204, 2010.

[3-16] H.W. Kim, W.S. Hwang, C. Lee, R. Reif, "Plasma cleaning of carbon species for silicon homoepitaxial growth," *J. Mater. Sci. Lett.*, vol. 22, pp. 1067–1068, 2003.

[3-17] J. Kim, P. Seidler, L. S. Wan, and C. Fill, "Formation, structure, and reactivity of amino-terminated organic films on silicon substrates," *J. Colloid Interface Sci.*, vol. 329, no. 1, pp. 114–119, 2009.

[3-18] J. Kim, G. J. Holinga, and G. A. Somorjai, "Curing induced structural reorganization and enhanced reactivity of amino-terminated organic thin films on solid substrates: Observations of two types of chemically and structurally unique amino groups on the surface," *Langmuir*, vol. 27, no. 9, pp. 5171–5175, 2011.

[3-19] S. Zlatanovic, L. W. Mirkarimi, M. M. Sigalas, M. A. Bynum, E. Chow, K. M. Robotti, G.W. Burr, S. Esener, and A. Grot, "Photonic crystal microcavity sensor for ultracompact monitoring of reaction kinetics and protein concentration," *Sens. Act. B Chem.*, vol. 141, pp. 13–19, 2009.

[3-20] S. Kita, S. Otsuka, S. Hachuda, T. Endo, Y. Imai, Y. Nishijima, H. Misawa and T. Baba, "Super-sensitivity in label-free protein sensing using nanoslot nanolaser," *Opt. Express*, vol. 19, no. 18, pp. 17683–17690, 2011.N. A. C. Cressie and H. J. Whitford, "How to use the two sampe *t*-test," *Biometrical J.*, vol. 28, no. 2, pp. 131–148, 1986.

Chapter 4
Sensing of model proteins

4. 1 Overview

This chapter demonstrates the sensing of the non-specific adsorption of BSA on a sensor surface with GA as well as the sensing of the specific adsorption of BSA through an antibody–antigen reaction using an anti-BSA antibody. In the process of sensing the non-specific adsorption, the dynamic range of the BSA concentration was evaluated and an improvement in the sensitivity of the coated protection layer after the deposition of the atomic layer was confirmed. To sense the specific adsorption, two sensing methods were used. By comparing the $\Delta\lambda$ values of both methods, the detection of the specific adsorption was confirmed.

4. 2 Sensing of non-specific adsorption

For this section, BSA [4-1] adsorption through GA [4-2] was sensed using the protein sensing model of non-specific adsorption with ananolaser (hereafter NS). BSA has often been investigated as a model protein for biosensing, because it is an abundant protein in serum and is easily purified. BSA has therefore been adopted as a model protein for the sensing of non-specific adsorption. Fig. 4.1(a) shows the sensing model. BSA is adsorbed on the sensor surface through GA, which is capable of coupling to an amino group on the sensor surface. As mentioned in Chapter 3, GA is a molecule with two aldehyde groups and protein absorbs on the sensor surface through the coupling of an amino group and an aldehyde group. $\Delta\lambda$ after immersion in 10-μM BSA was first measured for checking the BSA absorption. The sensing procedure was performed as follows:

1. The sensor chip was prepared with an APTES treatment, as shown in Chapter 3. However, to ensure stable detection, a surface treatment involving the thermal oxidization of the lasing nanolaser by strong pumping was adopted.
2. The chip was immersed in a 2.5% GA solution diluted with pure water at room temperature for 1 h.
3. The laser wavelength was measured in pure water after the rinse.

4. The chip was immersed in 10-μM BSA for 30 mins.
5. The laser wavelength was measured in pure water after the rinse and Δλ was then evaluated.

Fig. 4.1(b) shows the laser spectra before and after the immersion in 10-μM BSA. The laser spectrum was redshifted after the adsorption of BSA owing to an increase in the refractive index. The BSA was thus detected by the wavelength shift Δλ. If a nanolaser sensor shows a certain shift after immersion in a particular concentration of a biomarker, the concentration of the biomarker solution can be evaluated using Δλ.

For the evaluation of the sensitivity of the NS, BSA sensing in the dynamic range was performed. The sensing procedure was roughly the same as that above except for steps 1 and 4. Devices that had undergone a variety of surface treatments, such as laser pumping, thermal oxidization using an oven, and coating with a thin protection layer by ALD, were prepared. The sensor chip was immersed in a set of BSA solutions with low concentrations of BSA, and the immersion was repeated after the measurement of the wavelength Δλ. Fig. 4.2 shows the wavelength spectra after the adsorption of each concentration of BSA for the device that underwent advanced laser pumping oxidization. Although Δλ was blueshifted for low concentrations of BSA owing to oxidization or etching, as outlined in Chapter 3, it was redshifted from 1-nM BSA upwards. In previous work from our laboratory [4-3], the BSA dependency showed shift_L and shift_H owing to the difference between the inside and outside of the NS. However, the shift_L was suppressed because of blueshift noise in this sensing. It was therefore necessary to suppress the blueshift noise.

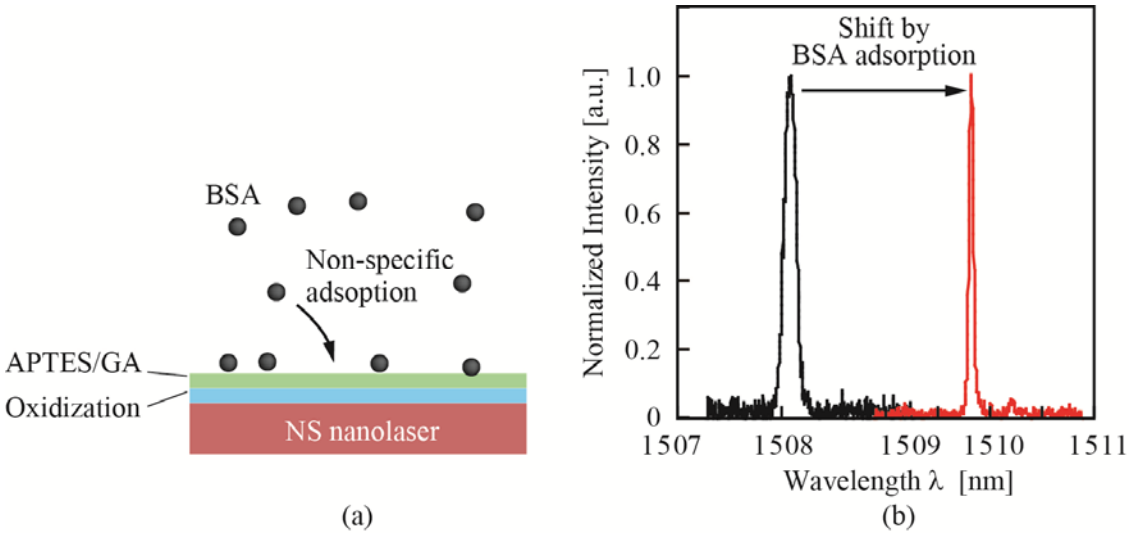

Fig. 4.1 (a) BSA sensing model through binding with GA. (b) Laser wavelength before and after 10 μM BSA adsorption. The blue and red lines show the wavelengths before and after the BSA treatment, respectively.

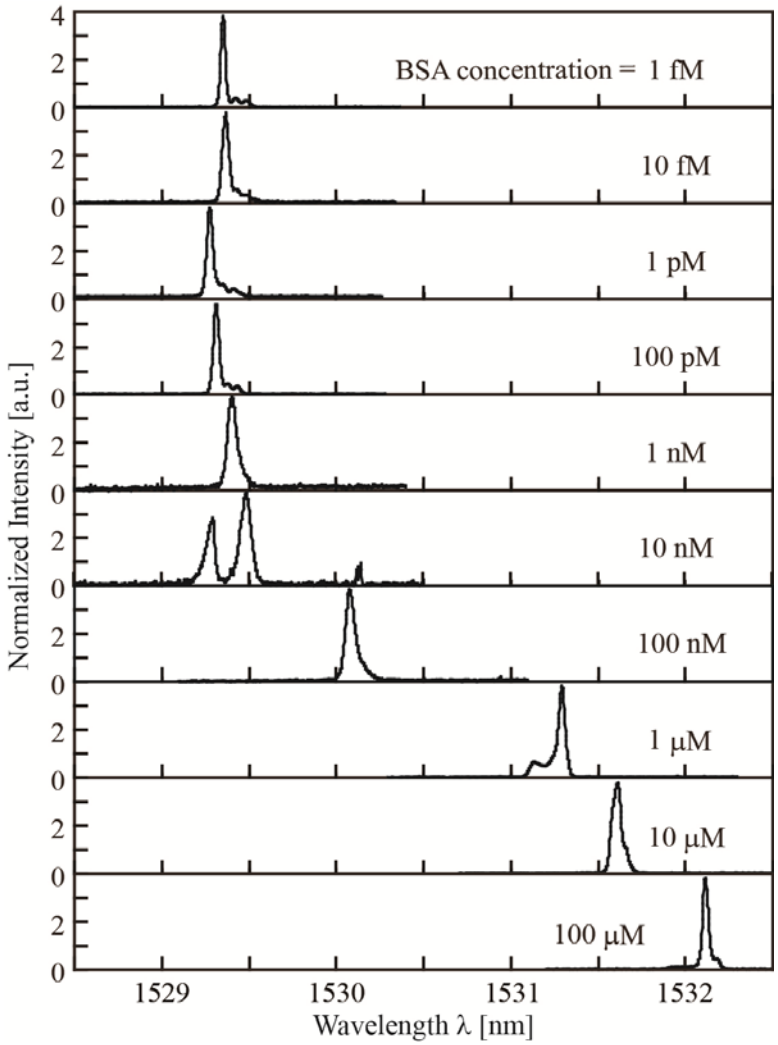

Fig. 4.2 Wavelength spectrum after the adsorption of each concentration of BSA.

Figure 4.3 shows $\Delta\lambda$ as a function of BSA concentration for comparison between the different surface treatments and Table1 shows the parameter of Langmiur fitting. $\Delta\lambda$, plotted with an orange color, was measured by S. Kita using an average value over many devices. As mentioned above, the shift_L and shift_H were observed for low and high concentrations, respectively. S. Kita proposed that the two-step shift originates from the saturated sensitivity inside the NS, which has a higher sensitivity than outside [4-3–5]. The detection limit of 255 fM BSA was evaluated with the NS, and the sensitivity was 1000 times greater than the general surface plasmon resonance sensor. However, the device that underwent surface treatment with an oven often showed blueshift noise because of the non-uniformity of the oxidization between the devices and the weak stability of the oxide of GaInAsP against etching. As mentioned in Chapter 3, a charged

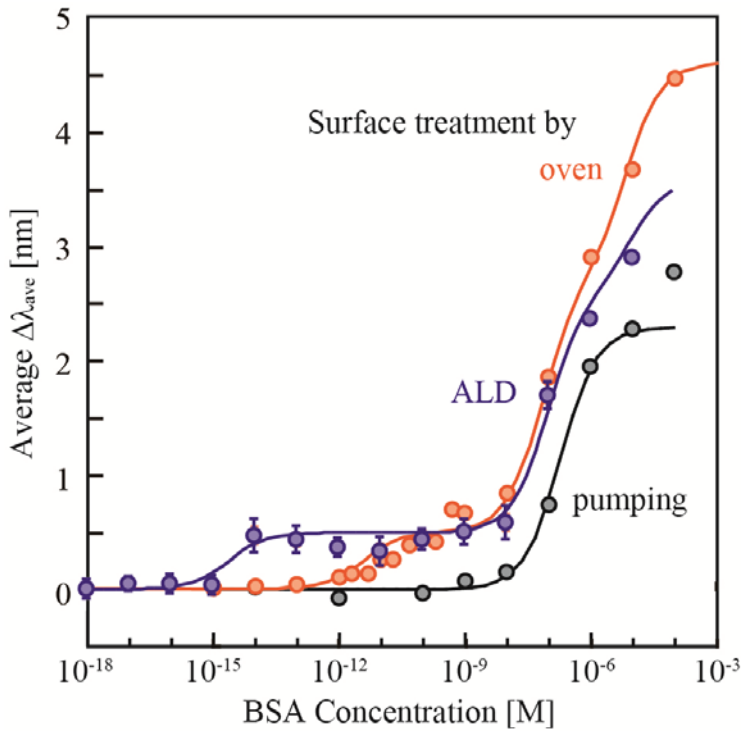

Fig. 4.3 (a) Sensing model of BSA using an NS nanolaser with HfO_2 as a thin protection layer. (b) Comparison of $\Delta\lambda$ with and without the HfO_2 coat. Solid lines were drawn from the Langmuir fitting assuming the linear combination of three different adsorption terms: two chemisorptions (inside and outside of NS) and one physisorption [4-3]. The fitting parameters were shown in Table 4.1.

polymer oxidizes and etches the surface and the etching cannot be suppressed enough by thermal oxidization. The red plot shows $\Delta\lambda$ for the device coated with HfO_2 as a protection layer by ALD. With the HfO_2 coat, the $shift_L$ occurred at a lower concentration than that without HfO_2, which had its blueshift suppressed by the thermal oxidization. This is caused by the suppression of blueshift causing redshift along with other reasons. The ultra-high sensitive detection achieved using NS was demonstrated above. Furthermore, a thin protection layer coated by ALD was shown to be effective for the suppression of the blueshift noise.

4. 3 **Sensing of specific adsorption**

As mentioned in Chapter 1, the specific adsorption has selectivity owing to the bind, which recognizes the target molecule. When a biomarker is diagnosed from a contaminated sample, such as human blood, selectivity against contaminants is necessary

Table 4.1 Fitting parameters evaluated from each solid line.

Surface treatment	Affinity constant [M^{-1}]			Maximam shift [nm]		
	K_{A1}	K_{A2}	K_{A3}	$\Delta\lambda_{max1}$	$\Delta\lambda_{max2}$	$\Delta\lambda_{max3}$
Pumping	—	5.0×10^{6}	—	—	2.5	—
Oven	2.5×10^{11}	1.5×10^{7}	1.5×10^{5}	0.5	2.2	1.9
HfO_2	4.0×10^{14}	1.0×10^{7}	1.0×10^{5}	0.5	2.1	1.0

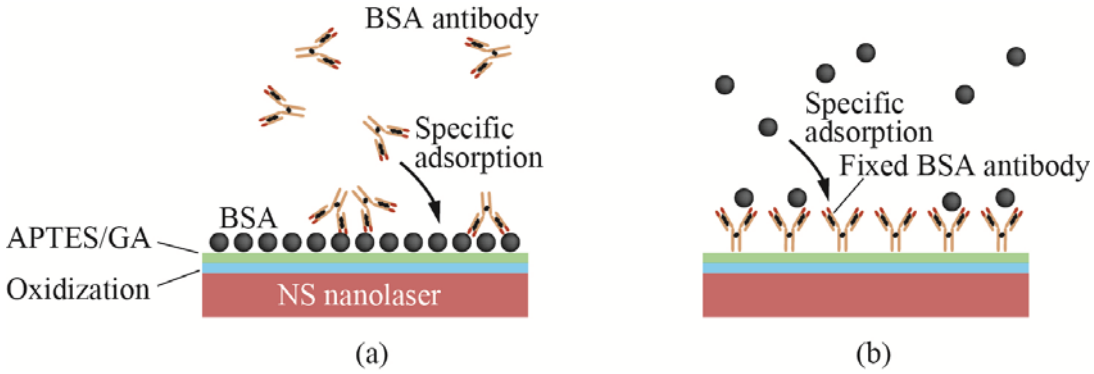

Fig. 4.4 Model for sensing the antibody–antigen reaction using BSA and anti-BSA antibodies. (a) BSA was immobilized on the sensor surface, and then, BSA antibodies were adsorbed to the BSA. (b) The BSA antibodies were immobilized on the sensor surface, and the BSA was then adsorbed to the BSA antibodies.

for the diagnosis. Therefore, it is necessary to construct a biointerface that is complementary. For example, antibodies, aptamer, and DNA are used as host molecules on sensor surfaces to analyze biomarker proteins, and these have binding sites that are complementary to those of the host molecule [4-6, 7]. For this section, antibody–antigen reactions were sensed using the NS. BSA and anti-BSA polyclonal antibodies were used for the model antibody–antigen reaction. Fig. 4.4 shows the model for sensing the antibody–antigen reaction. In Fig. 4.4(a), the BSA was immobilized on the sensor surface, and then, the BSA antibody was absorbed. On the other hand, in Fig. 4.4(b), the BSA antibody was immobilized on the sensor surface, and then, the BSA was absorbed. The sensing procedure was performed as follows:

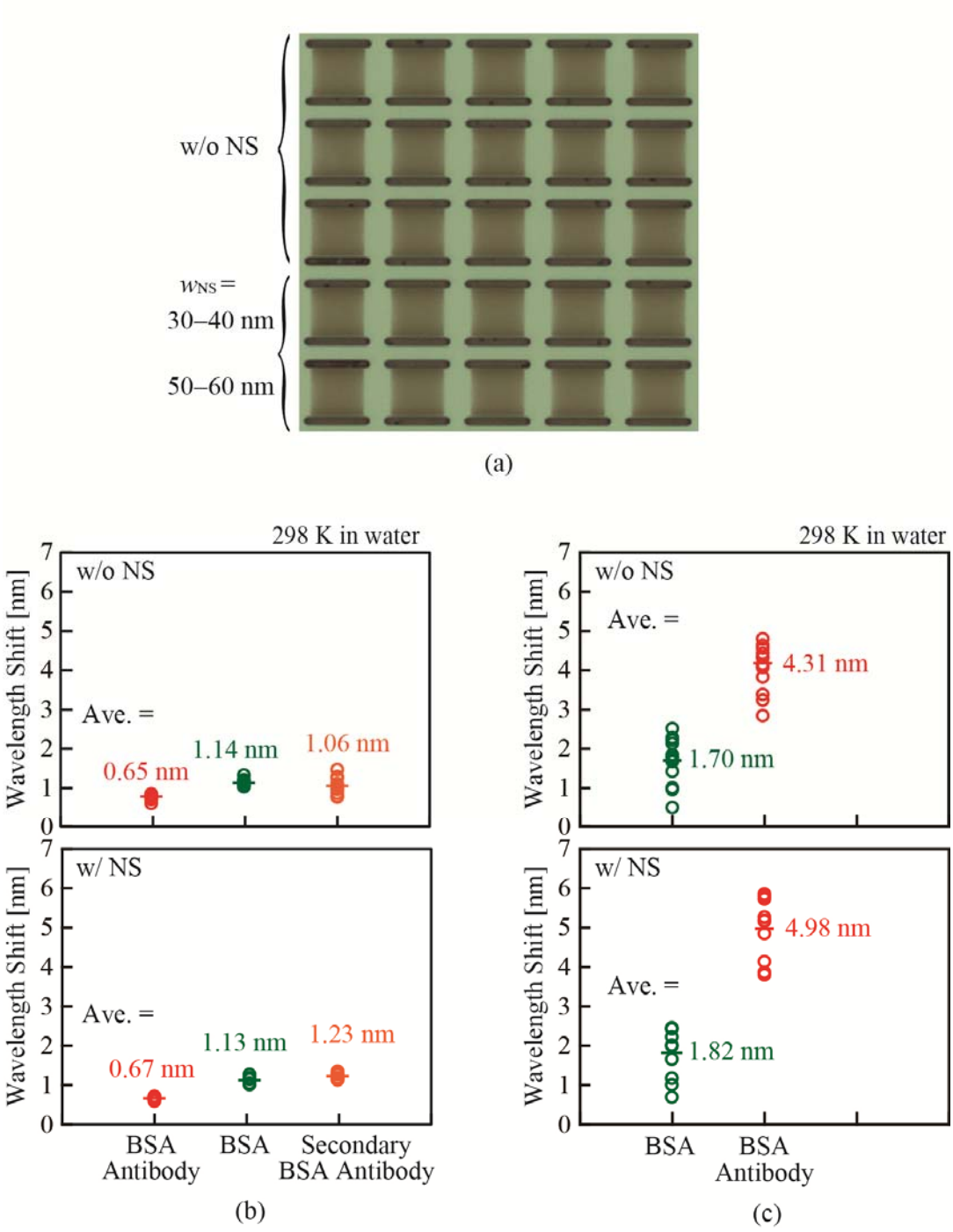

Fig. 4.5 Sensing of the antibody–antigen reaction of BSA. (a) A typical microscope image of a measured nanolaser array. (b) $\Delta\lambda$ from GA as a function of each process of BSA immobilization followed by BSA antibody specific adsorption. (c) $\Delta\lambda$ from GA as a function of each process of BSA antibody immobilization followed by BSA specific adsorption. The upper figures show the results without NS, and the bottom figures show the results with NS.

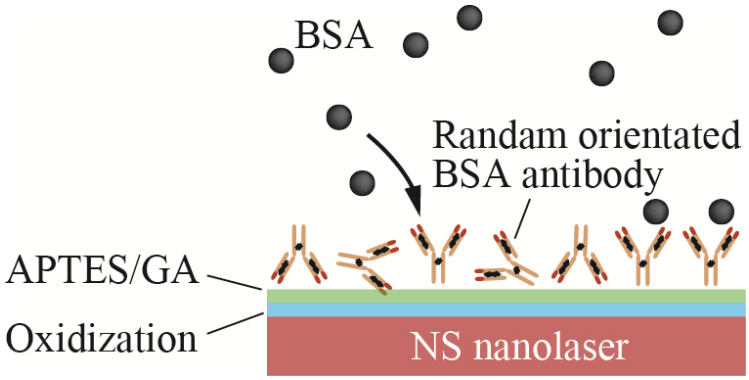

Fig. 4.6 Model of the limitations of the antibodies. When the antibodies were immobilized by GA, the antibodies were randomly orientated. The downward directed antibodies could not absorb to BSA.

BSA antibody adsorption on BSA

1. The sensor chip was prepared until GA functionalization, as described in Section 4.1. Thermal oxidization with an oven was the surface treatment adopted for stable detection.
2. The laser wavelength was measured in pure water after rinsing with water for a duration of 1 min.
3. The chip was immersed in 10-μM BSA and diluted with pure water for 30 mins.
4. The wavelength was measured in pure water after a rinse in 0.05% polyoxyethylene (20) sorbitan monolaurate (Tween 20) and pure water for 1 min, respectively.
5. The chip was immersed in 10-μM BSA antibody solution for 30 mins.
6. Step 4 was repeated.

BSA adsorption on BSA antibodies

1. The sensor chip was prepared until GA functionalization, as described in Section 4.1.
2. The laser wavelength was measured in pure water after rinsing with water for a duration of 1 min.
3. The chip was immersed in a 10-μM BSA antibody solution diluted with pure water for 30 mins.
4. The wavelength was measured in pure water after a rinse in 0.05% Tween 20 and pure water for 1 min, respectively.

5. The chip was immersed in a 10-μM BSA antibody solution for 30 mins.
6. Step 4 was repeated.

In these sensing procedures, Tween 20 was used as a surfactant to suppress the non-specific adsorption of the protein, and a high enough concentration of the protein was used for the evaluation of the saturated adsorption, in which BSA antibodies and BSA occupy the binding sites. Fig. 4.5 summarizes the sensing of the antibody–antigen reaction for both methods. Figure 4.5(a) shows a microscope image of a typical 5 × 5 nanolaser array used for this sensing. The upper three lines of devices in the nanolaser array were without NS, and the bottom two lines were with NS. In Fig. 4.5(b) and (c), $\Delta\lambda$ measured from GA by the two methods is summarized. In Fig. 4.5(b), the averaged $\Delta\lambda$ with and without NS for BSA were 1.82 and 1.70 nm and $\Delta\lambda$ values for the BSA antibodies were 4.98 and 4.31 nm, respectively. The $\Delta\lambda$ values were slightly larger than those without NS. Therefore, fluctuations occurred in $\Delta\lambda$, because the nanolasers were fabricated with various design w_{NS} and the functionalization of APTES was still unstable. Thus, this fluctuation can be suppressed through fabrication with a fixed design. Moreover, fluctuations of $\Delta\lambda$ between the nanolasers occurred owing to fabrication errors or the non-uniformity of the functionalization of APTES or GA. Therefore, it was necessary to optimize the functionalization. In Fig. 4.5(c), the averaged $\Delta\lambda$ with and without NS for the BSA antibodies were 0.67 and 0.65 nm and the $\Delta\lambda$ values for the BSA were 1.13 and 1.14 nm, respectively. Differences existed in $\Delta\lambda$ because of differences in the order of the adsorption processes. These differences arose from the suppression of the adsorption of BSA to the immobilized BSA antibodies owing to the limitations of the orientation of the antibody or steric interference. Fig. 4.6 shows an image of the limitations for the orientation of the antibodies. In the BSA immobilization process, the BSA antibodies can approach the binding sites of the BSA. On the other hand, in the BSA antibody immobilization process, the BSA cannot approach the BSA antibodies when the antibodies are fixed in the downward direction. It is believed that the observed differences occurred for this reason. However, the limitations related to orientation are derived from the specific adsorption process. Thus, the specific adsorption of BSA was schussed.

Reference

[4-1] M. Okubo, I. Azume, and Y. Yamamoto, "Preferential adsorption of bovine serum-albumin dimer onto polymer microspheres having a heterogeneous surface consisting of hydrophobic and hydrophilic parts," *Colloid Polym. Sci.*, vol. 268, pp. 598–603, 1990.

[4-2] I. Migneault, C. Dartiguenave, M. J. Bertrand, and K. C. Waldron, "Glutaraldehyde:

Behavior in aqueous solution, reaction with proteins, and application to enzyme crosslinking," *Biotechniques*, vol. 37, no. 5, pp. 790–802, 2004.

[4-3] S. Kita, "Photonic crystal nanolaser sensor," Doctoral thesis (*Yokohama Nat'l Univ.*), 2012.

[4-4] S. Kita, S. Otsuka, S. Hachuda, T. Endo, Y. Imai, Y. Nishijima, H. Misawa, and T. Baba, "Super-sensitivity in label-free protein sensing using nanoslot nanolaser," *Opt. Express*, vol. 19, no. 18, pp. 17683–17690, 2011.

[4-5] S. Kita, S. Otsuka, S. Hachuda, T. Endo, Y. Imai, Y. Nishijima, H. Misawa, and T. Baba, "Photonic crystal nanolaser bio-sensors," *IEICE Trans. Electron.*, vol. E95-C, no. 2, pp. 188–198, 2012.

[4-6] K. N. Houk, A. G. Leach, S. P. Kim, and X. Zhang, "Binding affinities of host–guest, protein–ligand, and protein–transition-state complexes," *Angew. Chemie Int. Ed.*, vol. 42, no. 40, pp. 4872–4897, 2003.

[4-7] Q. Chen, H. Chen, Y. Zhao, F. Zhang, F. Yang, J. Tang, and P. He, "A label-free electrochemiluminescence aptasensor for thrombin detection based on host–guest recognition between tris(bipyridine)ruthenium(II)-β-cyclodextrin and aptamer," *Biosens. Bioelectron.*, vol. 54, pp. 547–552, 2014.

Chapter 5
Sensing of streptavidin

5. 1 Overview

This chapter demonstrated ultra-high sensitivity of SA as a model of antibody-antigen reaction using a nanoslot nanolaser. The issue of the nanolaser sensor was introduced and the biointerface conditions and sensing conditions were improved for resolving the issues.

5. 2 Sensing in pure water

SA has extremely strong binding to the biotin [5-1, 2] and often have been used as a linkage of the functionalization of enzyme, antibody, DNA, etc [5-3, 4]. SA has been also used as a model of antibody-antigen reaction due to such a strong binding. In this chapter, the SA-biotin adsorption was used as a model of antibody-antigen reaction and DL was evaluated for the aim to demonstrate the ultra-high sensitivity of NS nanolaser. The sensing procedure was shown as follow:

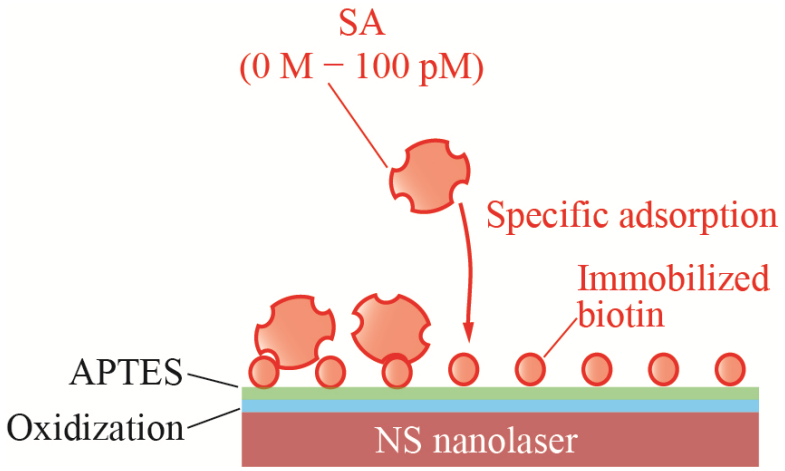

Fig. 5.1 SA sensing model. SA has 4 binding sites which bind to biotin. SA is absorbed to biotin through the binding sites.

1. Sensor chips were prepared with silanization of APTES by the process shown in Chapter 3. However, for the suppressing the blueshift noise, the advance thermal oxidization using an oven was adopted.
2. The chips were immersed in the mixed solution with 50 mM water-soluble carbodiimide (WSC) [5-5] and 50 μg/ml biotin for one hour.
3. The laser wavelength in pure water was measured after the rinse with pure water over 5 minutes.
4. The chips were immersed in a series of SA solution for 5 minutes at room temperature.
5. The procedure 3rd and 4th were repeated from lower concentration of PSA solution.

Figure 5.1 shows the sensing model of SA and Fig. 5.2 shows example lasing spectra, in which the spectral width of 150 pm is mainly limited by Q8383 used in this measurement. Clear wavelength shifts $\Delta\lambda$ larger than the spectral width are observed even at extremely low concentrations of SA. Figure 5.2(b) shows the $\Delta\lambda$ versus SA concentration characteristics for six devices with different w_{NS}. All the devices with $w_{NS} > 0$ exhibit such meaningful $\Delta\lambda$ at concentrations from 10 – 100 zM. Fundamentally $\Delta\lambda$ increases with increasing the concentration, but in some devices decreases in the fM – pM regime, which might be due to the slight oxidation of the device after repeated measurements. In addition, $\Delta\lambda$ increases with decreasing w_{NS}, which is attributed to the enhanced interaction of the laser mode and adsorbed SA in the NS [5-6].

Figure 5.2(c) compares the average $\Delta\lambda$ with and without NS [5-7]. Corresponding to (b), $\Delta\lambda$ starts appearing from the SA concentration of 10 – 100 zM. When the measurement was done without biotin, $\Delta\lambda$ did not increase until higher than 1 nM. Therefore, $\Delta\lambda$ at lower and higher than 1 nM are dominated by the specific binding of biotin-SA and the physisorption of SA, respectively. Solid lines were drawn from the expanded Langmuir fitting assuming the linear combination of three different adsorption terms: two chemisorptions and one physisorption [5-8]. Table I summarizes the parameters and DLs obtained from the fitting. In Fig. 5.2(c) and Table 5.1, the results for SA are also compared with our previous results for the non-specific adsorption of BSA [5-9]. Affinity constants K_{A1} and K_{A2} associated with chemisorptions of SA are 6 – 9 orders higher than those of BSA. Here, K_{A2} almost correspond to original affinity constants for SA and BSA seen in literatures [5-9, 10]. Therefore, the very low DL for SA arises primarily from the large affinity constant for SA. Furthermore, K_{A1} associated with $\Delta\lambda$ at lower concentrations is enhanced and the DL is reduced by 3 – 4 orders with the NS. Such a huge K_{A1} cannot be expected only from the

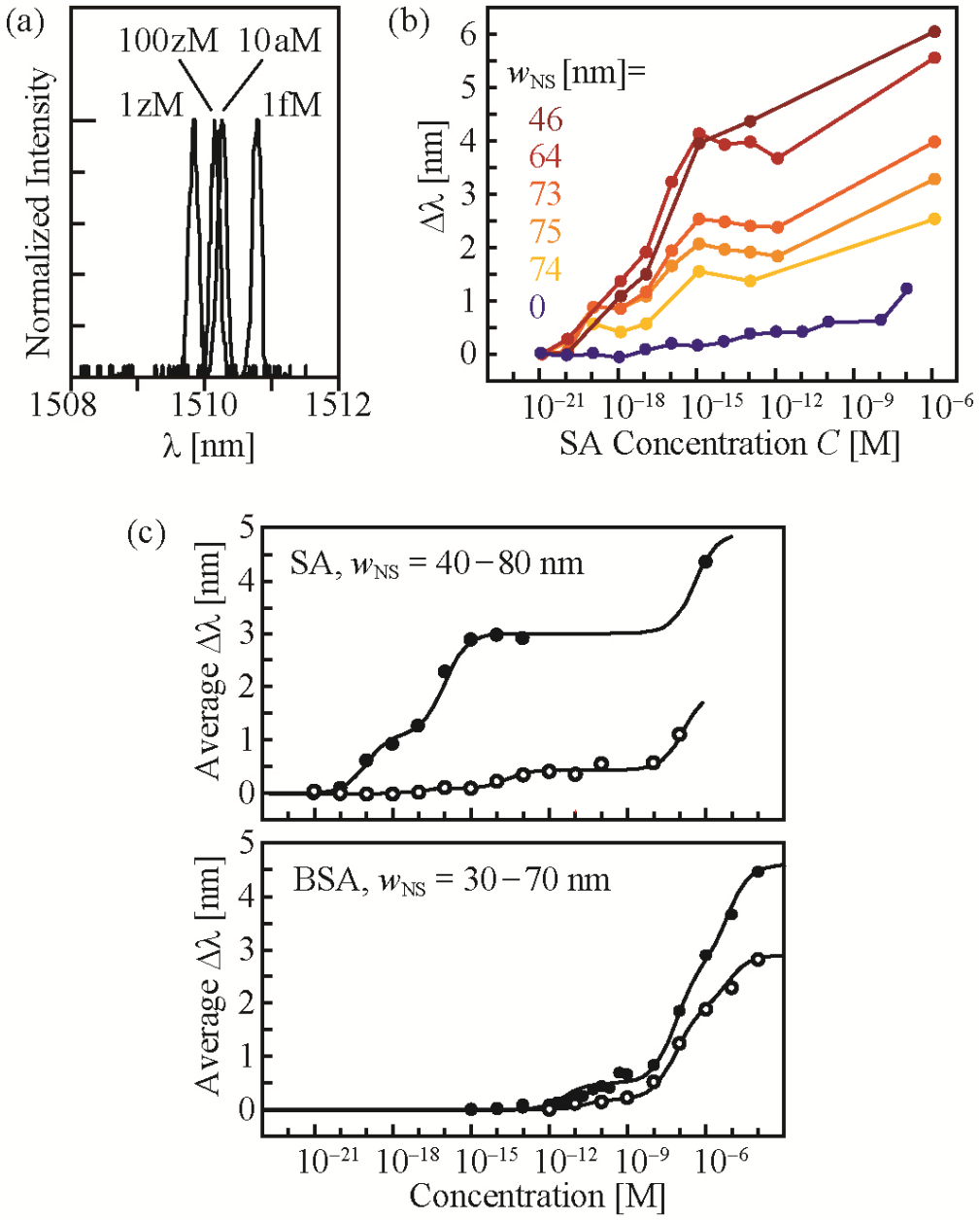

Fig. 5.2 Δλ due to adsorption of protein in pure samples. (a) Example laser spectra at different SA concentrations. (b) Δλ with SA concentration for six devices with different wNS. (c) Comparison of average Δλ for devices with NS (closed circles) and without NS (open circles). Data for SA were obtained in this study, while those for BSA are from Ref. [5-11]. These fitting curves were draw from Langmuir fitting [5-8] for the parameters shown in Table 5.1.

Table 5.1 Fitting parameters and DL evaluated from each solid line.

Samle	Affinity constant [M^{-1}]			Maximam shift [nm]			FWHM [nm]	DL
	K_{A1}	K_{A2}	K_{A3}	$\Delta\lambda_{max1}$	$\Delta\lambda_{max2}$	$\Delta\lambda_{max3}$	$\Delta\lambda_s$	
SA (w/ NS)	1.0×10^{19}	1.0×10^{16}	2.5×10^{6}	1.1	1.9	1.9	0.15	16 zM
SA (w/o NS)	1.0×10^{17}	4.0×10^{13}	7.0×10^{6}	0.10	0.34	1.5	0.30	188 fM
BSA (w/ NS) [5-8]	2.5×10^{11}	1.5×10^{7}	1.5×10^{5}	0.5	2.2	1.9	0.03	255 fM
BSA (w/o NS) [5-8]	4.0×10^{10}	1.5×10^{7}	1.5×10^{5}	0.2	1.7	1.0	0.60	38 nM

nature of the chemisorption. We have discussed previously the possibility that the optical gradient force captures the protein and enhances the affinity and sensitivity effectively [5-11]. In this experiment, however, the adsorption must take place during the soaking in the samples before the devices are operated in pure water. Therefore, the optical gradient force during the laser operation cannot contribute to the enhancement of the adsorption but only to the suppression of the desorption. Although the results shown here is reproducible in repeated experiments, its mechanism is still an open question.

5. 3 **Sensing in impure water**

For the biomarker sensing in human blood, it is necessary for suppressing the adsorption of contaminants such as albumin which account for 50–60% of the components of proteins in blood and for detecting the adsorption of the biomarker from the contaminated sample. Thus, the SA sensing in the mixture with SA as a target, BSA as a contaminant and Tween 20 [5-12] as a surfactant which was used for suppressing the non-specific adsorption was investigated as the selective detection model of antigen-antibody reaction. As mention in chapter 4, BSA is the albumin derived from a bovine and has often been used for the biosensing. Furthermore, the albumin account for 50–60% of the components of proteins in blood. For the above reason, BSA was adopted as the contaminant.

A surfactant is a molecule composed of two hydrophilic groups that are compatible with water and hydrophobic groups that are compatible with oil. Because surfactants self-assemble to form aggregates so as to achieve segregation of its hydrophobic groups from water for relaxing surface energy [5-13], the surfactant becomes stabilized by the formation of a micelle structure in water shown in Fig. 5.3(a). Considering the adsorption on a sensor surface in the mixture with the surfactant and proteins, the surfactant forms aggregates so as to achieve segregation of its hydrophobic groups from water and its hydrophobic groups from the surface. Furthermore, the surfactant is

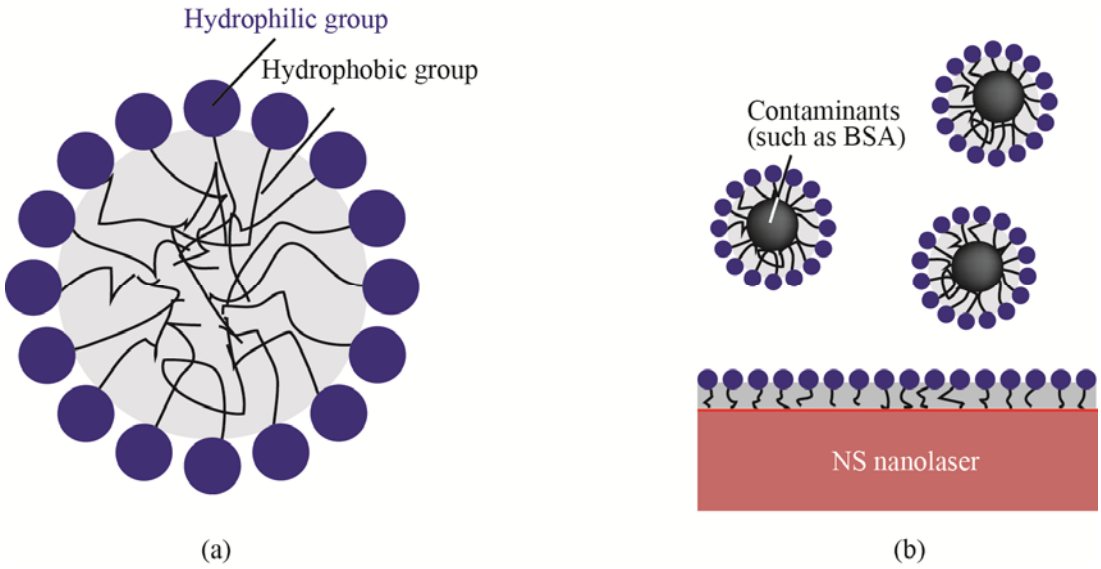

Fig. 5.3 (a) Schematic representation which surfactants self-assemble to form a micelle structure in water so as to relax the surface energy which occurs in the case of the hydrophobic groups. (b) Schematic image of the suppressing non-specific adsorption by the surfactant covered on contaminants and sensor surface.

wrapped around the protein so as to incorporate into the micelle [5-14], shown in Fig. 5.3(b). For relaxing the surface energy between protein and water by the surrounding surfactants, the surfactant suppresses the non-specific adsorption of proteins. In this sensing, surfactant Tween 20 hydrophilizes all the surfaces of proteins and devices and it suppresses the non-specific adsorption of BSA, while does not disturb the biotin-SA binding as it desorbs from SA on this condition.

The model of SA sensing in impure sample was shown in Fig. 5.4 and the method of the SA detection of impure sample is shown in Fig. 5.5. As seen in Fig. 5.4 and 5.5, the biotin-SA binding was detected from the comparison of the presence of biotin. The author considered that the adsorption of high concentration of BSA only occurs for the device without biotin and the adsorption of high concentration of BSA and low concentration of SA occurs for the device with biotin. Hence, the SA detection was evaluated by the comparison of the $\Delta\lambda$ between the device with and without biotin. Figure 5.4 summarizes the average $\Delta\lambda$ with different SA concentrations in the presence of three different concentrations of BSA as the contaminant [5-7]. Results in the absence of SA did not exhibit significant difference depending on the presence of biotin. When the BSA concentration is 100 nM, $\Delta\lambda$ increases with increasing SA concentration only with

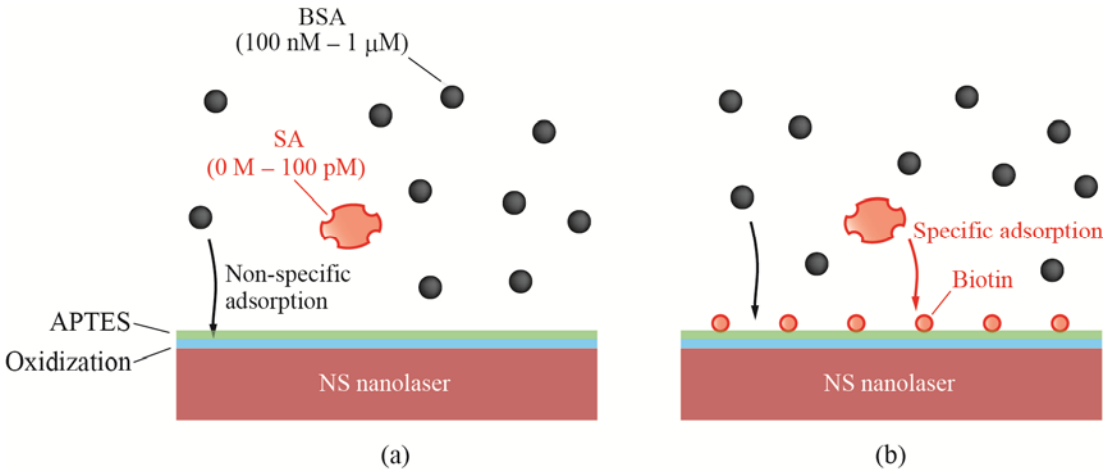

Fig. 5.4 The model of SA sensing in impure sample for the device (a) without and (b) with biotin. However, the surfactant Tween 20 was omitted to draw for the sake of simplicity.

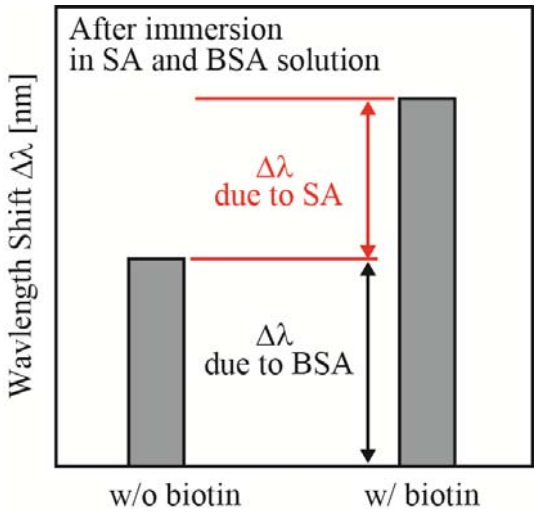

Fig. 5.5 The method of the selective detection by the comparison between Δλ without and with biotin.

the biotin; it was negligible without biotin. This indicates that biotin-SA specific binding occurs. When the BSA concentration is 1 μM, almost similar results are observed, although Δλ overall increased for both with and without biotin. This increase should be due to the increase in the non-specific physisorption of BSA even with Tween 20 because of the very high concentration of BSA. BSA might be adsorbed on the device surface as multi-layers and prohibits SA adsorption. The background noise increased more and obscured the main signal from the biotin-SA binding when the BSA

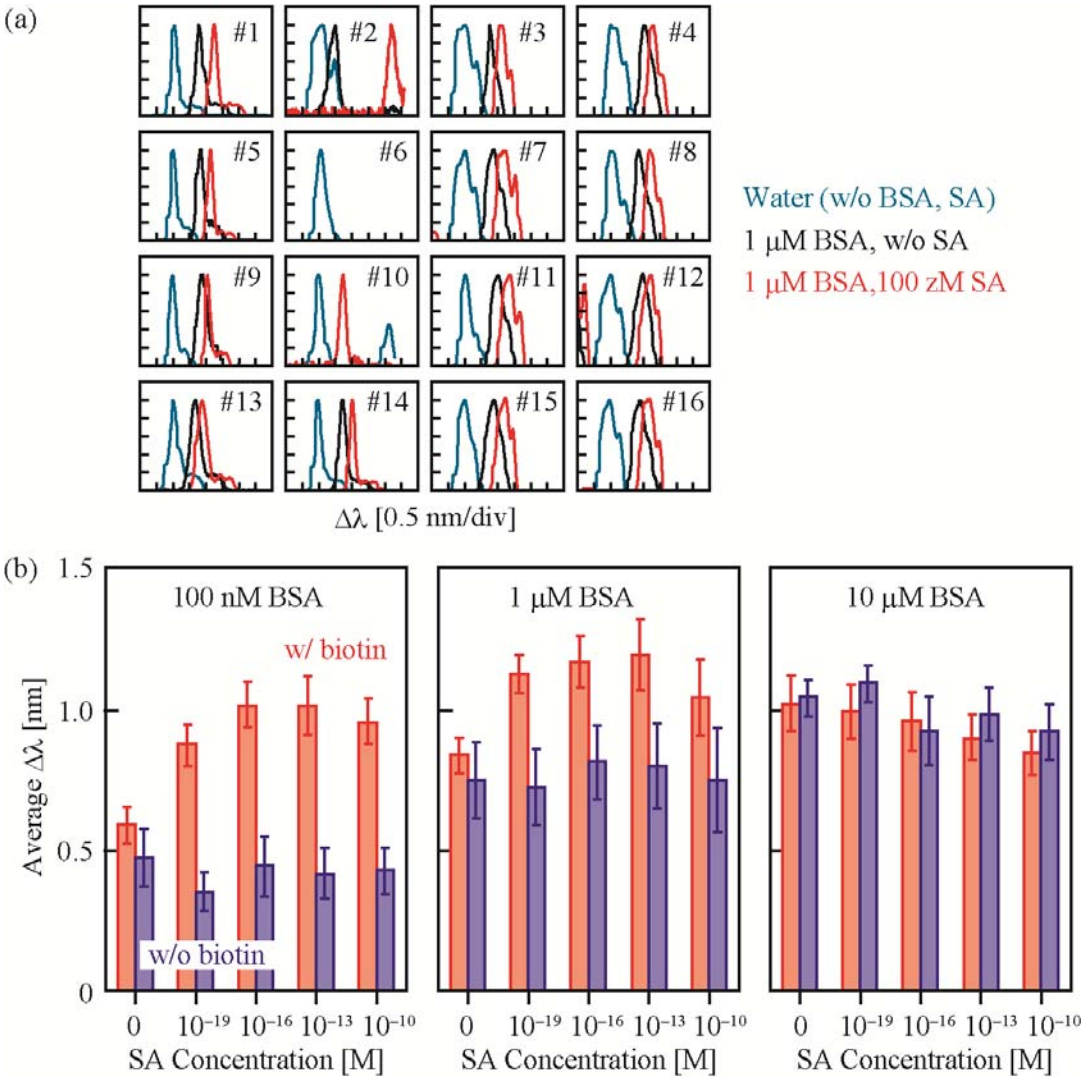

Fig. 5.6. Wavelength shifts due to adsorption of SA in impure samples. (a) Laser spectra of 16 devices under three different conditions. Some spectra for #6 and #10 were missing in the automatic measurement, which might be due to position errors of pump light and weak emission intensity from nanolasers. (b) Average Δλ due to the adsorption of SA in impure samples with three different concentration BSA as impurities. Red and blue plots show those with and without biotin, respectively. Error bars indicate the range for 95% confidence interval.

concentration was 10 μM. Here we can see the gradual decrease in Δλ with increasing the SA concentration. This might also be due to the aforementioned oxidation of the device after repeated measurements. Thus we confirmed that the biotin-SA adsorption was detected up to a SA concentration of 100 zM against 1 μM BSA. The

corresponding selectivity is as high as (SA/BSA) = 10^{13}. It is known that such albumin is included by ~1mM in human blood. Such high concentration completely hampers the detection of low concentration target biomarkers even using our nanolasers. Therefore, our strategy is such that we first dilute the blood plasma to ~1 μM, a thousand-fold lower concentration, and then detect the target. Antibodies of target biomarkers typically have affinity constants of 10^{9} – 10^{11} M^{-1} order, which are three orders lower than biotin-SA's. Considering the DL of our nanolaser sensor for biotin-SA, the DL of target biomarkers will be in the sub-fM regime, which is equivalent to sub-pM regime before the dilution. This is a very promising number that enables the detection of various biomarkers of interest for medical diagnoses.

5. 4 **Issues**

This sensing using NS nanolaser has some issues. First, the issues are listed as follow:

1. Blueshift noise occurred at the SA sensing.
2. The fluctuation of sensing in different trials.
3. The principle of the ultra-high sensitivity.
4. It was not confirmed whether the SA solution was diluted accurately.
5. The presence of blind area of the concentration which Δλ does not increase with.

First, the blueshift noise has occurred in BSA sensing as seen in Chapter 4. So far, the noise was suppressed by thermal oxidization using strong pumping or the heating by an oven (180°C, >1 hour). Thereby, the sensor surface was covered with oxide layer of GaInAsP. This oxide layer prevented the sensor from further oxidization by photo-pumping at the sensing. However, the device with the thermal oxidization still blueshifted in charged polymers solution such as PAA or PEI. Because the oxide GaInAsP has weak resistance against acid or alkali solution, the oxide GaInAsP was etched or further oxidized by the charged polymers [5-15, 16]. As mention in Chapter 3 and the next Section 5.5.1, the noise can be suppressed by the protection layer coated by ALD, which has strong resistance of such solution. Thus, the blueshift noise is no problem and the suppression was demonstrated next section.

Second, the fluctuations in different trials were observed due to the un-uniformity of functionalization such as APTES and biotin. So, the stable and uniformity biointerface was not still structured between different treatment due to the manual errors or environmental errors. Thus, the fluctuation will be able to be suppressed by optimizing the modification conditions. The optimization of APTES treatment was discussed latter

in Chapter 6. In the next section, the optimization of immunization of biotin was shown.

Thirdly, the principle of the ultra-high sensitivity is still open question. The ultra-high sensitivity has been discussed in ref. [5-8] and was described due to the light gradient force to the inside of NS and any forces in the wide area, which draw to the surrounding of the nanolaser cavity. However, this description cannot be explained for the SA sensing. SA was detected in pure water after the adsorption. So, light gradient force has nothing to do with the ultra-high sensitivity because there were no free-molecules surrounding the nanolaser. Furthermore, the adsorption in the sub-atto-molar means that in hundreds molecules in 1 ℓ and was the ration of (sensing area/other area) was roughly estimated as 0.02 if all SA was absorbed on the sensor. So, three molecules were estimated to absorb in the area where 5 × 5 nanolasers were integrated. In spite of the nanolaser sensing area of ~1 μm^2, the sub-atto-molars were detected by the multiple devices at the same time as seen in Fig. 5.6(a). Thus, only the description cannot be explained. The principle of the ultra-high sensitivity of the nanolaser might be due to something which senses in the wide area. At the current, it was discussed that the charge was related with the lasing or spontaneous emission light [5-15]. Thus, the charged ions such as H_3O^+ might be also related to be wavelength shift. However, the sensing principle is still resolved and it is necessary to investigate the principle. Fourthly, it was not confirmed whether the SA solution was diluted accurately. Thus, in the next section the accuracy of the dilution was checked.

Finally, there is a blind area of the concentration which $\Delta\lambda$ does not increase with [5-8]. At sensing the blind area concentration, the sensing by a NS nanolaser cannot be evaluated for showing the same $\Delta\lambda$. However, the blind area could be solved by the averaging $\Delta\lambda$ of the nanolasers which has various affinity constants. S. Kita reported the extension of sensing area by the averaging $\Delta\lambda$ using the devices with different w_{NS} (= 0–120 nm) [5-8]. It is consider that other method so as to verify the constants is use of multiple measurements of various antibodies which has affinity to other epitopes. The multi-measurement is one of merits of the nanolaser sensor and the blind area could be solved by above measurement.

5. 5 **Improvement**

To suppress the blueshift noise at the sensing, the thin layer as a protection by ALD was investigated. Furthermore, the modification condition of the biotin as a biointerface was investigated and accurate dilution by pipetting was checked by the use of multiple pipettes. The effect of Tween 20 as a surfactant was also investigated. Finally, improving the selectivity was tried by the additional polyethylene glycol (PEG).

5. 5. 1 **Suppression of blueshift noise by ALD protection layer**

In this section, the suppression of the blueshift noise at the biosensing by a protection layer of ALD was investigated. These materials are electrochemically stable. The sensing procedure was the same as the Section 5.1. However, the devices were coated a protection layer such as 3 nm ZrO_2, HfO_2 or SiO_2 by ALD before the procedure of the functionalization, in other words, immediately after etching for the air-bridge. To compare the three types of the nanolasers coated with ZrO_2, HfO_2 or SiO_2, with PSA antibody, Fig. 5.5 summarized $\Delta\lambda$ as a function of PSA concentration for each coating conditions. As seen in Fig. 5.5, the blueshift noise was suppressed for each coating condition. Furthermore, with ZrO_2 and HfO_2, the rising $\Delta\lambda$ occurred from the lower concentration than that of the device with SiO_2. ZrO_2 and HfO_2 were high dielectric materials and it was reported that spontaneous the charge on the sensor surface affected the intensity of the spontaneous emission and lasing. So, it has been discussed that there is some involvement of the charge and $\Delta\lambda$. For the reason, SiO_2 which is insulating material suppressed $\Delta\lambda$. Furthermore, the characteristics of ZrO_2 ,which is the isoelectric point near neutral, the transparency and the resistance for acid and alkali solution, was suitable for the protection layer of the nanolaser. Thus, 3 nm ZrO_2 was adopted as a protection layer. In the next chapter, ZrO_2 was used for the suppression of blueshift noise, if there is no notice.

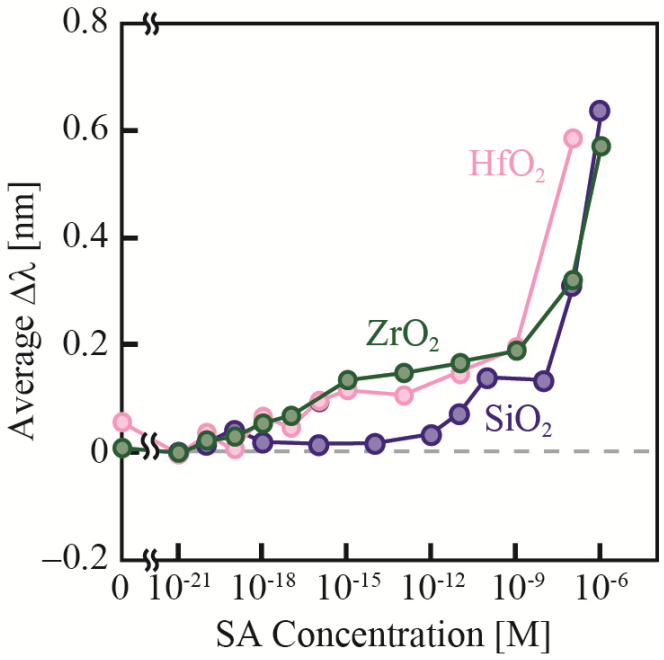

Fig. 5.7 $\Delta\lambda$ as a function of SA concentration for each protection layer condition.

5. 5. 2 Optimization of temperature at the biotin functionalization

For the optimization of the biointerface, the modification of the biotin was checked. The APTES which is based on the biointerface was discussed later in Chapter 6. This section checked temperature dependency at the biotin modification. The procedure of the biosensing was the same as Section 5.1 except temperature at the biotinylation. Fig. 5.6 summarized $\Delta\lambda$ as a function of SA concentration for each temperature. At the temperature of 25°C and 30°C, the redshift from sub-atto-molar occurred On the other hands, at the temperature of 20°C and 40°C, the shift did not occur until ~nM SA. Those are considered to be due to the low velocity of the biotinylation at 20°C and the effect of side reactions at 40°C. Thus, the temperature of the biotinylation was adopted as 25°C to observe the maximum $\Delta\lambda$ at the temperature.

5. 5. 3 Investigation of accurate dilution of SA solution

This section was checked whether the accurate dilution was done by pipetting. The dilution of SA solution was separated in four steps of individual pipetting at the SA concentrations which are less than 1 aM, no less than 1aM and no higher than 1 fM, no less than 1 fM and no higher than 1 pM, and higher than 1 pM. The procedure of the biosensing was the same as Section 6.1 except above the dilution procedure. Fig. 5.7 shows $\Delta\lambda$ as a function of SA concentration for the stepwise pipetting. $\Delta\lambda$ rose from 10

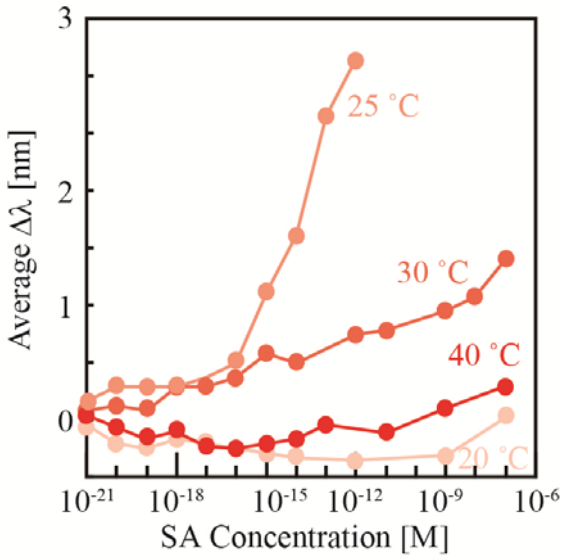

Fig. 5.8 $\Delta\lambda$ as a function of SA concentration for each temperature of the biotinylation.

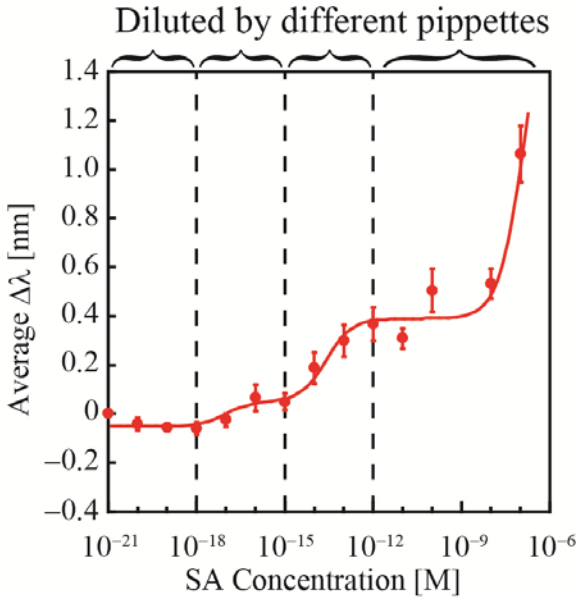

Fig. 5.9 Δλ as a function of SA concentration for the stepwise pipetting. Fitting curve was calculated by expanded Langmiur fitting [5-8] for K_{A1}= 10^{17} M^{-1}, K_{A2} = 4 ×10^{13} M^{-1}, K_{A3} =7 ×10^{6} M^{-1}, $\Delta\lambda_{max1}$ = 0.1 nm, $\Delta\lambda_{max2}$ = 0.34 nm, and $\Delta\lambda_{max3}$ = 1.5 nm.

aM as low as the concentration of SA detected in Section 6.1 and it proved that the dilution of SA was accurate. Furthermore, K. Watanabe also discussed the accuracy of the SA concentration using single-molecule imaging techniques [5-16] and reported 1 fM SA diluted by 9 times pipettings was evaluated as 8.51 fM and the dilution of SA had enough accuracy.

5. 5. 4 **Investigation of the treatment of Tween 20**

This section investigated the effect of Tween 20 used as a surfactant. This surfactant was used for the suppression of the physic adsorption because the surfactant covered and hydrophilized the surrounding PSA, impurities, and the sensor surface. For the investigation of Tween 20, the sensing using devices with biotin in the SA solution with and without 0.1% Tween 20 was performed. Fig. 5.8 compared the SA sensing with and without Tween 20. As seen in Fig. 5.8, Δλ was increased due to Tween 20 at the low concentration of SA and blue shift noise was observed at the rage of high concentration. The ingression of Dl is considered the relaxing the surface hydrophobicity which was discussed later in Chapter 6 and the blueshift noise was due to the absent of the protection layer of ZrO_2. Thus, the blueshift can be suppressed and it was confirmed that Tween 20 improved the performance of a NS nanolaser.

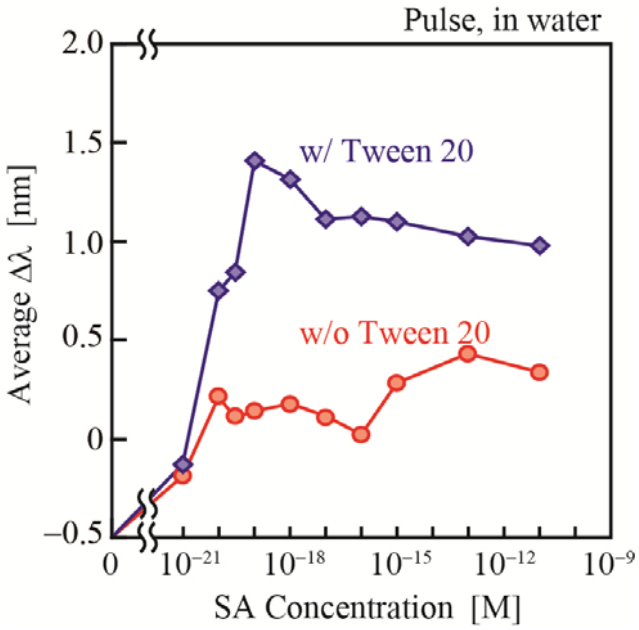

Fig. 5.10 Comparison of the SA sensing with and without Tween 20.

5. 5. 5 **Improvement of selectivity**

For the improvement of the selectivity against contaminants, it is the necessary to suppress the non-specific adsorption of contaminants. The use of PEG is one of the solutions. PEG is a polymer which has three characteristics such as non-immunogenic, hydrophilic and high flexibility [5-17]. In other words, PEG does not affect biomarkers, prevents non-specific binding and does not inhibit specific adsorption such as antibody-antigen reaction. Thus, the non-specific binding can be suppressed by the use of PEG. In this section, the improving selectivity was tried by the comparison of the PEG without and with biotin (mPEG-NHS ester and biotin-mPEG-NHS ester). Furthermore, the comparison of different long polymers of PEG which were long PEG (mPEG-NHS ester, average molecular weight 5000) and short PEG (PEG_{12}-NHS ester, the number of the ethylene glycol chains was 12) Figure 5.11 shows the structure of the both PEG and figure 5.12 shows the biointerface without and with biotin. The PEG polymers cotein N-hydroxysuccinimide (NHS) and NHS is a function group which efficiently couples to NH_2 group in the pH range of 7.0–8.5. Thus, the PEG polymers can be functionalized on the surface with APTES. Furthermore, the ref. [5-18] reported the optimization of the spacing of biotin by immersing in the mixed solution in which mPEG-NHS ester and biotin-PEG-NHS ester are mixed in a ratio of 5:1.The detail procedures of functionalizing PEG without and with biotin were as follow:

Procedure of functionalizing PEG without biotin for control.

1. Sensor chips were prepared with silanization of APTES by the process shown in Chapter 3. However, for the suppressing the blueshift noise, the advance thermal oxidization using an oven was adopted.
2. Mixed buffer was prepared with 150 mM KCl, 1 mM $CaCl_2$, 50 mM 4-(2-hydroxyethyl)-1-piperazineethanesulfonic acid (HEPES) and KOH so that pH become 7.4 by the addition of KOH.
3. mPEG-NHS ester or PEG_{12}-NHS ester was dissolved in the prepared buffer so that the concentration become 1 mg/ml. In the detail, 18mg mPEG-NHS ester was dissolved in 3.6 ml above HEPES buffer and 36 µl $mPEG_{12}$ ester solutions whose concentration was 100 mg/ml was mixed with 1164 µl HEPES buffer.
4. The chips were immersed in the PEG buffer prepared in the procedure of 3 for 1 hour.
5. The chips were rinsed in pure water for 1 minute.

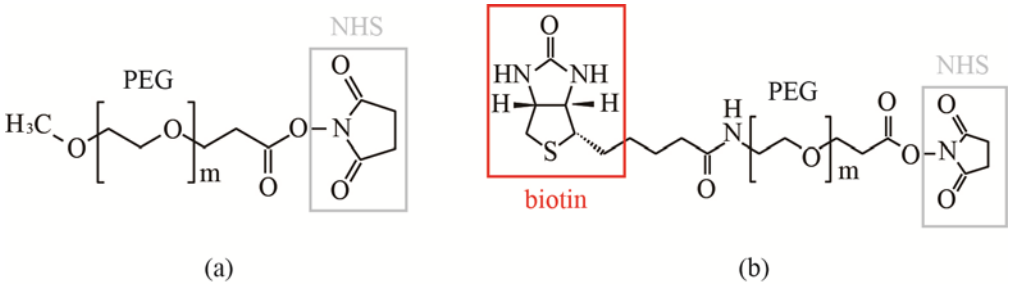

Fig. 5.11 Structure of used PEG (a) without and (b) with biotin. Different length PEG polymers were used (average molecular weight = 5000 or length of ethylene glycol m = 12).

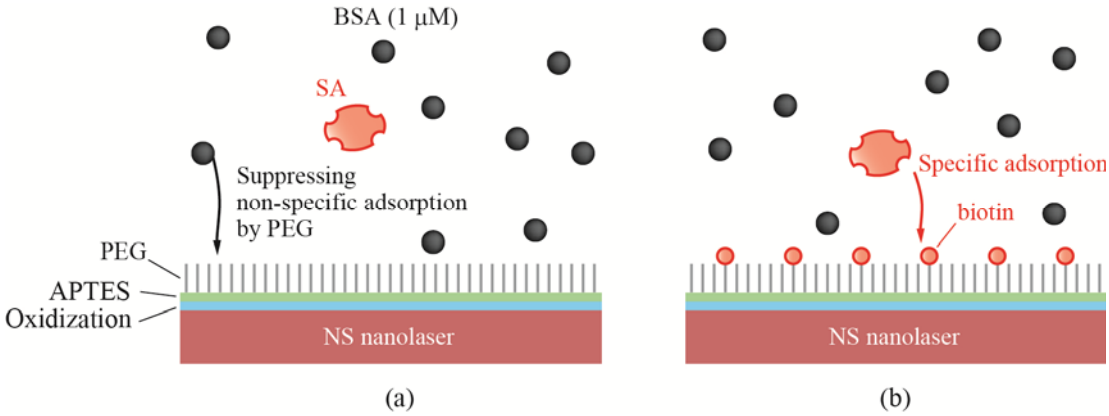

Fig. 5.12 The model of SA sensing in impure sample using PEG (a) without and (b) with biotin.

Procedure of functionalizing PEG with biotin for control.

1. Above procedures of 1–2 were done.
2. The mixture with mPEG-NHS ester or PEG_{12}-NHS ester, biotin-mPEG-NHS ester or biotin-PEG_{12}-NHS ester and HEPES buffer was prepared so that the volume ratio of become 5:1, respectively. In the detail, 15 mg mPEG-NHS ester and 3 mg biotin-PEG-NHS ester were dissolved in 3.6 ml HEPES buffer. 30 μl PEG_{12}-NHS ester solution and 24 μl biotin-PEG_{12} ester solution, whose concentrations were 100 mg/ml and 25 mg/ml respectively, were mixed with 1146 μl HEPES buffer.
3. Above procedures of 4 and 5 were done.

The SA sensing from impure sample was done by the process shown in Section 5.2. However, the concentration of BSA as a contaminant was 1 μM. Figure 5.13 shows Δλ as a function of SA concentration for the PEG condition (the length of PEG and the presence of biotin) and with 1 μM BSA and 0.1% Tween 20. With the long PEG shown in Fig. 5.13(a), there was no difference between the devices without and with biotin except of 1 fM SA. Furthermore, by the comparison of the results of Fig. 5.6(b) and Fig. 5.13(a), both Δλ for the device without biotin at 1 μM BSA was the approximately same level. With the short PEG shown in Fig. 5.13(b), on the other hand, there were differences between the device without and with biotin and Δλ without and with biotin

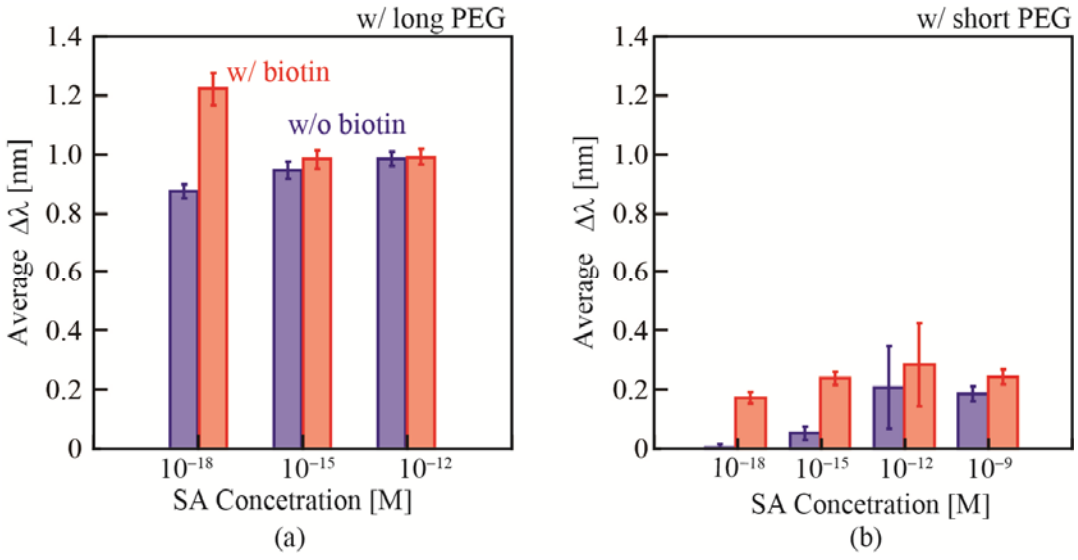

Fig. 5.13 Δλ due to adsorption of SA in impure samples included in 1 mM BSA and 0.1% Tween 20 using (a) long PEG and (b) short PEG for the biotin conditions. Red and blue plots show those with and without biotin, respectively. Error bars indicate the standard errors.

overall decreased. Thus, the non-specific adsorption can be decreased by the functionalization of short long PEG. However, $\Delta\lambda$ without biotin increased with SA concentration and the difference between $\Delta\lambda$ without and with biotin disappeared above the SA concentration of 1 pM by *t*-test. The cause of increasing $\Delta\lambda$ without biotin might be desorption of PEG and then adsorption of BSA at the same place. PEG might be desorbed due to etching the sensor surface because of the process of suppressing blueshift noise was adopted as thermal oxidization. Thus, the increasing due to the non-specific adsorption of BSA could be suppressed by the coating ALD protection layer. Therefore, the suppressing of non-specific adsorption noise was demonstrated by using short long PEG and the selectivity could be improved by the using of PEG and ALD coating.

Reference

[5-1] N. M. Green, "Avidin and streptavidin," *Methods in Enzymology*, vol. 184, pp.51–67, 1990.

[5-2] E. P. Diamandis and T. K. Christopoulos, "The biotin-(strept)avidin system: Principles and applications in biotechnology," *Clin. Chem.*, vol. 37, no. 5, pp. 625–636, 1991.

[5-3] K. N. Houk, A. G. Leach, S. P. Kim, and X. Zhang, "Binding affinities of host–guest, protein–ligand, and protein–transition-state complexes," *Angew. Chemie Int. Ed.*, vol. 42, no. 40, pp. 4872–4897, 2003.

[5-4] Q. Chen, H. Chen, Y. Zhao, F. Zhang, F. Yang, J. Tang, and P. He, "A label-free electrochemiluminescence aptasensor for thrombin detection based on host–guest recognition between tris(bipyridine)ruthenium(II)-β-cyclodextrin and aptamer," *Biosens. Bioelectron.*, vol. 54, pp. 547–552, 2014.

[5-5] N. Nakajima and Y. Ikada, "Mechanism of amide formation by carbodiimide for bioconjugation in aqueous media," *Bioconjug. Chem.*, vol. 6, no. 1, pp. 123–130, 1995.

[5-6] S. Kita, S. Hachuda, K. Nozaki, and T. Baba, "Nanoslot laser," *Appl. Phys. Lett.* 97(16), 161108 (2010).

[5-7] S. Hachuda, S. Otsuka, S. Kita, T. Isono, M. Narimatsu, K. Watanabe, Y. Goshima, and T. Baba, "Selective detection of sub-atto-molar Streptavidin in 10^{13}-fold impure sample using photonic crystal nanolaser sensors.," *Opt. Express*, vol. 21, no. 10, pp. 12815–21, 2013.

[5-8] S. Kita, "Photonic crystal nanolaser sensor," Doctoral thesis (*Yokohama Nat'l Univ.*), 2012.

[5-9] K. De Vos, I. Bartolozzi, E. Schacht, P. Bienstman, and R. Baets, "Silicon-on-insulator microring resonator for sensitive and label-free biosensing,"

Opt. Express, vol. 15, no. 12, pp. 7610–7615, 2007.

[5-10] H. Ukeda, T. Ishii, M. Sawamura, and H. Kusunose, "Dynamic analysis of the binding process of bovine serumalbumin on glutaraldehyde-activated controlled-pore glass," *Anal. Chim. Acta*, vol. 308, no. 1–3, pp. 261–268, 1995.

[5-11] S. Kita, S. Otsuka, S. Hachuda, T. Endo, Y. Imai, Y. Nishijima, H. Misawa and T. Baba, "Super-sensitivity in label-free protein sensing using nanoslot nanolaser," *Opt. Express*, vol. 19, no. 18, pp. 17683–17690, 2011.

[5-12] S. Mao, G. H. Lu, K. H. Yu, Z. Bo, and J. H. Chen, "Specific protein detection using thermally reduced grapheme oxide sheet decorated with gold nanoparticle-antibody conjugates," *Adv. Mater.*, vol. 22, no. 32, pp. 3521–3526, 2010.

[5-13] R. Nagarajan, "Theory of surfactant self-assembly: a predictive molecular thermodynamic approach," *Langmuir*, vol. 7, pp. 2934–2969, 1991.

[5-14] Kathryn L. Brogan, Jae Ho Shin and Mark H. Schoenfisch, “Influence of Surfactants and Antibody Immobilization Strategy on Reducing Nonspecific Protein Interactions for Molecular Recognition Force Microscopy,” *Langmuir*, vol. 20, pp. 9729 – 9735 (2004).

[5-15] K. Watanabe, Y. Kishi, S. Hachuda, T. Watanabe, M. Sakemoto, Y. Nishijima and T. Baba, "Simultaneous detection of refractive index and surface charges in nanolaser biosensors," *Appl. Phys. Lett.*, vol. 106, no. 2, pp. 021106, 2015.

[5-16] M. Ueda, Y. Sako, T. Tanaka, P. Devreotes, T. Yanagida,"Single-molecule analysis of chemotactic signaling in dictyostelium cells," *Science*, vol. 294, no. 5543, pp. 864–867, 2001.

[5-17] J. Kahovec, R. B. Fox, and K. Hatada, "Nomenclature of regular single-strand organic polymers - (IUPAC Recommendations 2002)," *Pure and Applied Chemistry*, vol. 74, pp. 1921-1956, Oct 2002.

[5-18] S. K. Kufer, E. M. Puchner, H. Gumpp, T. Liedl, and H. E. Gaub, "Single-molecule cut-and-paste surface assembly," *Science*, vol. 319, pp. 594-596, Feb 2008.

Chapter 6
Sensing of prostate-specific antigen

6. 1 Overview

This chapter demonstrates PSA sensing in pure and impure samples. Firstly, for accurate measurement, PSA is calibrated by two methods: Micro-BCA and ELISA. Secondly, PSA sensing is demonstrated in pure and impure samples. Thirdly, improvements on stable sensing are investigated and discussed. Finally, fluctuations in PSA sensing in different trials are discussed.

6. 2 Sample

PSA (33–34 kDa) is a well-known blood biomarker of prostate cancer [6-1, 2, 3, 4]. The critical concentration for positive diagnosis has been determined to be 4 ng/ml (approximately 100 pM) in the blood. Moreover, for the detection of prostate cancer recurrence postoperatively, it has been reported that an assay with a detection limit of 100 pg/ml (approximately 3 pM) [6-2] can identify the recurrence of prostate cancer approximately 1 year earlier than most assays in current use. Therefore, more sensitive detection of PSA will enable earlier identification and a high sensitivity of detection of rising PSA postoperatively will be effective. Thus far, labeling methods, such as enzyme linked immunosorbent assay (ELISA), have been used to detect these concentrations. However, the detection limit of standard ELISA is in the sub-pM range, which may not be sufficient for monitoring instances of recurrence. In addition, the associated costs remain relatively high [6-5].

We adopted PSA as a typical example using the antibody–antigen reaction for demonstration because PSA is a well-known biomarker in order to compare the nanolaser with other sensor devices and because of the high sensitivity of PSA detection that is required for the identification of prostate cancer recurrence. PSA derived from human semen (Sigma-Aldrich Co. LLC., P338-25UG) was used as a target. PSA monoclonal antibody (Mikuri Immune-Laboratory, clone No. 4D10) [6-6] was used as the primary antibody and mouse antibody obtained from pre-immune mouse serum (Sigma-Aldrich Co. LLC.) was used as a negative control.

6. 3 Adjustment of the concentration of PSA

For a number of the measurements, the original PSA solution was diluted in pure water and stored in small aliquots at −20 °C or −80 °C. The procedure for dilution and storage was as follows:

1. Pure water (735 ml) was injected in the original tube of PSA (1–5 mg/ml).
2. The PSA solution was mixed by pipetting 5–10 times to produce a uniform concentration.
3. The PSA solution was dispensed in 50 µl aliquots.
4. The diluted PSA was preserved at −20 °C or −80 °C.

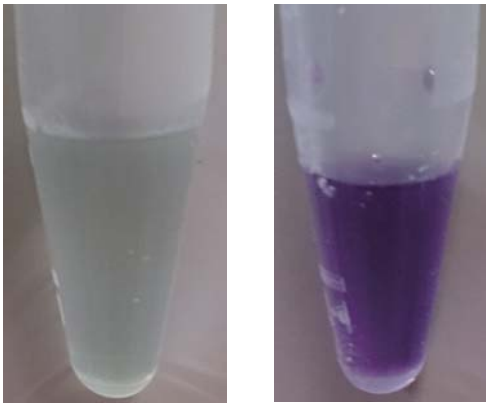

Fig. 6.1 Color reaction in the Micro-BCA assay. Left and right figures are before and after the reaction, respectively.

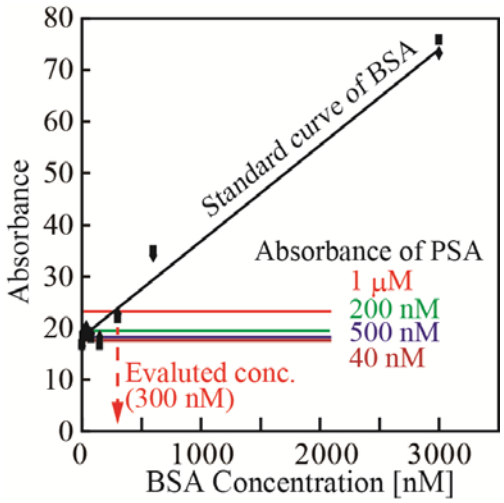

Fig. 6.2 Calibration of PSA concentration by Micro-BCA assay.

The concentration of the diluted solution used for PSA detection was estimated to be 1–5 mM. To measure PSA detection with accuracy, we checked the concentration of the diluted PSA solution for the retention of PSA reactivity. The following two assays were conducted.

6. 3. 1 **Micro-BCA Protein assay**

First, we verified the total protein concentration by the Micro-BCA assay [6-7]. Micro-BCA assay is the method that uses the color reaction of copper ions caused by the change in the valence. Amino groups, which are part of protein, bind the copper ion and change the valence from Cu^{+2} to Cu^{+1}. When bicinchoninic acid (BCA) is added to the solution containing reduced copper (Cu^{+1}) ions, the reduced ion and BCA form a complex that has an absorption peak at 540 nm (Fig. 6.1). To determine the concentration of the PSA solution, we compared the absorption peak of the diluted PSA solution (estimated concentrations: 40 nM, 200 nM, 500 nM, and 1 μM) with a known amount of BSA. The Micro BCA™ Protein Assay Kit (Thermo Fisher Scientific, Inc.) and a ChroMate® 4300 (Awareness Technology Inc.) microplate-reader were used for the assay.

Figure 6.2 shows the absorbance of the each concentration of the protein. The absorbance of BSA (standard curve) increased linearly in the range from 300 nM to 3000 nM and concentrations <300 nM gave an absorbance of approximately 20 and was considered to be background. On the other hand, the absorbances of the PSA solutions were at background level, except for 1 μM PSA. Comparing 1 μM PSA with the standard BSA curve, the concentration of 1 μM PSA estimated by dilution ratio was 300 nM.

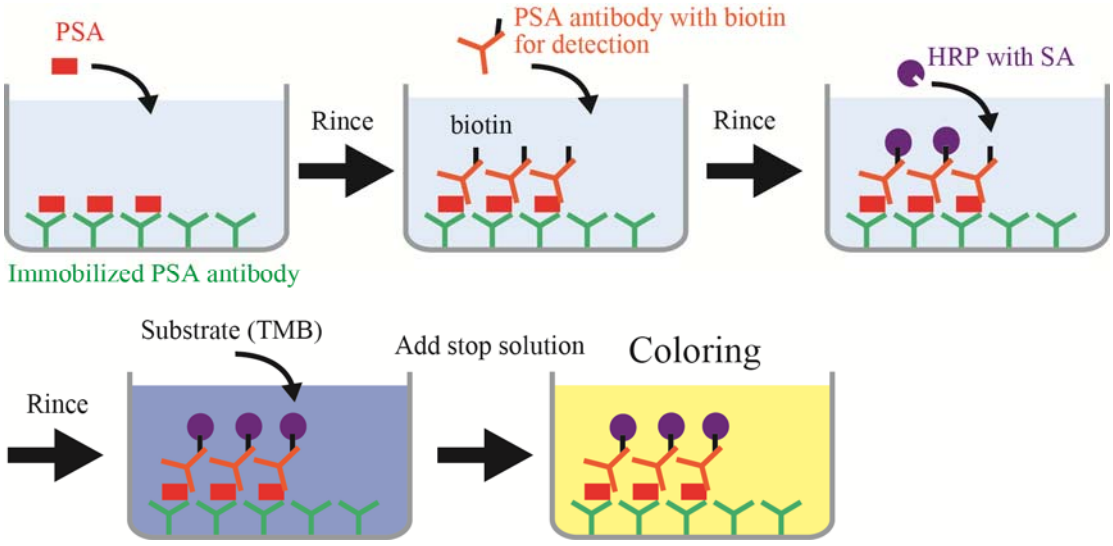

Fig. 6.3 Schematic procedure of ELISA.

6. 3. 2 **Assay of PSA by ELISA**

Then, we checked the concentration of active PSA by ELISA. ELISA is the method specific to biomarkers such as PSA due to the antibody–antigen reaction and quantitation based on the chromogenic enzyme reaction. Fig. 6.3 shows a schematic of the ELISA procedure. ELISA for PSA consists of five steps:

1. Diluted PSA solutions were injected into each well of an ELISA kit on which PSA antibody was immobilized for the adsorption of PSA.
2. The biotin-conjugated PSA antibody solution of constant concentration was injected into each well so that the PSA antibody adsorbed to the immobilized PSA for detection. The primary antibody was coupled to biotin because the biotin- SA interaction used is as a link between the primary antibody and the enzyme, horseradish peroxidase (HRP).
3. The solution of SA coupled to HRP was injected into each well for the immobilization of the enzyme through biotin-SA binding.
4. TMB regent, the substrate of peroxidase, was injected into each well to develop the color by enzyme reaction.
5. Stop solution (0.2 M H_2SO_4) was injected to halt the progression of the enzyme reaction.

The bonds between PSA and PSA antibody through the antibody–antigen reaction were formed in proportion to the concentration of PSA solution, as were those between SA and biotin. Thus, the intensity of the color change produced by the enzyme reaction was proportional to the concentration of PSA in the solution. Each PSA concentration was evaluated using a commercial ELISA kit (human PSA-total ELISA kit, Sigma-Aldrich Co. LLC.) and a microplate-reader, ChroMate® 4300 (Awareness Technology Inc.). TMB regent is the substrate buffer, which includes 3, 3', 5, 5'-tetra-methylbenzidine as a color former and H_2O_2. H_2O_2 is reduced by HRP; the resulting active oxygen oxidizes TMB. The reaction is stopped in a sulfuric acid environment and the oxidized TMB has an absorbance peak of 450 nm.

Figure 6.4(a) shows an optical microscope image before and after the injection of 0.2 M H_2SO_4 stop solution. Each well was filled with various concentrations of PSA, which was systematically diluted with the buffer for serum, provided with the ELISA kit. Color intensity is PSA concentration-dependent because the adsorption of HRP increases with the concentration of PSA, and the HRP enzyme reaction in turn increases with the amount of HRP adsorbed. Fig. 6.4(b) shows the comparison of the above dilutions of PSA and known amounts of PSA (standard sample provide with ELISA kit) according to absorbance. Fig. 6.4(b) shows that the absorbance of both samples increased linearly in

the absorbance range of 0.01–3, but the linear absorbance ranges for both samples occurred over different concentration ranges. We therefore calibrated the PSA concentration by comparison to the absorbance of 1 μM PSA, which, when estimated by dilution ratio, was evaluated as 100 nM. This value was less than the value obtained by Micro-BCA assay. Generally, the Micro-BCA assay quantitates the amount of total protein, regardless of protein activity. On the other hand, ELISA quantitates the amount of immunologically active protein because ELISA is based on the antibody–antigen reaction. Therefore, it is reasonable for the results of the Micro-BCA assay to differ from those of the ELISA. We evaluated the concentration of the above dilution of PSA as 100 nM because the nanolaser sensor also assays PSA on the basis of the antibody–antigen reaction. The calibrated concentration of PSA was used for the following measurement.

6. 4 Optimization of the concentration of PSA antibody

This section describes the optimization of the concentration of PSA antibody solution immobilized on the nanolaser sensor surface. The immobilization of PSA antibody is an important process because the PSA antibody provides nanolaser sensor specificity for PSA, and the adsorption of PSA depends on the PSA antibody. First, we checked the immobilization of PSA antibody by repeated and long-duration measurement in the PSA antibody solution. Then, we optimized the concentration of PSA antibody by comparison of the wavelength shift due to PSA at each concentration of PSA antibody.

6. 4. 1 Optimization of immersion time in the antibody solution

The process of immobilization of PSA antibody until silanization was shown in 3. 3. A sensor chip was immersed in 2.5% GA solution diluted water for 1 h and then rinsed in pure water for 5 min. Because GA has two aldehyde groups, which are coupled to an amino group, GA serves as a bridge between the sensor surface and PSA antibody. The chip was set in a brief micro-fluidic channel filled with 10 μM PSA solution and then the channel was set on the sample stage of a μ-PL set as shown in 2.4. The laser wavelength was measured repeatedly. Fig. 6.5 shows the wavelength shift by the absorption of PSA antibody as a function of time. The wavelength shift increased until the 60-min time point and was maintained over 1.5 h. A slight blueshift was observed at the time of water injection due to a decrease in the refractive index of the solution. The immobilization of PSA antibody was confirmed and we adopted 1 h as the optimal immersion time because wavelength shift saturation was observed after 1 h.

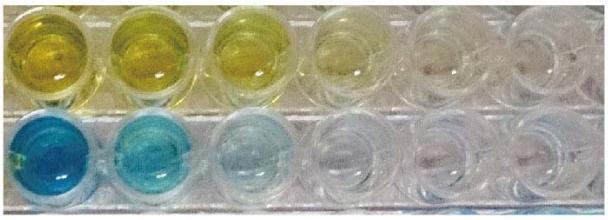

(a)

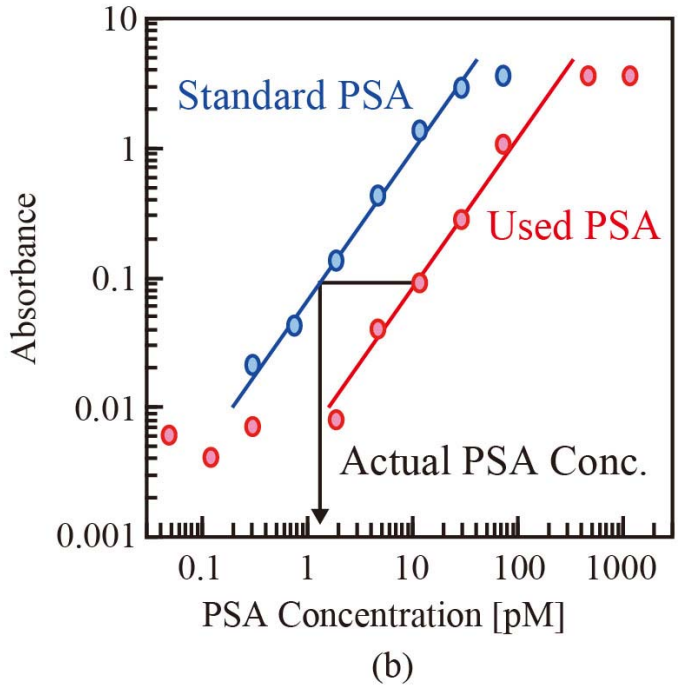

(b)

Fig. 6.4(a) Optical microscope images before (lower wells) and after (upper wells) the injection of stop solution. (b) Comparison between the absorbance of PSA standards and diluted PSA samples.

6. 4. 2 **Optimization of the adsorption of PSA antibody**

To optimize concentration of PSA antibody immobilized on the sensor chip, the wavelength shift by PSA was measured at each concentration of PSA antibody. The process of biosensing until functionalization of GA was the same as above. The processes of PSA antibody immobilization and absorption of PSA were as follows:

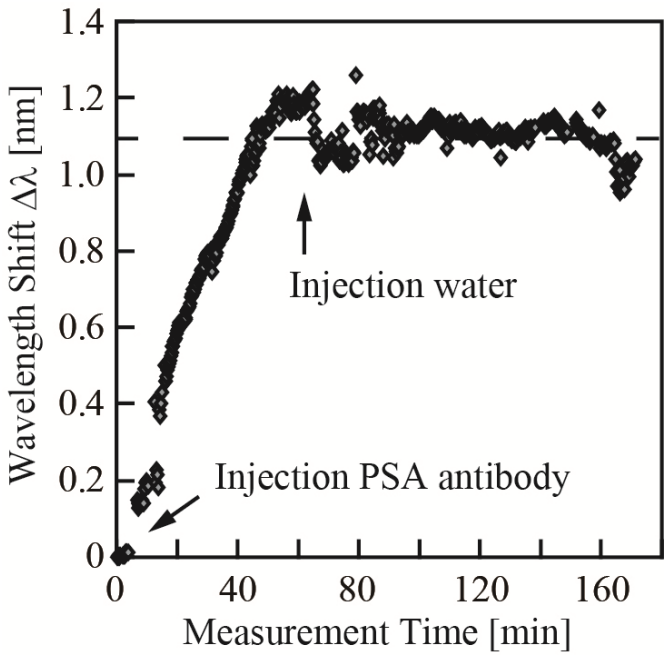

Fig. 6.5 Wavelength shift by PSA antibody as a function of measurement time.

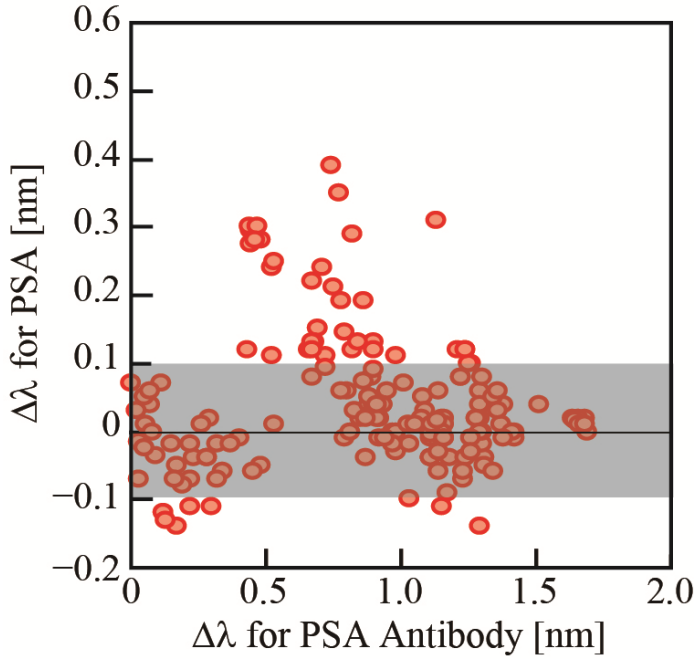

Fig. 6.6 Δλ due to PSA as a function of Δλ due to PSA antibody. The range of the wavelength shift from −0.1 nm to 0.1 nm shows no significant shifts due to the fluctuation of the nanolaser itself.

1. The sensor chip was immersed in 1–50 μM (6.7–335 nM) PSA antibody solution for 1 h at 25–37 °C.
2. The chip was rinsed in pure water for 5 min and $\Delta\lambda_{ant}$ was measured in pure water.
3. The chip was immersed in 1 pM PSA solution for 1 h at 25 °C.
4. The chip was rinsed in pure water for 5 min and $\Delta\lambda$ was measured in pure water.

Figure 6.6 shows $\Delta\lambda$ for 1 pM PSA plotted as a function of $\Delta\lambda_{ant}$ for the PSA antibody, where the antibody was immobilized with the various concentrations and temperatures. The fluctuation of the peak wavelength between repeated and long-duration measurements was ±0.06 nm. In this study, a shift of more than ±0.1 nm was considered to be significant. A significant shift in PSA was observed when the shift for the antibody was 0.7–0.8 nm. Figure 6.7 describes the concentration limits of the PSA antibody. When the shift in antibody concentration is small, PSA adsorption should be limited by the decrease in available antibody. When the shift is large, on the other hand, PSA adsorption might be limited by steric hindrance and other factors that are due to the excess adsorption of the antibody. In subsequent experiments, the concentration of the PSA antibody was set to 67 nM and the temperature to 37 °C, for which $\Delta\lambda$ for the antibody was 0.8 nm. The 13 nM control antibody was also used, for which $\Delta\lambda$ for the antibody was the same value.

6. 5 **Sensing in pure water**

For the demonstration of the high sensitivity detection of PSA-specific adsorption, the sensing of PSA in pure water was performed using the nanolaser. The PSA sensing process was as follows:

1. The sensor chip with the antibody was prepared by the process shown in Chapter 3. However, the concentration of PSA antibody was 67 nM, the concentration of mouse antibody was 13 nM and the temperature was 37 °C.
2. The wavelength in pure water was measured after rinsing with pure water for 5 min.
3. A series of PSA solutions was prepared and the chip was immersed in the PSA solution of lowest concentration for 20 min at 25 °C.
4. Steps 2 and 3 were repeated at lower concentrations of PSA solution.

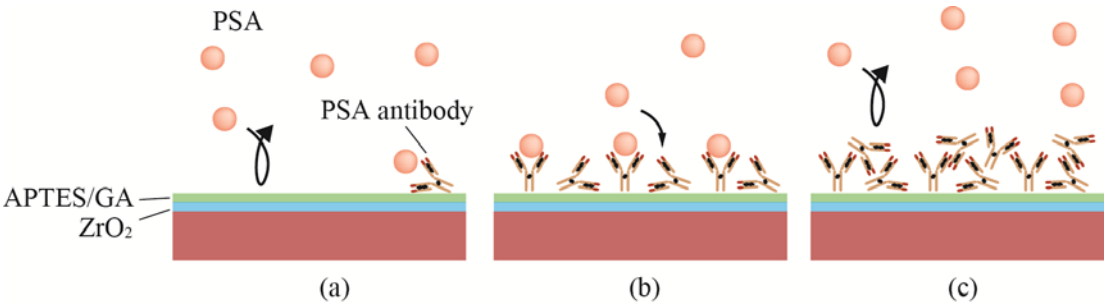

Fig. 6.7 Concentration limits of the PSA antibody. The PSA antibody concentration is (a) low, (b) optimal value and (c) high.

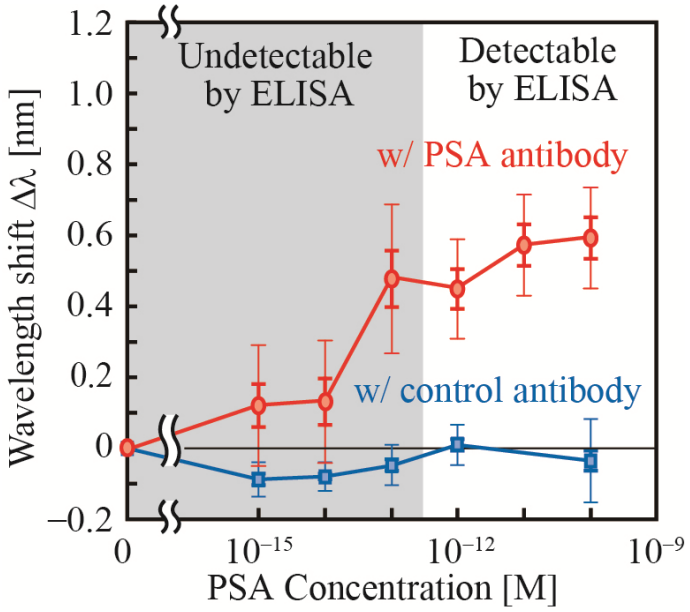

Fig. 6.8 PSA sensing in pure water. Circular and square plots show the wavelength shift with PSA antibody as a target and mouse antibody as a negative control, respectively.

Figure 6.8 summarized Δλ with the PSA concentration for the solution. The devices functionalized with anti-PSA antibody exhibit the wavelength redshifts at a PSA concentration of 100 fM, which is lower than the detection limit of the standard ELISA. On the other hand, the devices with the control antibody only exhibited a spectral fluctuation within 0.06 nm (noise level) regardless of the PSA concentration. Thus, PSA was specifically detected at very low concentrations. However, there was a problem which the fluctuation of this sensing between different trials.

6. 6 Sensing in impure water

To investigate selectivity against a contaminant, sensing in the impure sample was performed. The process of PSA sensing in impure sample was as follows:

1. Sensor chips were prepared with PSA antibody or control antibody as outlined in Section 6.5.
2. Δλ in pure water was measured after rinsing with pure water for 5 min.
3. The chips were immersed in a series of PSA solution mixed with 0.1% Tween 20 as a surfactant and the BSA series (100 nM, 1 μM, and 10 μM) for 1 h at room temperature.
4. Steps 2 and 3 were repeated for PSA solutions of lower concentration.

Fig. 6.9 shows Δλ as a function of each process, such as the immobilization of PSA antibody and the mixture without PSA (the solution including BSA and Tween 20). Δλ by the absorption of PSA antibody was 0.5 nm and that of mouse antibody as a control was 1.5 nm. The difference was due to the conditions of antibody adsorption. This sensing was not used under the above optimized conditions. Fig. 6.10 summarizes the PSA-concentration dependence of Δλ in impure samples to compare antibody conditions, with 100 nM, 1 μM, and 10 μM BSA. The Δλ was shown as the shift in wavelength after the solution was mixed without PSA. Δλ for PSA antibody redshifted from 10–100 fM PSA. On the other hand, Δλ for the control antibody did not redshift, except when 10 μM BSA was included. At the 10 μM BSA concentration, the difference between PSA and control antibody was not observed because of the high

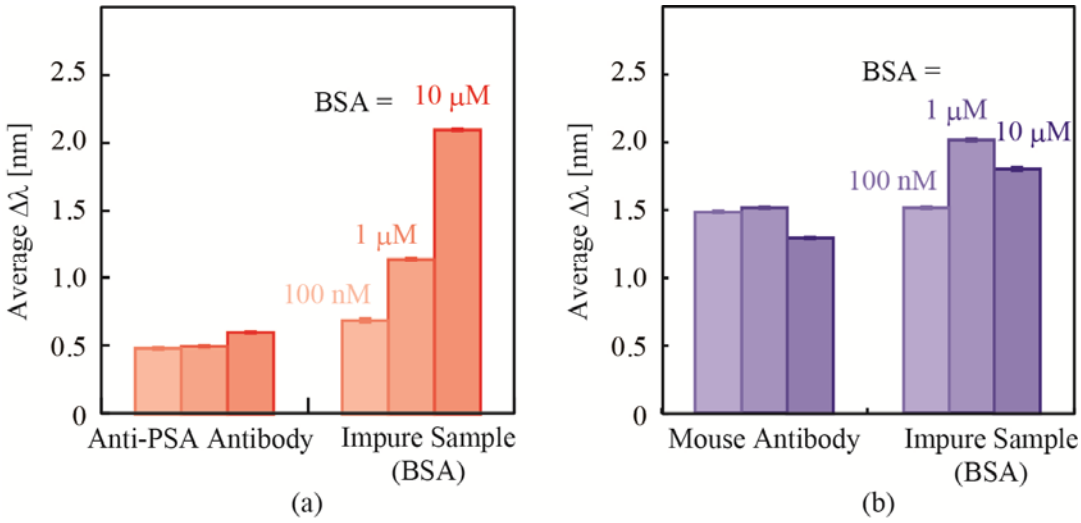

Fig. 6.9 Δλ as a function of each process of the adsorption of antibody and impure sample without PSA. (a) PSA antibody, (b) mouse antibody as a control.

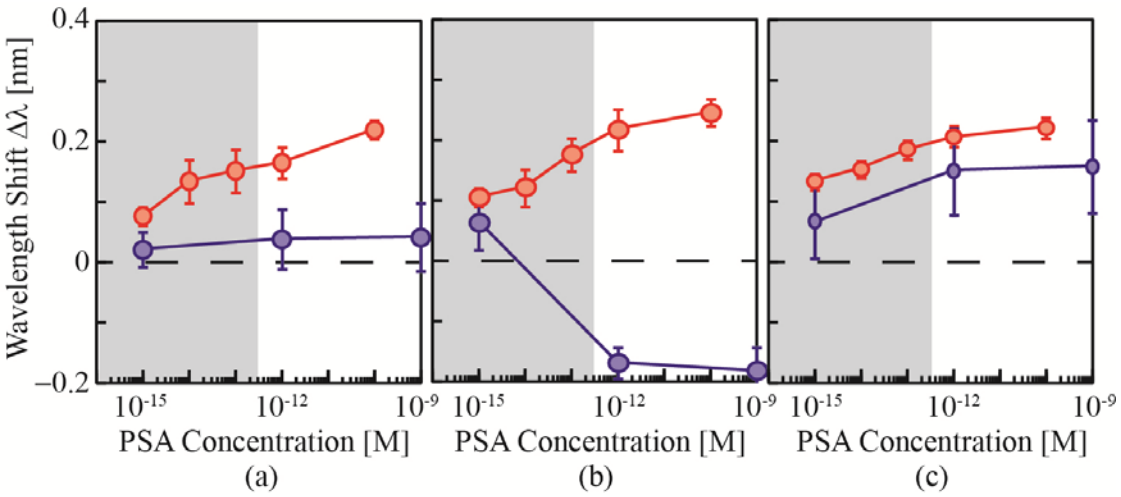

Fig. 6.10 PSA sensing in impure samples. (a) 100 nM BSA, (b) 1 μM BSA, (c) 10 μM BSA. Red and blue plots show Δλ with PSA antibody as a target and mouse antibody as a negative control, respectively. The gray area shows the area undetectable by ELISA.

concentration of a contaminant. At the 1 μM BSA concentration using the control antibody, Δλ blueshifted with PSA concentration. Excess adsorption of control antibody was considered to be desorbed by competitive adsorption. This blueshift was expected to be suppressed by the above optimized antibody immobilization. Furthermore, Δλ with PSA antibody redshifted at a lower concentration of PSA than that of PSA sensing in pure sample. This was because Tween 20 relaxed the surface hydrophobicity, as discussed in the following Section 6.7.4.

Detection of 10–100 fM PSA was demonstrated in impure samples with a contaminant of 1 μM BSA. However, this sensing with and without a contaminant has some fluctuation; therefore, the following section will investigate the source of the fluctuation and ways to improve upon the consistency of sensing.

6. 7 **Improvement**

To improve the stability of Δλ due to PSA adsorption, this section investigated the condition of the modification, the effect on the sensitivity by the nanolaser structure, and the EA modification. Firstly, the temperature and time of PSA adsorption was optimized. Secondly, the effects of fluctuation of NS width w_{NS} and circular diameter $2r$ was investigated. Thirdly, the APTES concentration of 0.5% and 0.05% was compared and discussed for the stable biosensing. Fourthly, to suppress the surface hydrophobicity, the EA modification was added and the effect was investigated.

6. 7. 1 Conditions of surface modification

This section investigated temperature and immersion time of PSA adsorption. The procedure was as follows:

Procedure for investigating temperature dependence:

1. Four sensor chips were prepared with PSA antibody as Section 6.5.
2. $\Delta\lambda$ in pure water was measured after rinsing with pure water for 5 min.
3. The chips were immersed in 1 pM PSA solution at 24 °C, 30 °C, 35 °C, and 40 °C for 20 min.
4. $\Delta\lambda$ were measured in pure water after rinsing with pure water for 5 min.

Procedure of investigating immersion time dependence:

1. The four sensor chips were prepared with PSA antibody as above.
2. $\Delta\lambda$ in pure water was measured after rinsing with pure water for 5 min.
3. The chips were immersed in 1 pM PSA solution at room temperature (26 °C) for each immersion time of 20, 40, and 60 min.
4. $\Delta\lambda$ was measured in pure water after rinsing with pure water for 5 min.

Figure 6.11 summarizes the temperature dependence and time dependence of adsorption. As seen in Fig. 6.11(a), a clear difference in $\Delta\lambda$ was not observed until 35 °C, and $\Delta\lambda$ at 40 °C redshifted slightly. Generally, the antibody–antigen reaction was effective at 37 °C and this temperature is considered a suitable condition. In Fig. 6.11(b), $\Delta\lambda$ increased linearly with immersion time. Thus, past sensing of PSA did not measure saturated adsorption at the concentration, but rising adsorption. The rising adsorption might cause fluctuation; therefore, an immersion time of 1 h was adopted because the adsorption was roughly saturated at 1 h. Therefore, 37 °C and 1 h were adopted as the optimal conditions of PSA adsorption.

6. 7. 2 Evaluation of sensitivity at different NS width and circular diameter

To investigate the source of the instability of PSA sensing, we checked w_{NS} and $2r$ dependency of $\Delta\lambda$ for 1 pM PSA. The process of surface modification was approximately the same as described in Section 6.5. However, the modification of GA and the absorption of PSA were done at 37 °C for 1 h. Four chips were modified for functionality at the same time to suppress fluctuation due to the modification. Fig. 6.12 summarizes w_{NS} and $2r$ dependency of $\Delta\lambda$ for 1 pM PSA. As seen in Fig. 6.11, w_{NS} dependency was not observed

and Δλ was 0–0.8 nm, regardless of w_{NS}. On the other hand, 2*r* dependency was observed and Δλ tended to increase with 2*r*. The calculated sensitivity as a function of w_{NS} and 2*r* was reported [6-8]. The calculated sensitivity with NS (w_{NS} = 40–100 nm) is doubled relative to without NS. This enhancement of sensitivity due to a NS was demonstrated by measuring refractive index in liquid [6-9] and SA sensing [6-10]. However, the enhancement of sensitivity due to a NS was not clearly confirmed from this experiment. PSA absorption on the inside of a NS was considered inefficient because antibody size is generally approximately 10 nm. On the other hand, the calculated sensitivity of 2*r* in the range of 220–300 nm is roughly constant [6-8], though it was confirmed that Δλ was increased with increasing 2*r*. Thus, it can be said that the increasing Δλ was not due to the sensitivity of a nanolaser but due to the enhancement of something derived from the increasing 2*r*, such as increasing the absorption on the aspect of holes or the under surface by facilitating the circulation of the solution and PSA. From the above, the design w_{NS} of 30 nm at which NS can be constantly fabricated and the design 2*r* of 220 —230 nm as a target of fabricated 2*r* of 230–240 nm were adopted.

6. 7. 3 **Evaluation of the concentration of APTES**

This section investigated the fluctuation due to APTES. As mentioned in Chapter 3, in the present situation, the coverage of the APTES layer is low [6-11] and the contact angle of water after the APTES process includes fluctuation. Furthermore, there is a possibility that a multi-layer of APTES is formed at the conventional concentration of 0.5% because of the saturated contact angle. The multi-layer APTES is applied on the nanolaser surface

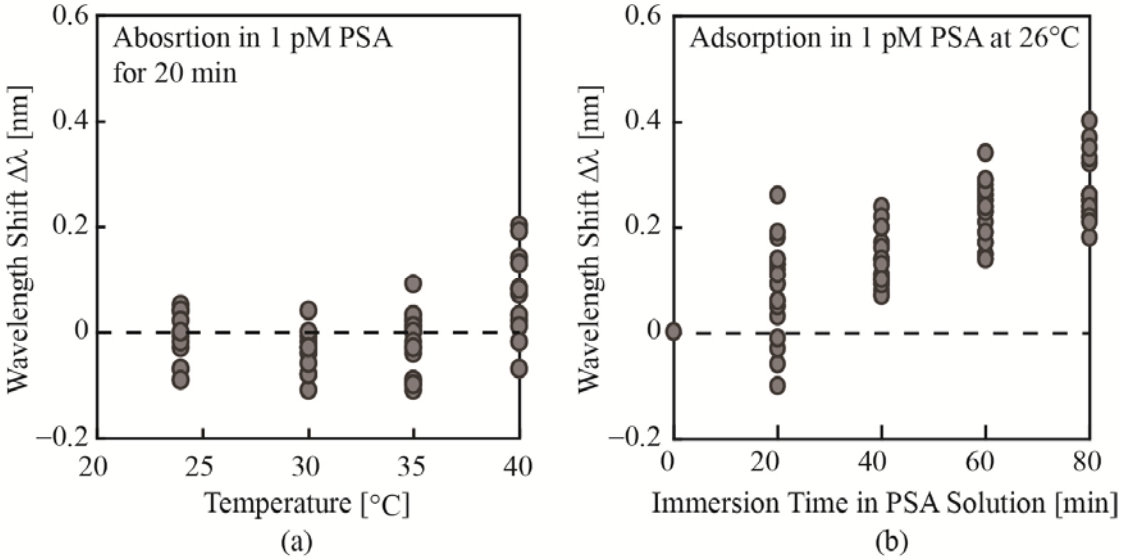

Fig. 6.11 (a) Temperature dependence of Δλ. (b) Immersion time dependence of Δλ.

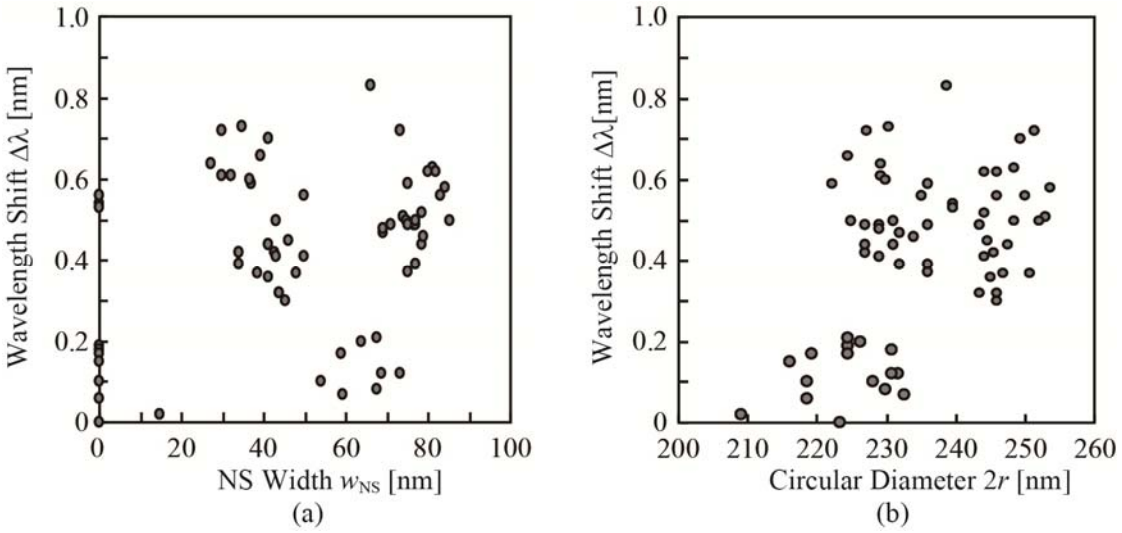

Fig. 6.12 $\Delta\lambda$ for 1 pM PSA as a function of (a) w_{NS} and (b) $2r$.

by the dehydration condensation of hydroxyl groups and also by physical adsorption [6-12]. The multi-layer APTES can become the source of background noise due to condensation of hydroxyl groups and also because physical adsorption is not a stable linkage as is the covalent bond. Thus, the modification of 0.05% APTES was compared with that of 0.5% APTES. The concentration of 0.05% was adopted because the contact angle did not saturate and a monolayer was considered to form at this concentration. The sensing process was the same as in section 6.7.2, except for the concentration of APTES and the additional process of ethanolamine (EA). The process of EA and its effect is shown later in Section 6.8.4. Three trials with PSA antibody were performed for each concentration of APTES. Fig. 6.13 shows $\Delta\lambda$ as a function of PSA concentration. When the concentrations of 0.5% and 0.05% were compared, the overall $\Delta\lambda$ shift with the 0.05% APTES modification was larger than with 0.5% APTES. Thus, it was concluded that the modification of the concentration to 0.05% prevented APTES from forming multi-layer. However, increasing fluctuation was observed in Trial 1, shown in Fig. 13(b). It was concluded that APTES partially covered the sensor surface and a difference in the modification ratio between each device occurred. To perform quantitative measurement, the stable modification of APTES has to been further investigated, but it can be said that the stability of biosensing improves by increasing the signal with the modification of 0.05% APTES.

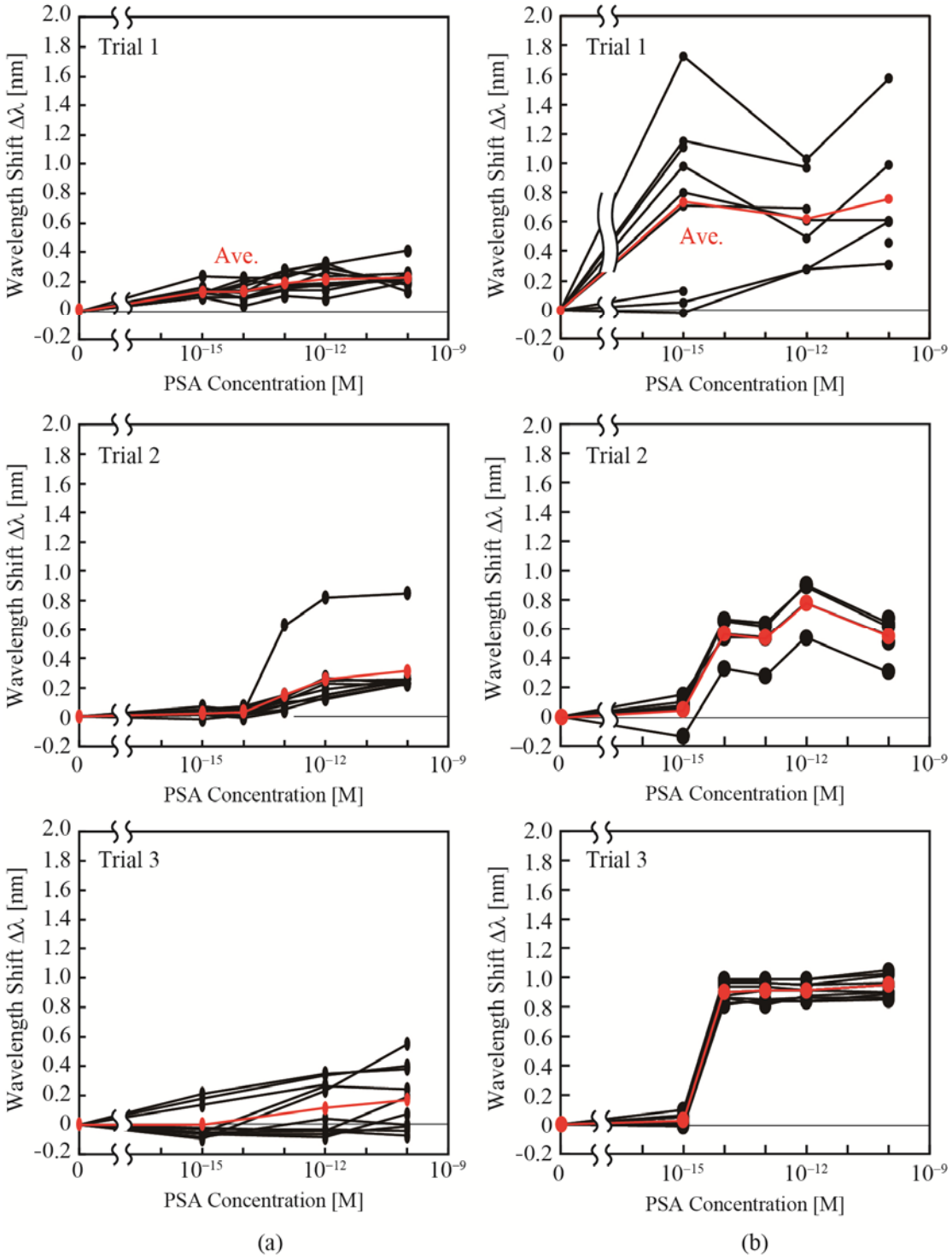

Fig. 6.13 Comparison of the concentration of APTES by Δλ as a function of PSA concentration. The concentrations are (a) 0.5% and (b) 0.05%. Black and red plots show Δλ of each device in a nanolaser array and averaged Δλ, respectively.

Fig. 6.14 Structure of EA.

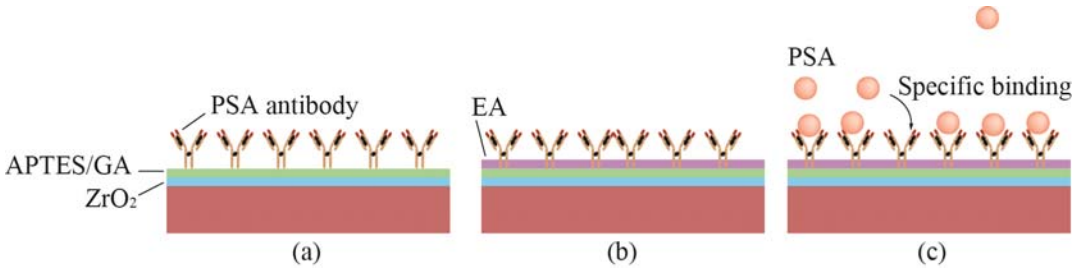

Fig. 6.15 A schematic of biosensing with the EA modification. Each procedure is (a) immobilization of PSA antibody, (b) a modification of EA and (c) PSA adsorption.

6. 7. 4 **Relaxing of the surface hydrophobicity by ethanolamine**

EA is a surfactant with an amino group and a hydroxyl group as shown in Fig. 6.14. Some effects were expected following EA treatment. First, EA was expected to wash the physically adsorbed antibodies by hydrophilization. Secondly, EA was expected to suppress additional physical adsorption of BSA by blocking unbound GA. Thirdly, EA was expected to suppress excessive hydrophobicity at the nanoscale rough surface by hydrophilizing the sensor surface so that biomarkers could efficiently penetrate the holes in the photonic crystal slab and approach the antibody. As described above, large 2*r* facilitated of the absorption on the aspect of holes or the under surface by facilitating the circulation of the solution and PSA. EA was expected to increase $\Delta\lambda$ of a device with PSA antibody and improve the sensitivity of detection. A schematic of biosensing was shown in Fig. 6.15 and the process added the modification of EA was as follows:

1. The sensor chips were prepared with the antibody (PSA antibody or control antibody) by the process shown in Chapter 3. However, the optimized conditions of APTES concentration, antibody concentration, and temperature for the immersion of GA solution and the concentration of PSA and control antibody were adopted: the concentration of APTES was 0.005%, temperature for the immersion of GA and antibody solutions was 37 °C, the concentration of PSA antibody was 67 nM and the concentration of control antibody was 13 nM.
2. The chips were immersed in 1 M EA solution diluted with pure water for 1 h at

37 °C. This concentration was not optimized and 1 M was adopted as a high enough concentration for the modification.

3. The chips were rinsed with pure water over 5 min and then Δλ was measured in pure water.
4. The chip was immersed in a series of PSA solutions. In the sensing of PSA in pure sample, a set of the concentration of PSA solution diluted pure water was used. In the sensing of PSA in impure sample, the PSA solution mixed with 1 μM or 10 μM BSA as a contaminant and 0.1% Tween 20 as a surfactant was used.
5. Δλ was measured after rinsing for 5 min.
6. The process of 4 and 5 from lower PSA concentration was repeated.

In the following section, the EA modification was evaluated by the PSA concentration dependency of Δλ in pure and impure samples.

6.7.4.1. Sensing in pure sample

Figure 6.16 summarizes Δλ as a function of PSA concentration to compare Δλ for various PSA concentrations, for antibody conditions, and with the inclusion of ethanolamine. Each plot shows an average value based on the results from 10 to 25 nanolasers measured simultaneously; the inner and outer error bars show the standard error and standard deviation, respectively. With the PSA antibody, a significant shift appeared from the PSA concentration of 100 fM even without EA as shown in Fig. 6.8. With EA, the shift appeared from 1 fM and the shift was approximately two times greater than that observed at 100 fM. In contrast, for the devices with the control antibody and without antibodies, no significant shifts were observed for any PSA concentrations; these observations were truly independent of the inclusion of EA in this experiment. However, some fluctuations were also observed in such selective detection between trials and evaluated in the Section 6.9. In general, EA as a surfactant is expected to suppress the physical adsorption of proteins by blocking unbounded GA and washing out the physically adsorbed antibodies and antigen by hydrophilization. However, the results suggest that the expectation that EA would suppress the shift for the control antibody was not valid. Another expectation of EA, which explains the observations, is the suppression of excessive hydrophobicity at the nanoscale level of rough surfaces by hydrophilizing the device surface. This allows the antigen to effectively penetrate holes in the photonic crystal slab and approach the antibody. Thus, the merit of the EA modification for PSA sensing using a nanolaser sensor was demonstrated and high sensitivity detection of 1 fM PSA was achieved.

6.7.4.2. Sensing in impure water

Figure 6.17 shows Δλ for the PSA concentration, where the wavelength in the impure samples without PSA was used as a reference. For the device with the PSA antibody, a significant shift occurred from the PSA concentration of 1 fM, which is comparable with the case without the contaminant. Increasing the concentration of contaminant from 1 μM to 10 μM, the shift in PSA decreased overall, but was still sufficient. Conversely, the device with the control antibody exhibited a blueshift with increasing PSA concentration. Similar blueshifts were observed repeatedly when the chip was soaked in the impure sample with the same concentration of contaminant, as shown in Fig. 6.18. This measurement used the above mixed solution without PSA and the biosensing process was the same. Furthermore, the trial without immersion in mixed solution, in other words, the trial in which only a rinse was performed, was checked, but the blueshift was not observed. The source of the blueshift was not considered to be due to the desorption of BSA but to the competitive adsorption of BSA. The APTES, which is the base used to immobilize the antibody, is applied on the nanolaser surface by the dehydration condensation of hydroxyl groups and also by physical adsorption. When the chip was soaked in the solution with a high concentration of the contaminant, the desorption of APTES without chemical coupling may have occurred due to competitive adsorption of

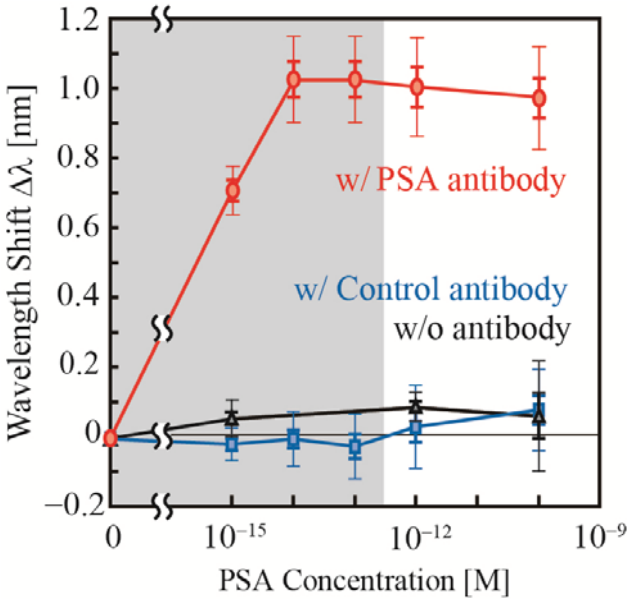

Fig. 6.16 SA sensing in pure water for the device with the modification of EA. Circular (red), square (blue) and triangular (black) plots show the wavelength shift with PSA antibody as a target, mouse antibody as a negative control, and without the antibody, respectively. Gray area shows the undetectable range of the concentration by ELISA.

the contaminant; this resulted in the desorption of the antibody and the blueshift.

PSA (1 fM), which is much lower than the detection limit of the standard ELISA technique, was detected using the nanolaser sensor even in 10^{10}-fold impure sample. This means that the nanolaser could detect 100 fM PSA from human serum, which include 1 mM contaminant such as albumin, after diluting it 100 times when the detection is performed in blood.

6. 8 **Evaluation of fluctuations**

There were fluctuations in $\Delta\lambda$ for PSA detection. Thus, the distribution of the wavelength shift in 3–6 experiments for the devices with the PSA antibody or with the control antibody, and the results, summarized by the histogram analysis, were evaluated. The method of the histogram analysis was as follows:

1. The values of $\Delta\lambda$ in the interval of 0.2 nm from −0.5 nm to 1.5 nm for each trial at the set concentration were summed.
2. The distribution of $\Delta\lambda$ was displayed as percentages.
3. The distribution between trials was summed and the total distribution was set at 100%.
4. Steps 1–3 were repeated for each concentration (1 fM, 10 fM, 100 fM, 1 pM, and 100 pM PSA)

Figure 6.19 summarizes the distribution of $\Delta\lambda$ for PSA detection for the comparison of antibody condition and EA condition. Fig. 6.19(a) displays the distribution of each trial in different colored bars and Fig. 6.19(b) displays the distribution sorted until −0.1 nm, from −0.1 nm to 0.1 nm, and over 0.1 nm for the comparison of the significant shift distinguishing from noise level ($|\Delta\lambda| < 0.1$ nm). Significant shifts appeared for the PSA antibody even without the inclusion of EA. The shifts were observed from 1 fM, but the majority of the shifts started from 1 pM. With EA, the yield was improved; shifts were observed from 1 fM in many nanolasers and trials. Even with the control antibody, the effect of EA was observed; the shift was almost suppressed without EA, while some devices exhibited significant shifts with EA.

Here, let us evaluate the fluctuation by standard deviation σ of $\Delta\lambda$. Limited to individual trials for antibody condition, PSA concentration and EA condition, σ was almost less than 0.1 nm and the increasing σ due to the EA modification was not observed. On the other hand, σ of $\Delta\lambda$ in the sum of trials for each concentration tended to increase. Without the EA modification, σ for the PSA antibody was 0.1–0.2 nm and that of the control antibody was approximately 0.1 nm. With the EA modification, σ for PSA

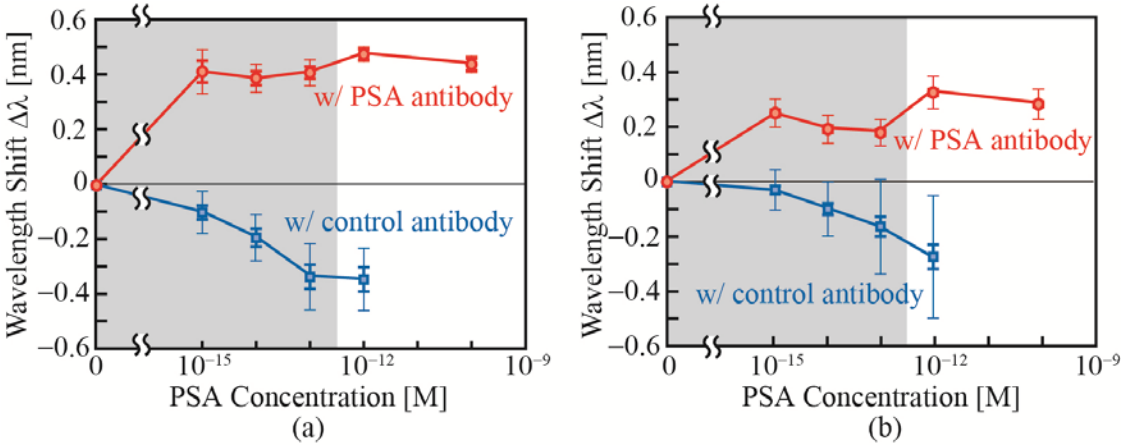

Fig. 6.17 PSA sensing in the impure sample, where ethanolamine was used. Concentrations of contaminant, BSA, were (a) 1 μM and (b) 10 μM.

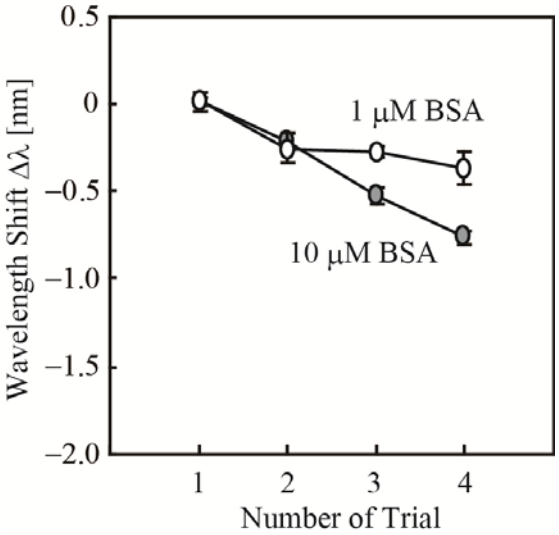

Fig. 6.18 Blueshift due to multiple trials of the above mixed solution. Filled plots and open plots show Δλ for 10 μM and 1 μM BSA.

antibody and control antibody was 0.3–0.4 nm. As aforementioned, the fluctuation between trials was larger than within trials and the fluctuation between trials was emphasized by the EA modification. We took into consideration that there were still differences in the functionality of the antibody between trials. Therefore, it may be necessary at the present stage to repeat the measurement in order to conduct statistical analysis. An important advantage of using nanolasers is that we can integrate a very large number of nanolasers on a chip and obtain statistical data easily from the automatic

measurement. This advantage is effective for decreasing the σ on a chip and in the quantification. The fluctuation between trials can be suppressed by further optimization of functionality. For instance, APTES coating of the ALD is expected to be a stabilizing modification. This method is predicted to suppress fluctuations in manual operation. Thus, the fluctuation between trials will be ideally decreased to the limit of the nanolaser sensor.

Reference

[6-1] M. K. Brawer, "Prostate-Specific Antigen," *Surg. Oncol.* Vol.18, pp. 3–9, 2000.

[6-2] H. Yu, E.P. Diamandis, A. F. Prestigiacomo, and T. A. Stamey, "Ultrasensitive assay of prostate-specific antigen used for early detection of prostate cancer relapse and estimation of tumor-doubling time after radical prostatectomy," *Clin. Chem.,* vol 41, pp. 430–434, 1995.

[6-3] American Cancer Society, "Cancer facts & figures 2010," < http://www.cancer.org/research/cancerfactsstatistics/cancerfactsfigures2010/index >.

[6-4] G. A. R. Y. Suaifan, C. Esseghaier, A. Ng, and M. Zourob, "Wash-less and highly sensitive assay for prostate specific antigen detection," *Analyst*, vol. 137, no. 23, p. 5614, 2012.

[6-5] Y. D. Ivanov, V. M. Govorun, V. A. Bykov, and A. I. Archakov, "Nanotechnologies in proteomics," *Proteomics.* vol. 6, no. 5, pp. 1399–1414, 2006.

[6-6] K. Matsumoto, N. Konishi, T. Samori, E. Kimura, M. Doi, S. Kato, and Y. I. Yuki, "ELISA for a complexed antigen with a monoclonal antibody blocking reaction with the free antigen - Assay-specific for complexed prostate- specific antigen," *J. Immunol. Methods*, vol. 234, no. 1–2, pp. 99–106, 2000.

[6-7] T. Osnes, O. Sandstad, V. Skar, M. Osnes, and P. Kierulf, "Total protein in common duct bile measured by acetonitrile precipitation and a micro bicinchoninic acid (BCA) method," *Scand. J. Clin. Lab. Invest.*, vol. 53, no. 7, pp. 757–763, 1993.

[6-8] S. Kita, "Photonic crystal nanolaser sensor," Doctoral thesis (*Yokohama Nat'l Univ.*), 2012.

[6-9] S. Kita, K. Nozaki, S. Hachuda, H. Watanabe, Y. Saito, S. Otsuka, T. Nakada, Y. Arita, and T. Baba, "Photonic crystal point-shift nanolaser with and without nanoslots --- design, fabrication, lasing and sensing characteristics," *IEEE J. Sel. Top. Quantum Electron.*, vol.17, no. 6, pp. 1632–1647, 2011.

[6-10] S. Hachuda, S. Otsuka, S. Kita, T. Isono, M. Narimatsu, K. Watanabe, Y. Goshima, and T. Baba, "Selective detection of sub-atto-molar Streptavidin in 10^{13}-fold impure sample using photonic crystal nanolaser sensors.," *Opt. Express*, vol. 21, no. 10, pp. 12815–21, 2013.

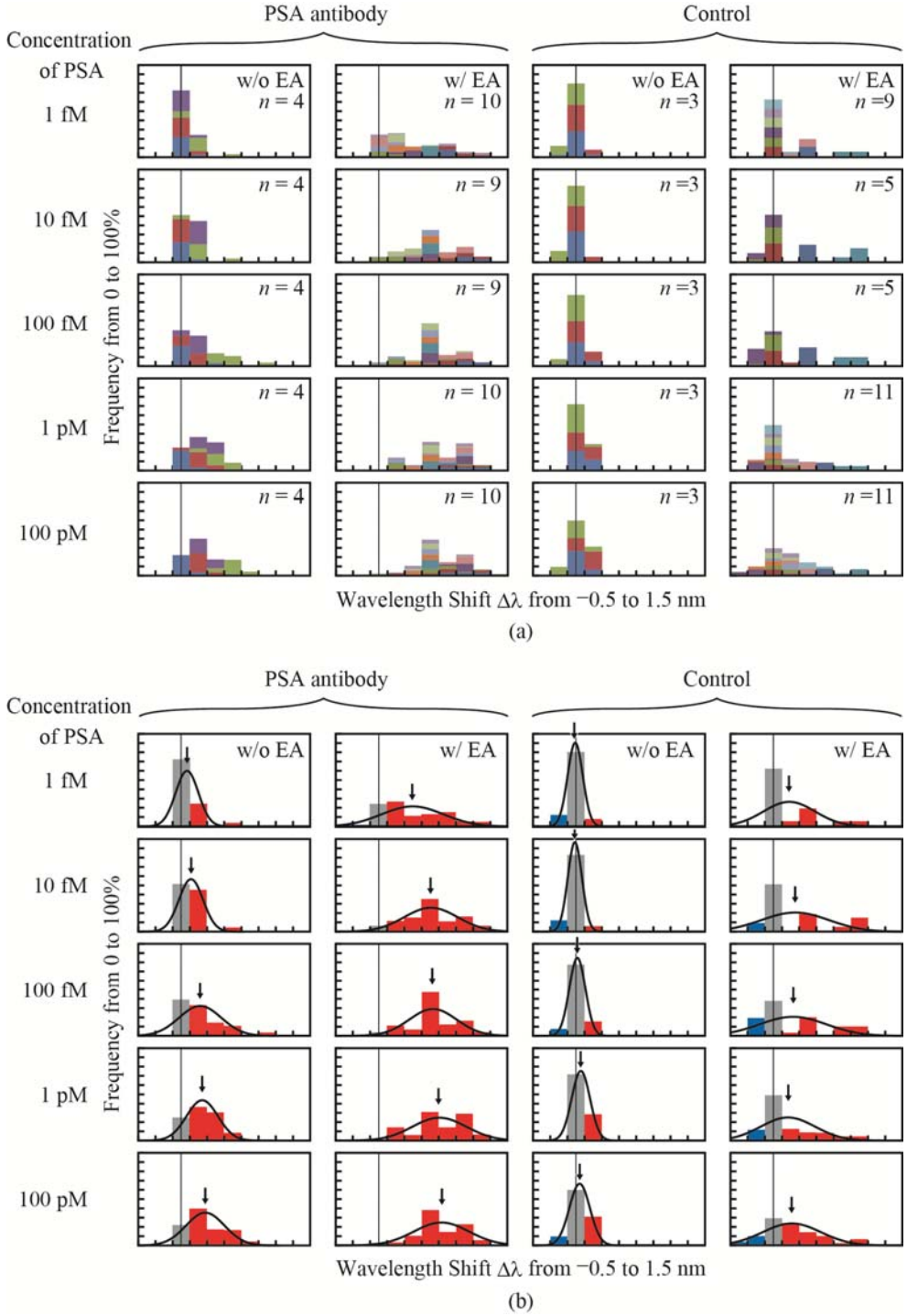

FIG. 6.19 Distribution of nanolasers showing the corresponding wavelength shifts in repeated trials. (a) Each color corresponds to a trial. (b) The red, blue, and gray bars show the frequencies that correspond to the redshift, blueshift, and no significant shifts, respectively. The black line shows the Gaussian fitting with the average value indicated by an arrow. The distribution of black lines was evaluated for the Gaussian distribution.

[6-11] P. G. Fernandes, H. J. Stiegler, M. Zhao, K. D. Cantley, B. Obradovic, R. A. Chapman, H. C. Wen, G. Mahmud, and E. M. Vogel, "SPICE macromodel of silicon-on-insulator-field-effect-transistor-based biological sensors," *Sensors Actuators, B Chem.*, vol. 161, no. 1, pp. 163–170, 2012.

[6-12] J. Kim, P. Seidler, L. S. Wan, and C. Fill, "Formation, structure, and reactivity of amino-terminated organic films on silicon substrates," *J. Colloid Interface Sci.*, vol. 329, no. 1, pp. 114–119, 2009.

Chapter 7
Comparison

This chapter evaluated the NS nanolaser performance by the comparison of other label-free sensor device and ELISA. For the fair evaluation of the performance, it is necessary to take into account the both value of K_A and DL because DL is limited by K_A between biomarkers and the corresponding to host molecules described in Chapter 1. To compare the performance, figure of merit (FOM) was difined as following equation [7-1]:

$$\mathrm{FOM} = \left(\mathrm{DL} \times K_A\right)^{-1} \tag{7-1}$$

This evaluation considered DL and K_A at the same time and normalized by those for ELISA shown in Chapter 6. Table 7.1 summarizes target biomarkers, K_A, DL and FOM. Here, the performance was evaluated by this FOM and Fig. 7.1 summarized the FOM for each biosensor. Our NS nanolaser achieves a very high FOM of 4×10^5 for BSA, 6×10^4 for SA and 10^6–10^7 (10^4–10^5) for PSA (w/o EA). FOM for each protein showed near value of 10^4–10^5 except of PSA with EA. Thus, it is reasonable that these values showed the performance of NS nanolaser. Other label-free biosensors such as PC waveguide/cavity, μ-toroidal, LSPR, SERS and FET also achieved higher FOM than that of 10^4 for ELSIA. As mentioned in Chapter 1, PC wavedguide/cavity measured the wavelength shift by the refractive chage around PC waveguide and cavity. The dsensor used the slow light effect of PC waveguide and the confinement of a cavity to improve the sensitivity. Furthermore, a NS strucuture was introducted for the more high sensitivity. However, this device has some issues such as complex measure setup and large scale device size. SPR sensor measures light intensity as a function of resonance angle of incident light through prism due to the light coupling to plasmon mode on the metal surface and it needs the device footprint is large (10^4–10^6 μm^2) resulting in high cost for the using sample. To improve the sensitivity and footprint, LSPR, which used the localization of electric field by the local pattern such as nanoparticles, was studied.and improved the sensitivity, the footprint and the special resolution. However, this method requires uniformity of nanoparticle size and shape and the stability of the

Table 7.1 The performance of biosensors

No.	Biosensor	Biomarker	K_A [M^{-1}]	DL [pM]	FOM	Reference
1	PC waveguide/cavity	BSA	10^5	1.5×10^5	67	[7-2]
		Anti-biotin	10^7	233	429	[7-3]
		SA	10^{15}	1.9×10^{-7}	5300	[7-4]
		CEA	10^{10}	5.6×10^{-4}	1.8×10^5	[7-5]
		avidin	10^{15}	10^{-3}	1	[7-6]
2	SiO_2 μ-toroidal	IL-2	10^9	5×10^{-6}	2×10^6	[7-7]
		IL-2	10^9	100	10	[7-8]
3	Ring	BSA	10^7	100	1000	[7-9]
		PSA	10^8–10^9	300	3–30	[7-10]
4	Interferometer	hCG	10^{10}	100	1	[7-11, 12]
5	SPR	IgG	10^8–10^9	0.27	10^3 – 10^4	[7-13]
		PSA	10^8–10^9	4.6	200–2000	[7-14–16]
6	LSPR	PSA	10^8–10^9	280	3–35	[7-17]
		Tau	10^7	0.2	5×10^6	[7-18, 19]
		CEA	–	8×10^{-6}	–	[7-20]
		PSA	10^8–10^9	30	30–300	[7-21]
		f-PSA	10^8–10^9	3×10^{-3}	10^5–10^6	[7-22]
7	SERS	PSA	10^8-10^9	0.12	10^4 – 10^5	[7-15, 16, 23]
		CEA	10^{10}	0.2	500	[7-24]
8	FET	SA	10^{15}	0.01	0.1	[7-25–27]
		PSA-ACT	10^{10}	11	9	[7-28]
		TnI	10^5–10^6	7000	1430	[7-29–31]
		CEA	10^{10}	5.5×10^{-4}	1.8	[7-31, 32]
		IgG	10^9	0.007	1.4×10^5	[7-33]
		PSA	10^8–10^9	2×10^{-3}	10^5 – 10^6	[7- 34]
		PSA	10^8–10^9	3×10^{-5}	10^7 – 10^8	[7-35]
		TnI	10^5–10^6	0.2	~10^7	[7-36]
		PSA-ACT	10^8–10^9	10^{-3}	10^5 – 10^6	[7-37]
9	NS nanolaser	BSA	10^7	0.26	4×10^5	[7-38]
		SA (this work)	10^{15}	1.6×10^{-8}	6×10^4	[7-39]
		PSA (w/o EA) (this work)	10^8–10^9	10^{-3} (0.1)	10^6 – 10^7 (10^4–10^5)	–
10	ELISA *	PSA	10^8–10^9	0.3	10^3 – 10^4	–

* This value was measured in Chapter 6 using commercial PSA ELISA kit.

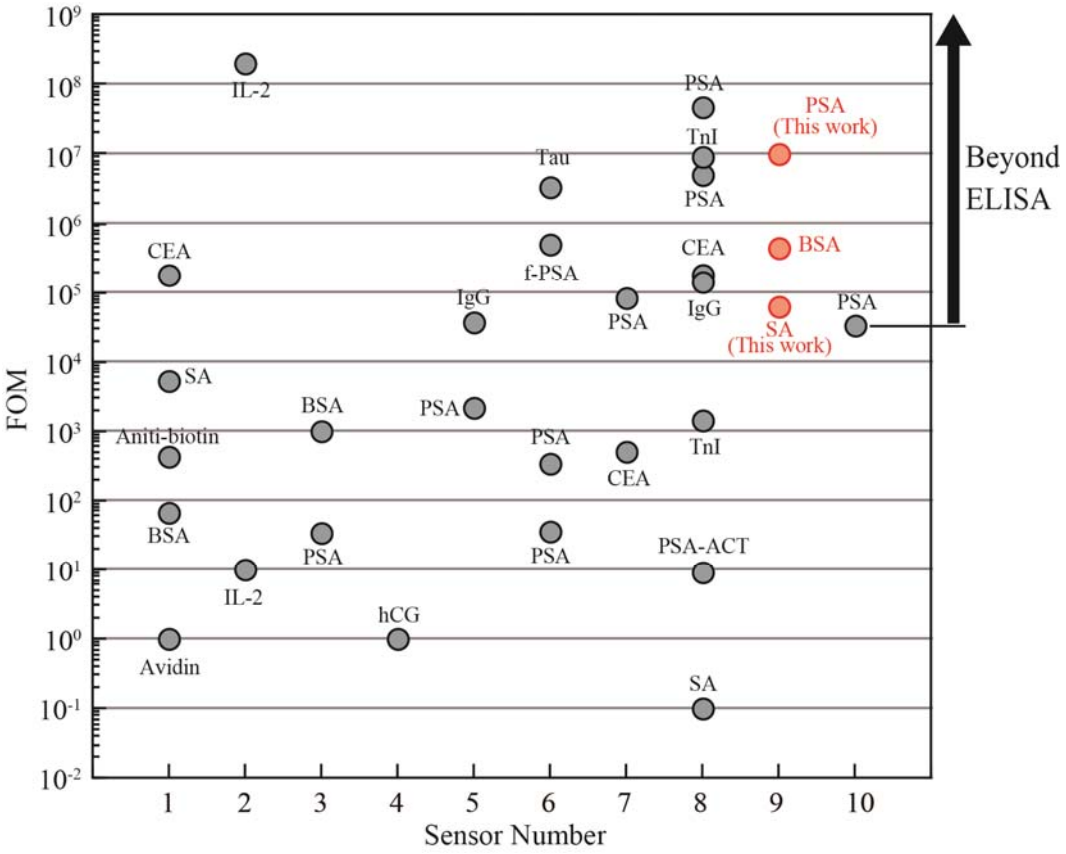

Fig. 7.1 Comparison of the sensor performance by FOM. Each of sensor number is corresponding to the number shown in Table 7.1.

attachment of the biomolecules to probe such as nanoparticles. Thus, the reproducibility is still a challenging. μ-toroidal biosensor measures resonance wavelength shift by whispering gallery mode and achieves high sensitivity by the very high *Q* factor. On the other hand, the sensing system is very complex. SERS identify sample from the spectrum of Raman scattering and is enhanced by local plasmon resonance which is one of most effective method for Raman scattering. However, the signal is noisy and unstable due to the lack of the uniformity of metal pattern which often has fabricated by Au nanoparticles. FET biosensor measures the changes in its electrical properties. FET biosensor has often improved by the modification of carbon nanotubes or grapheme, but the fabrication is the lack of reproducibility. Thus, it is not suitable for the large scale fabrication. As mentioned above, none of them simultaneously satisfy all the requirements of practical medical sensors. On the other hand, NS nanolaser has suitable characteristic for the biosensing, which are low cost, disposable use, simple procedure, and high sensitivity.

Furthermore, the nanolaser achieved a very high selectivity of (BSA/PSA) = 10^{10}. In this way, the nanolaser sensor could have all requirements for the biosensing.

Reference

[7-1] T. Baba, "Biosensing using photonic crystal nanolasers," *MRS Commun.*, vol. 5, no. 4, pp 555–564, 2015.

[7-2] R. G. Heideman and P. V. Lambeck, "Remote opto-chemical sensing with extreme sensitivity: Design, fabrication and performance of a pigtailed integrated optical phase-modulated Mach-Zehnder interferometer system," *Sensors Actuators, B Chem.*, vol. 61, pp. 100–127, 1999.

[7-3] S. Zlatanovic, L. W. Mirkarimi, M. M. Sigalas, M. A. Bynum, E. Chow, K. M. Robotti, G. W. Burr, S. Esener, and A. Grot, "Photonic crystal microcavity sensor for ultracompact monitoring of reaction kinetics and protein concentration," *Sensors Actuators, B Chem.*, vol. 141, no. 1, pp. 13–19, 2009.

[7-4] D. Yang, S. Kita, F. Liang, C. Wang, H. Tian, Y. Ji, M. Lončar, and Q. Quan, "High sensitivity and high *Q*-factor nanoslotted parallel quadrabeam photonic crystal cavity for real-time and label-free sensing," *Appl. Phys. Lett.*, vol. 105, no. 6, p. 063118, 2014.

[7-5] F. Liang, N. Clarke, P. Patel, M. Loncar, and Q. Quan, "Scalable photonic crystal chips for high sensitivity protein detection," *Opt. Express*, vol. 21, no. 26, pp. 6071–6077, 2013.

[7-6] S. Chakravarty, A. Hosseini, X. Xu, L. Zhu, Y. Zou, and R. T. Chen, "Analysis of ultra-high sensitivity configuration in chip-integrated photonic crystal microcavity bio-sensors," *Appl. Phys. Lett.*, vol. 104, p. 191109, 2014.

[7-7] A. M. Armani, R. P. Kulkarni, S. E. Fraser, R. C. Flagan, and K. J. Vahala, "Label-free, single-molecule detection with optical microcavities," *Science*, vol. 317, no. 5839, pp. 783–787, 2007.

[7-8] E. Ozgur, P. Toren, O. Aktas, E. Huseyinoglu, and M. Bayindir, "Label-free biosensing with high selectivity in complex media using microtoroidal optical resonators.," *Sci. Rep.*, vol. 5, p. 13173, 2015.

[7-9] K. De Vos, J. Girones, T. Claes, Y. De Koninck, S. Popelka, E. Schacht, R. Baets, and P. Bienstman, "Multiplexed antibody detection with an array of silicon-on-insulator microring resonators," *IEEE Photonics J.*, vol. 1, no. 4, pp. 225–235, 2009.

[7-10] T. Taniguchi, A. Hirowatari, T. Ikeda, M. Fukuyama, Y. Amemiya, A. Kuroda, and S. Yokoyama, "Detection of antibody-antigen reaction by silicon nitride slot-ring biosensors using protein G," *Opt. Commun.*, vol. 365, pp. 16–23, 2016.

[7-11] I. T. Huhtaniemi, C. C. Korenbrot, and R. B. Jaffe, "hCG binding and stimulation of testosterone biosynthesis in the human fetal testis," J. Clin. Endocrinol. Metab., vol. 44, no. 4, 963–967, 1977.

[7-12] B. H. Schneider, J. G. Edwards, and N. F. Hartman, "Hartman interferometer: versatile integrated optic sensor for label-free, real-time quantification of nucleic acids, proteins, and pathogens," *Clin. Chem.*, vol. 43, no. 9, pp. 1757–1763, 1997.

[7-13] W. C. Law, K. T. Yong, A. Baev, R. Hu, and P. N. Prasad, "Nanoparticle enhanced surface plasmon resonance biosensing: Application of gold nanorods, " *Opt. Express*, vol. 17, pp. 19041–19046, 2009.

[7-14] G. A. J. Besselink, R. P. H. Kooyman, P. J. H. J. van Os, G. H. M. Engbers, and R. B. M. Schasfoort, "Signal amplification on planar and gel-type sensor surfaces in surface plasmon resonance-based detection of prostate-specific antigen," *Anal. Biochem.*, vol. 333, pp. 165–173, 2004.

[7-15] D. A. Zubtsov, E. N. Savvateeva, A. Yu. Rubina, S. V. Pan'kov, E. V. Konovalova, O. V. Moiseeva, V. R. Chechetkin, and A. S. Zasedatelev, "Comparison of surface and hydrogel-based protein microchipsm," *Anal. Biochem.*, vol. 368, no. 2, pp. 205–213, 2007.

[7-16] P. S. Katsamba, I. Navratilova, M. Calderon-Cacia, L. Fan, K. Thornton, M. Zhu, T. V. Bos, C. Forte, D. Friend, I. Laird-Offringa, et al., "Kinetic analysis of a high-affinity antibody/antigen interaction performed by multiple Biacore users," *Anal. Biochem.*, vol.352, pp. 208–221, 2006.

[7-17]S. W. Lee, K. S. Lee, J. Ahn, J. J. Lee, M. G. Kim, and Y. B. Shin, "highly sensitive biosensing using arrays of plasmonic Au nanodisks realized by nanoimprint lithography," *ACS Nano*, vol. 5, pp. 897–904, 2011.

[7-18] M. Vestergaard, K. Kerman, D. K. Kim, H. M. Hiep, and E. Tamiya, "Detection of Alzheimer's tau protein using localised surface plasmon resonance-based immunochip," *Talanta*, vol. 74, pp. 1038–1042, 2008.

[7-19] G.o A. Farias, J. P. Muñoz, J. Garrido, and R. B. Maccioni, "Tubulin, actin, and tau protein interactions and the study of their macromolecular assemblies," *J. Cell. Biochem.*, vol. 85, no. 2, pp. 315–324, 2002.

[7-20] D. Wang, Y. Li, Z. Lin, B. Qiu, and L. Guo, "Surface-enhanced electrochemiluminescence of Ru@SiO_2 for ultrasensitive detection of carcinoembryonic antigen," *Anal. Chem.*, vol. 87, no. 12, pp. 5966–5972, 2015.

[7-21] S. S. Aćimović, M. A. Ortega, V. Sanz, J. Berthelot, J. L. Garcia-Cordero, J. Renger, S. J. Maerkl, M. P. Kreuzer, and R. Quidant, "LSPR chip for parallel, rapid, and sensitive detection of cancer markers in serum," *Nano Lett.*, vol. 14, no. 5, pp. 2636–2641, 2014.

[7-22] M. Sanders, Y. Lin, J. Wei, T. Bono, and R. G. Lindquist, "An enhanced LSPR

fiber-optic nanoprobe for ultrasensitive detection of protein biomarkers," *Biosens. Bioelectron.*, vol. 61, pp. 95–101, 2014.

[7-23] D. S. Grubisha , R. J. Lipert , H.-Y. Park , J. Driskell, and M. D. Porter, "Femtomolar detection of prostate-specific antigen: an immunoassay based on surface-enhanced Raman scattering and immunogold Labels," *Anal. Chem.*, vol. 75, no. 21, pp. 5936–5943, 2003.

[7-24] X. Miao, S. Zou, H. Zhang, and L. Ling, "Highly sensitive carcinoembryonic antigen detection using Ag@Au core-shell nanoparticles and dynamic light scattering," *Sensors Actuators, B Chem.*, vol. 191, pp. 396–400, 2014.

[7-25] Y. Cui, Q. Q. Wei, H. K. Park, and C. M. Lieber, "Nanowire nanosensors for highly sensitive and selective detection of biological and chemical species," *Science*, vol 293, pp.1289–1292, 2001.

[7-26] E. Stern, J.F. Klemic, D. A. Routenberg, P. N. Wyremebak, D. B. Turner-Evans, A. D. Hamilton, D. A. Lavan, T. M. Fahmy, and M. A. Reed, "Laabel-free immunodetection with CMOS-compatible semiconducting nanowires," *Nature*, vol. 445 pp. 519–522, 2007.

[7-27] E. Stern, R. Wagner, F. J. Sigworth, R. Breaker, T. M. Fahmy, and M. A. Reed, "Importance of the Debye screening length on nanowire field effect transisitor sensors," *Nano Lett.*, vol. 7, pp. 3405–3409, 2007.

[7-28] Jun Pyo Kim, Byung Yang Lee, Joohyung Lee, Seunghun Hong, and Sang Jun Sim, "Enhancement of sensitivity and specificity by surface modification of carbon nanotubes in diagnosis of prostate cancer based on carbon nanotube field effect transistors," *Biosens. Bioelectron.*, vol. 24, no. 11, pp. 3372–3378, 2009.

[7-29] T. W. Lin, P. J. Hsieh, C. L. Lin, Y. Y. Fang, J. X. Yang, C. C. Tsai, P. L. Chiang, C. Y. Pan, and Y. T. Chen, "Label-free detection of protein-protein interactions using a calmodulin-modified nanowire transistor," *Proc. Natl. Acad. Sci. U. S. A.*, vol. 107, pp. 1047–1052, 2010.

[7-30] X. Liu, J. Wei, D. Song, Z. Zhang, H. Zhang, and G. Luo, "Determination of affinities and antigenic epitopes of bovine cardiac troponin I (cTnI) with monoclonal antibodies by surface plasmon resonance biosensor," *Anal. Biochem.*, vol. 314, no. 2, pp. 301–309, 2003.

[7-31] L. V. Levin, T. W. Griffin, L. R. Childs, S. Davis, and D. E. HaagensenJr., "Comparison of multiple anti-CEA immunotoxins active against human adenocarcinoma cells," *Cancer Immunol. Immunother.*, vol. 24, no. 3, pp. 202–206, 1987.

[7-32] G. Zheng, F. Patolsky, Y. Cui, W.U. Wang, and C.M. Lieber, "Multiplexed electrical detection of cancer marlers with nanowire sensor arrays," *Nat. Biotechnol.*, vol. 23, pp. 1294–1301, 2005.

[7-33] J. P. Kim, B. Y. Lee, S. Hong, and S. Jun Sim, "Ultrasensitive carbon nanotube-based biosensors using antibody-binding fragment," *Anal. Biochem.*, vol. 381, no. 2, pp. 193–198, 2008.

[7-34] E. Stern, A. Vacic, N. K. Rajan, J. M. Criscione, J. Park, B. R. Ilic, D. J. Mooney, M. A. Reed, and T. M. Fahmy, "Label-free biomarker detection from whole blood," *Nat. Nanotechnol.*, vol. 5 pp. 138–142, 2010.

[7-35] A. Kim, C. S. Ah, H. Y. Yu, J. H. Yang, I. B. Baek, C. G. Ahn, C. W. Park, M. S. Jun, and S. Lee, "Ultrasensitive, label-free, and real-time immunodetection using silicon field-effect transistors," *Appl. Phys. Lett.*, vol. 91, p. 103901, 2007.

[7-36] K. Kim, C. Park, D. Kwon, D. Kim, M. Meyyappan, S. Jeon, and J. S. Lee, "Silicon nanowire biosensors for detection of cardiac troponin I (cTnI) with high sensitivity," *Biosens. Bioelectron.*, vol. 77, pp. 695–701, 2016.

[7-37] D. J. Kim, I. Y. Sohn, J. H. Jung, O. J. Yoon, N. E. Lee, and J. S. Park, "Reduced graphene oxide field-effect transistor for label-free femtomolar protein detection," *Biosens. Bioelectron.*, vol. 41, no. 1, pp. 621–626, 2013.

[7-38] S. Kita, S. Otsuka, S. Hachuda, T. Endo, Y. Imai, Y. Nishijima, H. Misawa and T. Baba, "Super-sensitivity in label-free protein sensing using nanoslot nanolaser," *Opt. Express*, vol. 19, no. 18, pp. 17683–17690, 2011.

[7-39] S. Hachuda, S. Otsuka, S. Kita, T. Isono, M. Narimatsu, K. Watanabe, Y. Goshima, and T. Baba, "Selective detection of sub-atto-molar Streptavidin in 1013-fold impure sample using photonic crystal nanolaser sensors.," *Opt. Express*, vol. 21, no. 10, pp. 12815–21, 2013.

Chapter 8
Conclusion

Identification of severe diseases and advanced medical diagnoses are of increasing importance in aging societies. Therefore daily examinations of diagnostic biomarkers in blood and humor will have long demands. Although some easily-detectable biomarkers are already being serviced in health clinics, low-cost and high-throughput detection of very small amounts of specific biomarkers suitable for earlier and more reliable diagnoses is still a challenge. For the purpose of easy and non-invasive diagnosis, the various biosensors were studied until now. In our laboratory, a photonic crystal nanolaser as a label-free sensor was developed and the super-sensitivity has achieved 1000-fold times than that of the common surface resonance plasmon sensor. Furthermore, it is expected to be less than the expendable cost of ELISA because of the sensing method which does not require a secondary antibody and enzyme. Thus, the nanolaser sensor is potentially candidate for the medical application such as the diagnosis of the low concentration biomarkers. However, the nanolaser has some issues. Those are the blueshift noise at the sensing, the fluctuation of sensing in different trials, and the unexamined actual biomarkers and selectivity against impurity. Accordingly, author tried to investigate the detection of streptavidin (SA) as a model of antibody-antigen reaction and prostate specific antigen (PSA). Furthermore, author tried to investigate the sensing in solution with contaminants. Finally, the fluctuation of the sensing was tried to suppress by the construction of the stable biointerface and relaxing the sensor surface hydrophobicity.

First, bovine serum albumin (BSA) was used as the modal protein for the evaluation of the non-specific adsorption and specific adsorption. At the non-specific adsorption, BSA was adsorbed to the sensor surface though the coupling with glutaraldehyde (GA). Compared the device with and without a protection layer which suppresses the etching of GaInAsP surface, the improving the sensitivity for the device with the layer was confirmed. At the specific adsorption, BSA was adsorbed to the sensor surface though the anti-BSA antibody. The specific adsorption was detected from the evaluation of the difference between the methods which differed to the order of immobilization.

Next, SA-biotin binding was detected from pure sample and impure sample. The

nanolaser observed the biotin-SA specific binding for which the detection limit concentration was evaluated from the Langmuir fitting to be 16 zM. Author also succeeded in detecting 100 zM SA in the impure sample with 1 μM BSA as the contaminant. This means that the ultra-high selectivity (SA/BSA) = 10^{13} was achieved. Furthermore, the improving the stability was confirmed by the coated a protection layer by ALD, and the optimization of the modification of biotinylation and adsorption conditions. Particularly, the effect of Tween 20 as a surfactant increased the wavelength shift. Furthermore, suppressing non-specific adsorption of BSA was demonstrated using PEG polymers.

PSA was detected from pure sample and impure sample. We selectively detected 1 fM PSA, which is much lower than the detection limit of the standard ELISA technique. This enables the monitoring of potential recurrences of prostate cancer after surgical procedures. Detection was possible even with the introduction of 10 μM BSA as a contaminant; the corresponding selectivity is ten billion. This selectivity is smaller than that obtained in the detection of the biotin-SA specific binding in a sample with BSA, but reasonably large, considering 5–6 orders of lower affinity constant of the PSA antibody-antigen binding compared with the case of biotin-SA. Furthermore, the increasing wavelength shift by ethanolamine was confirmed. The expectation of ethanolamine is the suppression of excessive hydrophobicity at the nanoscale level of rough surfaces by hydrophilizing the device surface. This allows the antigen to effectively penetrate into holes of the photonic crystal slab and approach the antibody. Thus, the merit of the surfactant modification such as EA for biomarker sensing using nanolaser sensor was demonstrated and high sensitivity detection of 1 fM PSA was also demonstrated even from mixture with 10 μM BSA. This effect of relaxing surface hydrophobicity was also observed at the SA detection with 0.1% polyoxyethylene (20) sorbitan monolaurate (Tween 20). This experiment supports the expectation.

The sensor performance was evaluated by figure of merit (FOM). A NS nanolaser achieved a very high FOM of 1.9-300. μ-toroidal, local SPR (LSPR), surface enhanced Raman scattering (SERS) and field effect transistor (FET) biosensors also achieved high FOM of > 1. However, these biosensors do not satisfy the requirement of the biomarker sensing which are low cost, disposable use, simple procedure, high sensitivity, and high selectivity against contaminants. The nanolaser sensor will become more suitable device as a biomarker sensor because the sensor potentially satisfies those requirements.

Those results of this study provided evidence that nanolaser sensors are instruments of ultrahigh sensitivity and are capable of selecting for bio-molecules of interest. It is known that total amount of serum albumin included in human blood is 1 mM. When the detection is conducted from blood, the nanolaser could detect 100 fM PSA in a sample with 1 mM albumin after diluting it 100 times. We also confirmed that more reliable sensing is

possible with the inclusion of ethanolamine. Thus, the nanolaser sensor was found to be a promising candidate for practical biomarker sensing in medical diagnoses.

Acknowledgements

I would like to express my heartfelt thanks to Prof. Toshihiko Baba (Yokohama Nat'l Univ.) for the full educations, the advices, the encouragements and the pep talks like the laser pumping. I would like to express my heartfelt thanks to Prof. Toshio Ogino (Yokohama Nat'l Univ.) for the educations, especially biointerface. I was educated about the basic knowledge of the surface science at the first year of master course.

I would like to express my heartfelt thanks to Prof. Yasuo Kokubun (Yokohama Nat'l Univ.), Associate Prof. Yoshiaki Nishijima (Yokohama Nat'l Univ.), Associate Prof. Takahide Oya, and Associate Prof. Taro Arakawa (Yokohama Nat'l Univ.) for the discussion and the educational and profitable advices.

I would like to express my heartfelt thanks to Prof. Eiichi Tamiya (Osaka Univ.) and Assistant Prof. Masato Saito (Osaka Univ.) for the discussion of the biointerface and the biosensing, especially the interface of APTES. I would like to express my heartfelt thanks to Associate Prof. Junji Fukuda (Yokohama Nat'l Univ.) for the discussion of the biosensing. I would like to express my heartfelt thanks to Prof. Yoshio Goshima (Yokohama City Univ.) for the advices at the view of medical front.

I would like to express my heartfelt thanks to Dr. Shota Kita (now of NTT basic Research Laboratories) for pioneering the photonic crystal nanolaser sensor in our laboratory. When I was assigned in Baba laboratory, he was direct senior associate and I was educated about everything related to the photonic crystal nanolaser sensor. I would like to express my heartfelt thanks to Dr. Toshinari Isono (now of Pharmaceuticals and Medical Devices Agency) for the advices. The behavior of his research and the word of "I have studied because knowing the new things is fun" are my motive ideas. I would like to express thanks to Mr. Hiroshi Abe (Yokohama Nat'l Univ.) for the discussions of the nanolaser arrays. I would like to express my heartfelt thanks to Mr. Shota Otsuka (now of TDK) for the contribution of the SA sensing, Mr. Keisuke Watanabe (now of Sony) for the contribution of ALD and the discussion of sensing principle, Mr. Takumi Watanabe (Yokohama Nat'l Univ.) for the discussion of the sensing principle, Mr. Michimasa Narimatsu (now of Simadzu) for the contribution of improvement of the photonic crystal nanolaser by FDTD, Mr. Yoji Kishi (now of Tokyo Seimitsu) for the investigation of NS and the charge effect, Mr. Atsuhiro Tanaka (Yokohama Nat'l Univ.) for the investigation of APTES, Mr. Naoki Okamura (now of Hitachi) for the discovery of the charge effect to

the nanolaser, Mr. Tomoki Tanaka (now of Adachi Lab. of Yokohama Nat'l Univ.) for the improvement of the nanolaser design, and Mr. Yuji Saito (now of Yokohama city office) for the contribution of the thermal chirping of the laser wavelength. I would like to express heartfelt thanks to Mr. Daichi Takahashi (Yokohama Nat'l Univ.), Ms. Mai Sakemoto (Yokohama Nat'l Univ.), Mr. Yuki Furuta (Yokohama Nat'l Univ.) and Mr. Ryota Hirano (Yokohama Nat'l Univ.) for the discussion of the biosensing.

I would like to express heartfelt thanks to colleagues in Baba laboratory for the discussion, advisements, and in some cases plays. I would like to express heartfelt thanks to Ms. Makiko Koyanagi, Ms. Yukie Iguchi, Ms. Harumi Oikawa, Ms. Toshiyo Takahashi and Ms. Tomoko Mando, who were office administrators, for the support of the academic life.

Finally, I would like to express heartfelt thanks to my parents and sisters for the mental and financial supports.

This work was supported by the Grant-In Aid projection of Ministry of Education, Culture, Sports, Science and Technology (MEXT) and by the global COE program of Japan Society for the Promotion of Science (JSPS).

Presentations of this work

I. Journal papers

Full papers

[1] S. Hachuda, S. Otsuka, S. Kita, T. Isono, M. Narimatsu, K. Watanabe, Y. Goshima and T. Baba, "Selective detection of sub-atto-molar streptavidin in 10^{13}-fold impure sample using photonic crystal nanolaser sensors," *Opt. Express*, vol. 21, no. 10, pp. 12815–12821, 2013.

[2] S. Hachuda, T. Watanabe, D. Takahashi, and T. Baba, "Sensitive and selective detection of prostate-specific antigen using photonic crystal nanolaser," *Sensors Actuators B Chem.*, (under review).

[3] S. Kita, K. Nozaki, S. Hachuda, H. Watanabe, Y. Saito, S. Otsuka, T. Nakada, Y. Arita and T. Baba, "Photonic crystal point-shift nanolaser with and without nanoslots --- design, fabrication, lasing and sensing characteristics," *IEEE J. Sel. Top. Quantum Electron.*, vol. 17, no. 6, pp. 1632–1647, 2011.

[4] S. Kita, S. Hachuda, S. Otsuka, T. Endo, Y. Imai, Y. Nishijima, H. Misawa and T. Baba, "Super-sensitivity in label-free protein sensing using a nanoslot nanolaser," *Opt. Express*, vol. 19, no. 18, pp. 17683–17690, 2011.

[5] S. Kita, S. Otsuka, S. Hachuda, T. Endo, Y. Imai, Y. Nishijima, H. Misawa and T. Baba, "Photonic crystal nanolaser bio-sensors," *IEICE Trans. Electron.*, vol. E95-C, no. 2, pp. 188–198, 2012.

Letters

[1] S. Kita, S. Hachuda, K. Nozaki and T. Baba, "Nanoslot laser," *Appl. Phys. Lett.*, vol. 97, no. 16, pp. 161108, 2010.

[2] K. Watanabe, Y. Kishi, S. Hachuda, T. Watanabe, M. Sakemoto, Y. Nishijima and T. Baba, "Simultaneous detection of refractive index and surface charges in nanolaser biosensors," *Appl. Phys. Lett.*, vol. 106, no. 2, pp. 021106, 2015.

[3] D. Takahashi, S. Hachuda, T. Watanabe, Y. Nishijima and T. Baba, "Detection of

endotoxin using a photonic crystal nanolaser," *Appl. Phys. Lett.*, vol. 106, no. 13, pp. 131112, 2015.

II. International conferences

[1] S. Kita, S. Hachuda and T. Baba, "Photonic crystal nanolaser with nano-slit structure," *Int. Sympo. Compound Semicon.*, Takamatsu, no. FrD3-3, June 2010.

[2] S. Kita, S. Hachuda, N. Yoshiaki, M. Hiroaki and T. Baba, "High resolution biosensing using photonic crystal nano-slit H0 nanolaser," *Int. Sympo. Compound Semicon.*, Takamatsu, no. FrD3-7, June 2010.

[3] S. Kita, S. Hachuda and T. Baba, "Nano-slit photonic crystal nanolaser with mode localization in air," *IEEE Int. Semicon. Laser Conf.*, Kyoto, no. ThA4, October 2010.

[4] S. Kita, S. Hachuda T. Endo, Y. Nishijima, H. Misawa and T. Baba, "High-sensitivity biosensing using nanolaser," *IEEE Sensors Conf.*, Hawaii, no. C1L-E6, November 2010.

[5] T. Baba, S. Kita, H. Abe, S. Hachuda, M. Narimatsu, S. Otsuka and K. Nozaki, "Photonic crystal nanolasers with nanoslot structure for sensing applications," *SPIE Optics and Photonics*, San Diego, no. 8095-30, August 2011 (Invited Paper).

[6] T. Isono, S. Kita, S. Otsuka, S. Hachuda, N. Okamura, Y. Goshima and T. Baba, "Specific detection of protein molecules using photonic crystal nanolaser sensor", *Int. Sympo. Surface Sci.*, Tokyo, no. 14PN-114, December 2011 (Poster).

[7] S. Kita, S. Hachuda, S. Otsuka, T. Isono and T. Baba, “Photonic crystal nanoslot nanolaser array for statistical analysis of protein detection”, *Int. Sympo. Photonic and Electromagnetic Crystal Structures*, Santa Fe, no. 125, June 2012.

[8] T. Baba, S. Kita, S. Hachuda and S. Otsuka, "Photonic crystal nanoslot nanolaser for super-sensitivity bio-sensing," *IEEE Int. Conf. Transparent Opt. Networks*, Coventry, no. We.A6.4, July 2012 (Invited Paper).

[9] S. Hachuda, S. Kita, T. Isono, S. Otsuka and T. Baba, "Selective detection of streptavidin in impure sample using nano-slot photonic crystal nanolaser," *IUMRS-Conf. Electron. Mat.*, Yokohama, no. B-9-O25-010, September 2012.

[10] S. Kita, S. Hachuda, S. Otsuka, N. Okamura, T. Isono and T. Baba, "Photonic crystal nanoslot nanolaser for ultra-high sensitivity and selectivity protein sensing," *IEEE Int. Semicon. Laser. Conf.*, San Diego, no. WC2, October 2012.

[11] T. Isono, S. Hachuda, S. Kita, Y. Goshima and T. Baba, "Supersensitive detection of

target molecules in a presence of excess non-targets using photonic crystal nanolaser sensor array," *MRS Fall Meet.*, Boston, no. XX3.16, November 2012.

[12] S. Hachuda, S. Otsuka, S. Kita T. Isono, K. Watanabe and T. Baba, "Selective detection of sub-atto-molar streptavidin in 10^{13} fold impure sample using nanoslot photonic crystal nanolaser," *SPIE Photonics West*, San Francisco, no. 8594-16, February 2013.

[13] K. Watanabe, S. Hachuda, T. Isono and T. Baba, "Photonic crystal nanolaser sensors with ALD coating," *Conf. Laser & Electro-Opt. Pacific Rim and Optoelectronic & Commun. Conf. / Photonics Switching*, Kyoto, no. TuJ2-2, July 2013.

[14] T. Isono, S. Hachuda, K. Watanabe, N. Yamashita, Y. Goshima, and T. Baba, "Specific detection of marker protein related with Alzheimer's disease using photonic crystal nanolaser sensor array," *MRS Fall Meet.*, Boston, no. K5.09, December 2013.

[15] S. Hachuda, T. Watanabe, D. Takahashi and T. Baba, "Ultra-sensitive and selective detection of prostate specific antigen beyond ELISA using photonic crystal nanolaser," *Conf. Laser and Electro-Opt.*, San Jose, no. AM1J.3, May 2015.

[16] D. Takahashi, S. Hachuda, T. Watanabe, Y. Nishijima and T. Baba, "Detection of endotoxin using a photonic crystal nanolaser," *Conf. Laser and Electro-Opt. Pacific Rim*, Busan, no. 25I3-3, August 2015.

III. Demestic conferences

[1] 羽中田祥司, 北翔太, 馬場俊彦, “ナノスリット構造フォトニック結晶 H0 ナノレーザ”, 応用物理学会春季講演会, no. 19a-M-4, 2010.

[2] 北翔太, 羽中田祥司, 西島喜明, 三澤弘明, 馬場俊彦, “ナノスリット構造フォトニック結晶 H0 ナノレーザによる高分解能バイオセンシング”, 応用物理学会春季講演会, no. 19a-M-5, 2010.

[3] 北翔太, 大塚翔太, 羽中田祥司, 遠藤達郎, 西島喜明, 三澤弘明, 馬場俊彦, “ナノスロット構造フォトニック結晶ナノレーザを用いたバイオセンサ”, 応用物理学会秋季講演会, no. 15a-ZW-18, 2010.

[4] 馬場俊彦, 北翔太, 羽中田祥司, 大塚翔太, 阿部紘士, 成松道正, “フォトニック結晶ナノレーザを用いたバイオセンシング”, 電子情報通信学会総合大会, no. CI-1-10, 2011 (招待講演).

[5] 馬場俊彦, 北翔太, 羽中田祥司, 大塚翔太, 阿部紘士, 成松道正, “フォトニック結晶ナノレーザ---究極のナノスロット構造とその応用”, 応用物理学会

春季講演会, no. 26p-BN-8, 2011 (招待講演).
[6] 馬場俊彦, 北翔太, 羽中田祥司, 大塚翔太, 渡邊敬介, 磯野俊成, “フォトニック結晶ナノレーザによる超高感度バイオセンシング”, 科学術振興機構光科学公開シンポジウム, 2012.
[7] 羽中田祥司, 北翔太, 大塚翔太, 成松道正, 磯野俊成, 馬場俊彦, “ナノスロットナノレーザによる不純物環境下でのストレプトアビジン選択的吸着検出”, 応用物理学会春季講演会, no. 17a-F8-4, 2012.
[8] 羽中田祥司, 北翔太, 成松道正,磯野俊成, 馬場俊彦, “ナノスロットナノレーザによる不純物環境下でのストレプトアビジン選択的吸着検出(II) --選択比のさらなる向上”, 応用物理学会秋季講演会, no. 12p-H3-8, 2012.
[9] 磯野俊成, 羽中田祥司, 北翔太, 大塚翔太, 五嶋良郎, 馬場俊彦, “フォトニック結晶ナノレーザセンサアレーによる不純物溶液中におけるターゲット分子の高感度検出”, 応用物理学会秋季講演会, no. 12p-H4-17, 2012.
[10]磯野俊成, 羽中田祥司, 北翔太, 五嶋良郎, 馬場俊彦, “フォトニック結晶ナノレーザアレーを用いた高選択性バイオセンシング”, 表面科学会学術講演会, no. 22Ca05, 2012.
[11]馬場俊彦, 羽中田祥司, 渡邊敬介, 磯野俊成, 大塚翔太, 北翔太, “フォトニック結晶ナノレーザによる高感度バイオセンシング”, 電子情報通信学会総合大会, no. C-4-22, 2013 (招待講演).
[12]磯野俊成, 羽中田祥司, 渡邊敬介, 五嶋良郎, 馬場俊彦, “フォトニック結晶ナノレーザアレイによる高感度/高選択性バイオセンシング”, 応用物理学会春季講演会, no. 27p-G17-9, 2013.
[13]羽中田祥司, 渡邉敬介, 磯野俊成, 馬場 俊彦, “ナノスロットナノレーザによる超低濃度タンパク質センシング”, 応用物理学会春季講演会, no. 28p-C1-16, 2013.
[14]渡邊敬介, 羽中田祥二, 磯野俊成, 馬場俊彦, “ALD 被膜によるフォトニック結晶ナノレーザセンサのノイズ抑制と特性評価”, 応用物理学会春季講演会, no. 30a-PB1-12, 2013.
[15]羽中田祥司, 磯野俊成, 渡邊敬介, 馬場俊彦, "ナノスロットナノレーザによる前立腺がんマーカ検出", 応用物理学会秋季講演会, no. 18a-P5-11, 2013.
[16]磯野俊成, 羽中田祥司, 渡邊敬介, 山下直也, 五嶋良郎, 馬場俊彦, "フォトニック結晶ナノレーザセンサアレイによるアルツハイマー病関連分子マーカの検出", 応用物理学会秋季講演会, no. 16p-C6-8, 2013.
[17]渡邊敬介, 羽中田祥司, 磯野俊成, 西島喜明, 馬場俊彦, "フォトニック結晶ナノレーザバイオセンサにおける極低濃度波長シフトの電気的効果の調査", 応用物理学会秋季講演会, no. 18a-P5-10, 2013.

[18]渡邊敬介, 羽中田祥司, 磯野俊成, 西島喜明, 馬場俊彦, “フォトニック結晶ナノレーザバイオセンサにおける屈折率・電荷同時検出の可能性”, 応用物理学会春季講演会, no. 18a-PG5-5, 2014.
[19]高橋大智, 羽中田祥司, 渡邊敬介, 磯野俊成, 西島喜明, 馬場俊彦, “フォトニック結晶ナノレーザバイオセンサを用いたエンドトキシン検出”, 応用物理学会春季講演会, no. 18a-PG5-15, 2014.
[20]磯野俊成, 羽中田祥司, 渡邊敬介, 山下直也, 五嶋良郎, 馬場俊彦, “フォトニック結晶ナノレーザセンサアレイによるアルツハイマー病関連分子マーカの検出 (II)”, 応用物理学会春季講演会, no. 19p-E15-10, 2014.
[21]高橋大智, 羽中田祥司, 西島喜明, 馬場俊彦, “フォトニック結晶ナノレーザバイオセンサとリムルス試薬を用いた高速・高感度エンドトキシン検出”, 応用物理学会秋季講演会, no. 18a-PA2-14, 2014.
[22]岸洋次, 渡邊敬介, 羽中田祥司, 渡部工, 酒本真衣, 西島喜明, 馬場俊彦, “フォトニック結晶ナノレーザバイオセンサにおける屈折率・電荷同時検出の可能性(II)”, 応用物理学会秋季講演会, no. 19a-A2-3, 2014.
[23]羽中田祥司, 高橋大智, 渡部工, 田中智基, 馬場俊彦, “フォトニック結晶ナノレーザによる不純物を含む試料からの前立腺癌マーカの高感度検出”, 応用物理学会秋季講演会, no. 19a-A2-4, 2014.
[24]渡部工, 渡邊敬介, 羽中田祥司, 高橋大智, 西島喜明, 馬場俊彦, “フォトニック結晶ナノレーザバイオセンサにおけるデバイ遮蔽効果の検証”, 応用物理学会秋季講演会, no. 20a-A3-3, 2014.
[25]馬場俊彦, 羽中田祥司, 渡部工, 高橋大智, 古田裕樹, 渡邊敬介, 阿部紘士, 岸洋次, 酒本真衣, 北翔太, “GaInAsP 半導体デバイスを用いたバイオセンシング／イメージング”, 電子情報通信学会光エレクトロニクス研究会, 2015 (招待講演).
[26]高橋大智, 羽中田祥司, 渡部工, 西島喜明, 馬場俊彦, "フォトニック結晶ナノレーザバイオセンサとリムルス試薬を用いた高速・高感度エンドトキシン検出(Ⅱ)", 応用物理学会春季講演会, no. 12a-P11-15, 2015.
[27]羽中田祥司, 渡部工, 馬場俊彦, "フォトニック結晶ナノレーザによる不純物を含む試料からの前立腺癌マーカーの高感度検出(Ⅱ)", 応用物理学会春季講演会, no. 13a-D6-9, 2015.
[28]渡部工, 羽中田祥司, 古田祐樹, 岸洋次, 西島喜明, 馬場俊彦, "フォトニック結晶ナノレーザバイオセンサにおけるセンサ界面の考察", 応用物理学会春季講演会, no. 13p-D5-2, 2015.
[29]高橋大智, 羽中田祥司, 渡部工, 西島喜明, 馬場俊彦, "フォトニック結晶ナノレーザバイオセンサとリムルス試薬を用いた高速・高感度エンドトキシン

検出(III)", 応用物理学会秋季講演会, no. 15p-2B-13, 2015.
[30] 渡部工, 羽中田祥司, 西島喜明, 馬場俊彦, "フォトニック結晶ナノレーザにおける試料吸着による屈折率変化の考察", 応用物理学会秋季講演会, no. 15p-2B-14, 2015.